



BACHELOR PROJECT, 15 ECTS-POINTS

---

# Closed-Loop Lambda Control of Ecocar Engine

---

*Author:*

Nikolaj DAGNÆS-HANSEN,  
s093232

28th June 2013

### Abstract

In today's society, the demands for vehicle fuel economy and low emissions are continually increasing. Ways of meeting these demands may include; using small engines running at wide open throttle, and an accurate control of the air/fuel ratio (lambda-value) because this value correlates strongly with the engine efficiency. This thesis focuses on the problems concerning closed loop lambda-control of a small single-cylinder engine running only at wide open throttle tantamount to running under transient conditions. A lambda control system has been developed for the DTU ecocar. Various control systems in relation to a performance specification for the ecocar have been analysed and tested. It was found that a simple version of an engine map combined with a simple version of closed loop lambda control was able to meet the control system requirements well, resulting in the pivotal contribution of the lambda control system in relation to the excellent results of the ecocar at the Shell Eco Marathon in May 2013. It was also found that a laminar flow meter can be used to improve the control system significantly and to facilitate the construction of the engine map.

## Contents

<b>1 Foreword</b>	<b>1</b>
<b>2 Problem statement</b>	<b>2</b>
<b>3 Introduction</b>	<b>3</b>
<b>4 Effect of excess air ratio on fuel efficiency</b>	<b>5</b>
<b>5 Performance specification of the control system</b>	<b>9</b>
5.1 Transient problems concerning $\lambda$ control . . . . .	11
5.2 Problems concerning the application of the control system in a real car in contrast to a test stand . . . . .	14
<b>6 Sensors</b>	<b>15</b>
6.1 Lambda-sensor . . . . .	15
6.2 Flow sensors . . . . .	18
6.2.1 Hot wire MAF sensor . . . . .	18
6.2.2 Laminar flow meter . . . . .	19
6.3 Axe encoder . . . . .	20
<b>7 Types of excess air ratio control systems</b>	<b>22</b>
7.1 Conventional $\lambda$ -control . . . . .	22
7.1.1 Conventional $\lambda$ control in relation to the requirement specification . . . . .	25
7.2 Control using the speed-density function . . . . .	26
7.2.1 Speed-density control in relation to the requirement specification . . . . .	26
7.3 Transient closed-loop $\lambda$ control . . . . .	27
7.3.1 Transient closed-loop $\lambda$ control in relation to the requirement specification	28
<b>8 Dynamometer testing of a speed-density function control system</b>	<b>30</b>
<b>9 Experimental tests concerning a closed-loop <math>\lambda</math> control system</b>	<b>39</b>
<b>10 Laminar flow meter experiment</b>	<b>48</b>
<b>11 Further work</b>	<b>73</b>
<b>12 Final conclusion</b>	<b>74</b>

<b>A Additional plots concerning the Shell Eco Marathon 2012 final race</b>	<b>77</b>
<b>B Additional plots concerning Shell Eco Marathon 2013</b>	<b>79</b>
<b>C Deduction of calibration formula</b>	<b>82</b>
<b>D Additional figures concerning the laminar flow meter experiment</b>	<b>83</b>
<b>E Core dimensions of the prototypes</b>	<b>92</b>
<b>F Prototype 5 drawings and dimensions</b>	<b>93</b>
<b>G LabVIEW code</b>	<b>96</b>
G.1 Speed-density control system . . . . .	96
G.2 Flow measurements . . . . .	98
G.3 Control of injection . . . . .	102
G.4 Closed-loop control . . . . .	108
<b>H Final engine map struct</b>	<b>112</b>
<b>I Matlab code for data processing, Shell Eco Marathon 2012 data</b>	<b>113</b>
<b>J Matlab code for data processing, Closed-loop <math>\lambda</math> control experiment</b>	<b>117</b>
<b>K Matlab code for data processing, laminar flow meter experiment</b>	<b>120</b>
<b>L Certification for the Meriam laminar flow meter</b>	<b>124</b>
<b>M Manual for the Meriam laminar flow meter</b>	<b>128</b>

## List of Figures

1	Emission of greenhouse gases (GHG) . . . . .	3
2	$\eta_e$ as a function of $\lambda$ - theoretical basis . . . . .	6
3	$\eta_e$ as a function of $\lambda$ - ecocar engine . . . . .	8
4	Three-way catalytic converter . . . . .	9
5	Velocity curve for ecocar - whole race . . . . .	10
6	Velocity curve for ecocar - one burn cycle . . . . .	10
7	Narrowband oxygen sensor . . . . .	15
8	NBO <sub>2</sub> output . . . . .	16
9	Wideband oxygen sensor . . . . .	16
10	Laminar flow element . . . . .	19
11	Axle encoder output . . . . .	21
12	Backbone of engine map . . . . .	22
13	Simple engine map . . . . .	25
14	Diagram for control system using speed-density function . . . . .	26
15	Simplified closed-loop principle . . . . .	28
16	First test of the system in 1st gear . . . . .	32
17	First test of the system in 2nd gear . . . . .	32
18	$\lambda$ as a function of engine speed, Shell Eco Marathon 2012 . . . . .	36
19	Injection length, Shell Eco Marathon 2012 . . . . .	36
20	$\lambda(N)$ 1st race 2013 . . . . .	43
21	$\lambda(N)$ 3rd race 2013 . . . . .	43
22	$\lambda(N)$ 2nd race 2013 . . . . .	43
23	$\lambda(N)$ 4th race 2013 . . . . .	43
24	Average of $\lambda$ -values for each lap . . . . .	44
25	Sketch of laminar flow meter calibration . . . . .	48
26	Experimental setup of laminar flow meter calibration . . . . .	50
27	Downscaling of air flow with a gap . . . . .	51
28	Sketch of the capillary tubing used for the prototypes . . . . .	53
29	Preparation of foil . . . . .	53
30	Corrugation of foil . . . . .	53
31	Coiling of foil . . . . .	54
32	The inside of a laminar flow element . . . . .	54
33	Laminar flow element, prototype 1 . . . . .	55
34	Laminar flow meter in testing stand . . . . .	56

35	Laminar flow meter mounted in car . . . . .	57
36	Preliminary laminar flow meter test . . . . .	58
37	Laminar flow meter test, prototype 1 . . . . .	59
38	Laminar flow meter test, prototype 5 . . . . .	60
39	Pressure oscillations A . . . . .	61
40	Pressure oscillations B . . . . .	62
41	Outside test of ecocar with the laminar flow meter . . . . .	63
42	Fuel mass determined from laminar flow meter 1 . . . . .	64
43	Fuel mass determined from laminar flow meter 2 . . . . .	64
44	$\lambda$ as a function of engine speed, Shell Eco Marathon 2012, all values . . . . .	77
45	Injection length during one burn 2012 . . . . .	77
46	Various values during whole race 2012 . . . . .	78
47	Various values during one burn 2012 . . . . .	78
48	$\lambda(N)$ 2nd race 2013, zoomed plot . . . . .	79
49	$\lambda(N)$ 3rd race 2013, zoomed plot . . . . .	79
50	$\lambda(N)$ 1st race 2013, all values . . . . .	80
51	$\lambda(N)$ 3rd race 2013, all values . . . . .	80
52	$\lambda(N)$ 2nd race 2013, all values . . . . .	80
53	$\lambda(N)$ 4th race 2013, all values . . . . .	80
54	$\lambda(N)$ 5th race 2013, all values . . . . .	81
55	$\lambda(N)$ 5th race 2013, average values . . . . .	81
56	Improved experimental setup of laminar flow meter calibration . . . . .	83
57	Laminar flow meter test, prototype 2 . . . . .	84
58	Laminar flow meter test, prototype 3 . . . . .	85
59	Laminar flow meter test, prototype 4 . . . . .	86
60	Laminar flow meter test, prototype 4b . . . . .	87
61	Laminar flow meter test, prototype 5, second test . . . . .	88
62	Engine oscillations C . . . . .	89
63	Engine oscillations D . . . . .	89
64	Pressure oscillations E . . . . .	90
65	$\lambda$ -values for outdoor test, May 12th . . . . .	91
66	Volumetric efficiency of ecocar engine . . . . .	91
67	Sketch of prototype with core dimensions . . . . .	92
68	Drawing of laminar flow meter prototype 5 . . . . .	93
69	Drawing of laminar flow meter prototype 5, intersected . . . . .	94
70	Drawing of laminar flow meter prototype 5 with core dimensions . . . . .	95

71	LabVIEW - Speed-density control, true case . . . . .	97
72	LabVIEW - Speed-density control, false case . . . . .	98
73	LabVIEW - Flow measurements 1 . . . . .	100
74	LabVIEW - Flow measurements 2 . . . . .	101
75	LabVIEW - Fuel injection code . . . . .	107
76	LabVIEW - Closed-loop code . . . . .	110
77	LabVIEW - Closed-loop code, case structure true . . . . .	111
78	Final engine map . . . . .	112

## List of Tables

1	Examples of lookup tables . . . . .	24
2	Calibration factors for speed-density control . . . . .	31
3	Core dimensions of prototypes . . . . .	92

## Acronyms

Abbreviation	Meaning
ABS	Acrylonitrile Butadiene Styrene
BDC	Bottom Dead Center
BTDC	Before Top Dead Center
ECU	Engine Control Unit
IEA	International Energy Agency
LED	Light-emitting Diode
MAF	Mass Air Flow
NBO <sub>2</sub>	Narrowband oxygen sensor
SI	Spark-ignition
TWC	Three-way catalytic converter
WBO <sub>2</sub>	Wideband oxygen sensor
WOT	Wide Open Throttle

## Nomenclature

Symbol	Meaning	Units
$B$	Bore diameter	m
$BMEP$	Brake mean effective pressure	kPa
$BP$	Brake power	kW
$BSFC$	Brake specific fuel consumption	g/kW-h
$CAD$	Crank angle degrees	CAD (degrees)
$D$	Hydraulic diameter	m
$FA$	Fuel air ratio	kg/kg
$FP$	Friction power	kW
$H_u$	Lower heating value	kJ/kg
$f$	Frequency	Hz
$IMEP$	Indicated mean effective pressure	kPa
$IP$	Indicated power	kW
$k$	calibration factor	-
$L$	Length	m
$m_f$	Fuel mass per injection	mg
$\dot{m}$	Mass flow	g/s
$N$	Rotation speed	Rev/min
$p_{in}$	Absolute inlet manifold pressure	kPa
$RPM$	Revolutions per minute	min <sup>-1</sup>
$S$	Stroke	m
$T_{in}$	Inlet manifold temperature	K
$\dot{V}_{air}$	Air volume flow through one capillary	m <sup>3</sup> /s
$V_d$	Displacement/swept volume	m <sup>3</sup>
$x$	Engine revolutions per engine cycle	Rev/cycle
$\Delta p$	Pressure difference	Pa
$\Delta V$	Voltage	V
$\varepsilon$	Compression ratio	-
$\eta_e$	Fuel conversion efficiency	-
$\eta_i$	Indicated efficiency	-
$\eta_m$	Mechanical efficiency	-
$\eta_v$	Volumetric efficiency	-
$\lambda$	Excess air ratio	-
$\mu$	Fluid dynamic viscosity	N · s/m <sup>2</sup>
$\rho$	Density	kg/m <sup>3</sup>

## 1 Foreword

This thesis has been completed in collaboration with DTU Ecocar and DTU Mechanical Department of Engineering as the final project required to complete a Bachelor degree in Mechanical Engineering at the Technical University of Denmark. All work related to this project has been carried out in the months between February and June 2013 and the project is rated at 15 ECTS points.

Firstly, I would like to thank Associate Professor Jesper Schramm and Postdoc Kim Rene Hansen for impeccable supervision and for making this project very exciting. Also, I would like to thank Erika Taras for thoroughly proof reading this thesis. I would also like to thank the whole ecocar team which it has been a privilege to work with, in particular Emil and Lasse Møller for electro-technological aid, Kris Retoft and Erik Gotfredsen for helping in the design of 3d-drawings, and Nils Refstrup, Maibrit S. Andersen, Marina Ejlertsen, Mie Bach-Pedersen and Morten Bæk for great teamwork concerning the programming of the engine control unit. I would especially like to thank teacher's assistant Claus S. Nielsen whose help and guidance have been essential and who has made the whole process towards the making of this report extremely instructive. Finally I would like to give a huge thanks to Associate Professor Elbert Hendricks whose experience, knowledge, and helpfulness has helped to raise the academic level of this project significantly and made it an even greater instructive and exciting experience.

Nikolaj Dagnæs-Hansen, 28th June 2013

## 2 Problem statement

This project deals with the electronic control of the fuel/air ratio in a combustion engine during speed and throttle transients. The engine is a single-cylinder, 4-stroke, 50cm<sup>3</sup> high-end moped spark ignition engine running on 2nd generation bio-ethanol. The engine is used in the DTU ecocar which participated in the 2013 European Shell Eco Marathon in Rotterdam.

The excess air ratio is controlled using a control system consisting of sensors and of software code written in LabVIEW. The purpose of this project is to examine the best choice of sensors and the best design of the control system in order to obtain accurate lambda control. In this study the focus will be on how to obtain closed loop lambda control - that is - how to utilise the feedback from a fuel/air ratio sensor placed in the exhaust manifold to improve control.

Based on a performance specification of the ecocar engine, different approaches to the control of lambda will be discussed. This discussion will be supported by experiments testing the applicability of various control systems.

### 3 Introduction

In 2012 transport accounted for 22% of global energy-related CO<sub>2</sub> emissions [2, page 9]. Therefore, fuel consumption reduction in the transport sector has to play a major role for the overall reduction of greenhouse gases. One of the most important strategies for this is the optimisation of vehicle efficiency. Regarding reduction in the transport sector, the International Energy Agency (IEA) has stated; "improvements in transport energy efficiency offer the largest and least expensive CO<sub>2</sub> reductions, at least over the next ten years" [1, page 31]. This shows in their emission-reduction strategy which is called "BLUE map". The BLUE map scenario and other scenarios can be seen on figure 1.

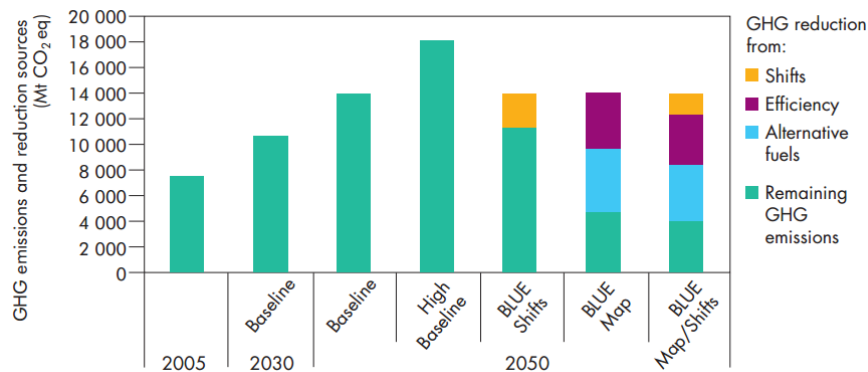


Figure 1: Emission of greenhouse gases (GHG) in 2005 and in the future when different scenarios are to occur. The graph is taken from: [1, page 31]. Explanation of different columns: **"Baseline:** Current and expected future trends in the absence of new policies. **High Baseline:** Considers the possibility of higher growth rates in car ownership, aviation and freight travel. **BLUE map:** Strong improvements in vehicle efficiency and introduction of advanced technologies and fuels. **BLUE shifts:** Travel is shifted to more efficient modes [for example; using public transportation instead of cars]" [1, page 30]

An effective and more commonly used way of developing more energy efficient vehicles is by better engine control. This project aims to demonstrate how engine control in practice can be used effectively to obtain higher fuel efficiency. A system for electronic control of the excess air ratio in a combustion engine will be developed and implemented in a car participating in the Shell Eco Marathon. By implementing the system in this particular car, the project contributes to the excellent fuel economy of the Shell Eco Marathon car. Thereby the necessary actions for reducing emissions are brought into focus by putting vehicle fuel-usage in perspective. A strong

perspective considering the results of Danish Technical University's car in May 2013. Here, a new world record of 612.3 km/l (gasoline equivalent) was set by the car.

As mentioned above, this report will demonstrate how engine control can be used to obtain a better fuel economy. This demonstration will be conducted through experiments testing various types of engine control systems. However, many different approaches can be made to optimise fuel consumption by engine control thus before experiments are presented, it is necessary to clarify why these particular experiments have been chosen.

This is done by discussing different types of engine control systems. An important tool in this discussion is the *performance specification* of the DTU ecocar control system which specifies what requirements the control system should meet to obtain the best fuel economy. Another crucial part in the discussion of control systems is the characterisation of the required sensors, hence a characterisation of the relevant sensors is also necessary prior to the experimental section.

There is however one crucial part that all control systems discussed in this report will have in common - they will all aim to control the instantaneous lambda-value, also called the excess air ratio. Therefore, an explanation of why this report focuses on lambda-control is initially presented. Summarised, the structure of this report will be:

- Explanation of why the fuel economy can be optimised by controlling the lambda-value (excess air ratio).
- Performance specification of the DTU ecocar control system.
- Characterisation of the relevant sensors for optimum control.
- Discussion of different control systems and how well they fulfil the performance specification.
- Experimental section. Here, different control systems are evaluated through tests and relevant data-processing.
- Further work and conclusion.

#### 4 Effect of excess air ratio on fuel efficiency

Throughout this report the efficiency of the engine will be expressed using the fuel conversion efficiency given by the brake power,  $BP$ , relative to the chemical energy input to the engine:

$$\eta_e = \frac{BP}{\dot{m}_f H_u} \quad (1)$$

where  $\dot{m}_f$  is the fuel mass flow and  $H_u$  is the lower heating value. Brake power is the usable power delivered by the engine:

$$BP = IP - FP \quad (2)$$

Where  $IP$  is the indicated power characterising the work induced on the piston by the pressure in the combustion chamber. The friction power,  $FP$ , is the power lost to friction. Pumping losses will in this report also be accounted for as friction and will be a part of  $FP$ . Another important term characterising the work induced on the piston is the indicated mean effective pressure,  $IMEP$ , which is the indicated work of the engine,  $W_i$ , relative to the displacement volume of the engine,  $V_d$ :

$$IMEP = \frac{W_i}{V_d} \quad (3)$$

Analogous to  $IMEP$ , an important indicator for brake power is the brake mean effective pressure,  $BMEP$ . The correlation between  $IP$ ,  $IMEP$ ,  $BP$  and  $BMEP$  is: [24, equation (1.9) and (1.10)]:

$$IMEP = \frac{60x \cdot IP}{V_d \cdot N} \quad (4)$$

$$BMEP = \frac{60x \cdot BP}{V_d \cdot N} \quad (5)$$

Where  $N$  is the engine rotation speed and  $x$  equals 2 for a four-stroke engine. Throughout this report the indicated mean effective pressure will be used to characterise the indicated work of the engine and the brake mean effective pressure will be used to characterise the load on the engine.

The fuel conversion efficiency can be expressed as a product of the indicated efficiency,  $\eta_i$  and the mechanical efficiency  $\eta_m$ .

$$\eta_e = \eta_i \cdot \eta_m \quad (6)$$

The mechanical efficiency characterises the relationship between brake power and indicated power:

$$\eta_m = \frac{BP}{IP} = \frac{IP - FP}{IP} \quad (7)$$

This is important to note because it shows that  $\eta_m$  and ultimately  $\eta_e$  will, all other things being equal, always be highest when the engine is producing its maximum output - for example, if more air is put into the engine, the fuel conversion efficiency will be higher because of the increased brake power which makes the friction power a smaller fraction of the indicated power.

Considering  $\eta_e$ , the mixture composition is of crucial importance because it dictates the development of the combustion process. A convenient indicator for the mixture composition is the excess air ratio,  $\lambda$  defined as:

$$\lambda \equiv \frac{FA_s}{FA} \quad (8)$$

where  $FA$  is the fuel-air mass ratio  $\equiv \frac{\text{fuelmass}}{\text{airmass}}$  and  $FA_s$  is the stoichiometric fuel-air mass ratio - the chemically correct ratio for oxidation of all the fuel with no oxygen from the air being left in the combustion products.

The excess air ratio's effect on  $\eta_e$  and its effect on the indicated mean effective pressure (IMEP) can be seen on figure 2. Even though there is enough oxygen to burn all of the fuel

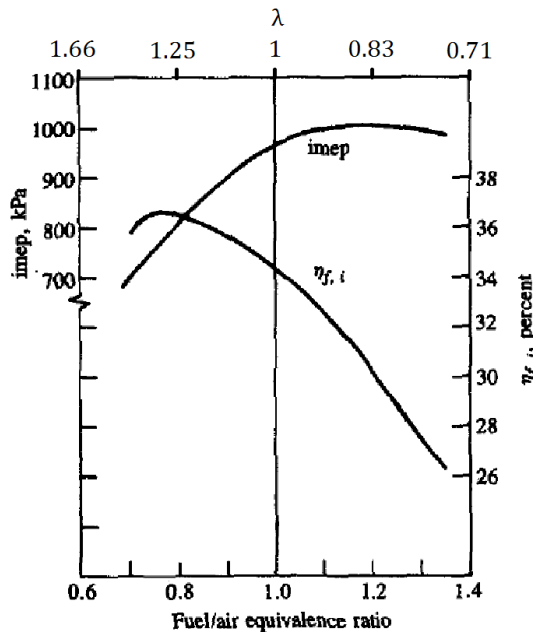


Figure 2:  $\eta_e$  and IMEP as a function of  $\lambda$  for a six-cylinder spark-ignition (SI) engine running with wide open throttle (WOT) and 1200 revolutions per minute (RPM). The graph is taken from [21] and the equivalence ratio has been converted to excess air ratio by the author of this paper.

at  $\lambda = 1.0$  the efficiency is normally not highest at the stoichiometric fuel-air ratio. This is because the fuel and air are not mixed perfectly resulting in a lack of oxygen locally. This local shortage is decreased with increasing  $\lambda$  which combined with lower combustion temperatures at higher  $\lambda$  makes  $\eta_e$  increase. The increase in  $\eta_e$  with increasing  $\lambda$  is however limited by decreasing flame speed at increasing excess air ratio. Also, as seen on figure 2 the induced power decreases as  $\lambda$  increases, making engine friction losses a bigger fraction of *IMEP*. All in all, the above factors make the fuel conversion efficiency peak at a  $\lambda$ -value slightly above 1.0. If  $\lambda$  is below 1.0, the fuel-air ratio is lower than the stoichiometric fuel-air ratio and a fraction of the fuel will stay unburned and will be wasted resulting in a lower fuel conversion efficiency. However, the high temperatures of combustion makes CO<sub>2</sub> and H<sub>2</sub>O dissociate, making more O<sub>2</sub> available for combustion, resulting in a peak of *IMEP* at a  $\lambda$ -value slightly lower than 1.0.

The engine of the DTU ecocar (which is the relevant engine for this report) is a one-cylinder four-stroke 50 cm<sup>3</sup> SI moped engine with fuel injection running on ethanol. The fuel conversion efficiency for this particular engine as a function of  $\lambda$  and spark timing can be seen on figure 3. As seen on the figure, the efficiency follows the same trend as described above. The efficiency peaks around  $\lambda = 1.1$  thus this will be the target value when trying to control the mixture composition. It can be seen that there is not much difference in efficiency for  $\lambda = 1.1$  and 1.2 when spark timing is optimized. However, if the spark timing is set to  $\lambda = 1.1$  (35 CAD for 6000 RPM), the efficiency will be significantly lower if  $\lambda$  turns out to be 1.2 instead - from 30.5% at  $\lambda = 1.1$  to 29.0% at  $\lambda = 1.2$ . Therefore, in practice, there will be a big difference in efficiency for  $\lambda = 1.1$  and 1.2 when the spark timing is set to  $\lambda = 1.1$  and therefore an excess air ratio of 1.2 should be avoided. When comparing  $\lambda = 1.0$  and  $\lambda = 1.2$ ; even though the peak in efficiency is lower for  $\lambda = 1.0$ , this value gives a higher efficiency if spark timing is set accordingly to  $\lambda = 1.1$  - from 30.5% at  $\lambda = 1.1$  to 29.9% at  $\lambda = 1.0$ . It is however important that  $\lambda$  will not fall below 1.0 because this will inevitably result in wasted fuel.

According to the above discussion, the excess air ratio has a strong influence on the fuel conversion efficiency which underlines the relevance of focusing on controlling the excess air ratio when trying to develop more energy efficient vehicles. Using the results from figure 3 it is found that the fuel conversion efficiency for this specific engine peaks at  $\lambda = 1.1$ . There is a minor decrease in efficiency from  $\lambda = 1.1$  to 1.0. When  $\lambda$  reaches 1.2 the change in conversion efficiency is starting to become noticeable. The desirable interval for the  $\lambda$ -value is therefore between 1.0 and 1.1 and most importantly it is crucial that the excess air ratio is kept above 1.0 and does not exceed 1.2.

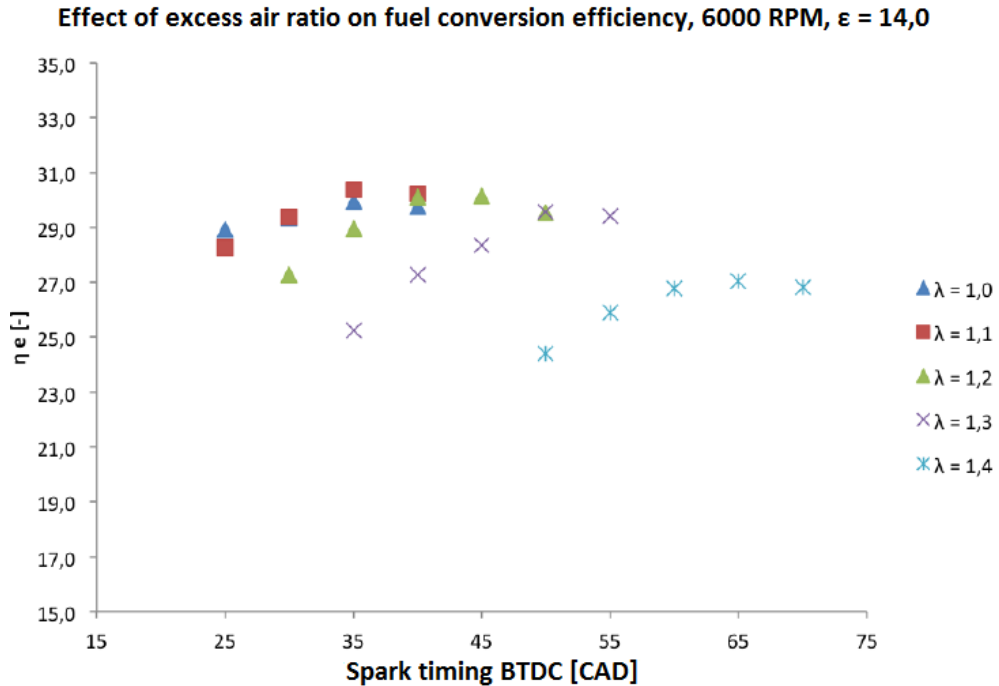


Figure 3:  $\eta_e$  and as a function of  $\lambda$  and spark timing for the ecocar engine running with WOT and 6000 RPM. BTDC means 'Before Top Dead Center', CAD stands for 'Crank Angle Degrees' and  $\varepsilon$  is the compression ratio. The graph is taken from [18] with permission from the owners and the text has been translated to English by the author of this paper.

It should be noted that energy efficiency is not the only argument for the relevance of  $\lambda$ -control. The concentration of various combustion products are also dependant on  $\lambda$ , thus emissions can be reduced by control of the fuel/air ratio. For example, the three-way catalytic converter (TWC) is only fully effective in a very narrow interval of the excess air ratio. See figure 4 where it is seen that the conversion efficiency for all of the three target emission components (nitrogen oxides, hydrocarbons and carbon monoxide) are only high around  $\lambda = 1.00$ .

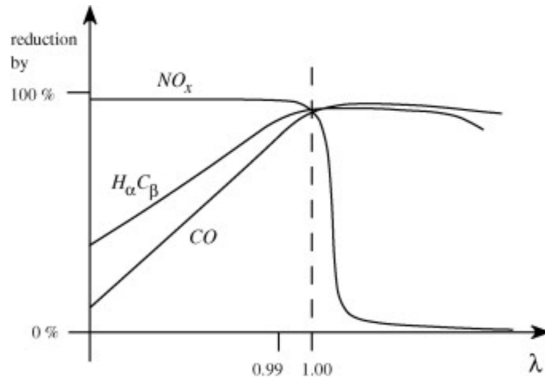


Figure 4: "Conversion efficiency (100% full conversion of harmful species to innocuous ones) of TWC as a function of  $\lambda$ " From [8]

## 5 Performance specification of the control system

The control system addressed in this report has a very specific function; to optimize the fuel efficiency of the DTU ecocar when it is participating in the Shell Eco Marathon. The requirements of the system will thus be based on an analysis of the conditions under which the Shell Eco Marathon is carried out. First of all, the race has a specific set of rules. One of them, article 123 [23], states that the total distance to cover during the race is 16.117 km which must be completed in maximum 39 minutes and that the race has 10 laps where a complete stop is required after each lap. This means that the car must be able to drive at an average speed of approximately 25 km/h including 9 stops. The track consists of standard urban roads with natural bumps and sharp turns.

The car must be driven according to the coast and burn principle so that the engine is only running with WOT. This is to increase *IMEP* so that friction losses will become the smallest possible fraction of the indicated power as mentioned earlier. The number of burns in each lap will be discussed later. The initial performance specification drawn up in this section will be based on the 2012 Shell Eco Marathon where one lap consisted of two burns. The above requirements to the driving strategy result in the velocity curve for the car at the Shell Eco Marathon 2012 as seen on figure 5. It can be seen that in the first burn, the car accelerates from 0 to above 30 km/h (for example as from 1731 s - 1744 s), and in the second burn the car accelerates from 20-25 km/h to around 35-40 km/h (for example as from 1807 s - 1814 s). Other increases in speed shown on the graph are due to hills and wind. A speed of 40 km/h corresponds to an engine speed of around 5000 RPM with the specific gearing used. A closer look at one burn cycle

can be seen on figure 6. In the 2013 version of the DTU ecocar the clutch will have been replaced with a centrifugal clutch, hence the engagement phase will look slightly different. It can be seen that the first burn takes around 10 seconds, taking into account that there is no burning when the gear is changed from first to second. The second burn lasts for a little less than 10 seconds.

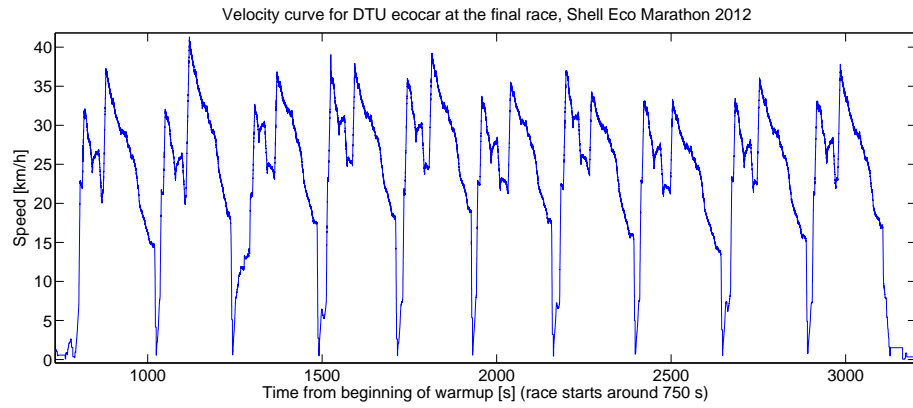


Figure 5: Speed of DTU ecocar as a function of time during final attempt at the Shell Eco Marathon 2012

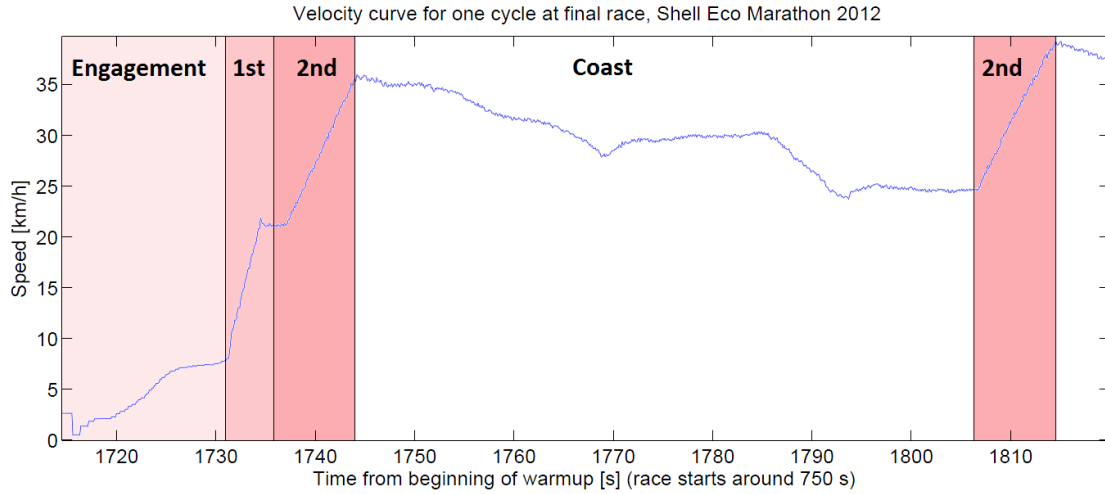


Figure 6: Speed of DTU ecocar as a function of time during one burn cycle of the final attempt at the Shell Eco Marathon 2012. Engagement is before the clutch is released, 1st denotes first gear, 2nd denotes second gear and coast is when the engine is off.

Because of the coast and burn tactic the  $\lambda$ -control problem is of a more transient character, see for example figures 5 and 6. During the race the engine is at no time running at constant speed but will accelerate making parameters such as friction power and the air mass flow into the engine change constantly. This requires a control system with a very low response time which creates a demand to the applied sensors of the control system to react rapidly. It is however still important that the sensors do not decrease the fuel conversion efficiency of the engine in other ways, for example; by increasing the weight of the car or by increasing the pumping losses of the engine.

As seen on figure 6, the engine is driven mostly in 2nd gear. The main focus of the control system will therefore be the  $\lambda$ -value in 2nd gear while the  $\lambda$ -value in 1st gear will be of less importance. On figure 6 it is also seen that the engine is working under very transient conditions in 1st gear which means that it will be a more difficult task to design the control system for 1st gear than for 2nd gear.

### 5.1 Transient problems concerning $\lambda$ control

To design a proper system for transient  $\lambda$  control one has to be aware of certain phenomena that would not create problems under steady-state engine operation, yet will create problems under transient operation. In this section, five phenomena that can create problems under transient engine operation will be discussed. These are the wall-wetting phenomenon, manifold filling phenomenon, engine pumping fluctuations, poor sensor response and time delays.

#### Wall-wetting phenomenon

When fuel is injected into the intake manifold some of the fuel will be deposited on the manifold walls and the intake valves. Afterwards, this layer of fuel will evaporate with a delay and a time constant, hence it will not enter the cylinder immediately and thereby not being immediately available for combustion [24, page 296].

#### Manifold filling phenomenon

Under transient operation the pressure and temperature in the manifold will change due to the filling and emptying of the intake manifold volume. For example; the throttle position is changing (not relevant for the ecocar) or the car accelerates increasing the air mass flow through the manifold. Because of these changes the flow into the manifold is different than the flow out of the manifold when the engine is not operated under steady-state conditions [24, 300].

## Pumping fluctuations

Pumping fluctuations make the volumetric efficiency of the engine vary at different engine speeds. The volumetric efficiency,  $\eta_v$ , is the air mass flow into the engine relative to the potential air mass flow into the engine [24, eq. (1.35)];  $\eta_v \equiv \frac{\dot{m}_{air}}{\dot{m}_{air,ideal}} = \frac{\dot{m}_{air}}{\frac{\rho_{in}V_{in}}{60s}}$ . The periodic motion of valves and piston makes the flow through the engine oscillate creating pressure pulsations travelling through the engine. The pulsations are approximately travelling at the speed of sound. The oscillation frequency is dependant on the length that the pulsations have to travel, thereby dependant on the length of the intake pipe and the exhaust pipe. During the intake and exhaust phase the piston works as a pump. This periodic pumping work creates a forced response to the oscillations. When the frequency of this forced response is equal to the frequency of the oscillations, resonance occurs and the sonic pressure pulsations supports the piston pumping work, significantly increasing the mass of fuel-air mixture input to the engine, thereby increasing *IMEP*. Therefore, the volumetric efficiency changes dependant on whether the oscillations from the pressure pulsations support or work against the piston, thus the volumetric efficiency is dependant on the engine speed. This dependency can be expected to be strong in the ecocar because the engine consists of only one cylinder in contrast to a multi-cylindrical engine where pumping fluctuations of the different cylinders tend to average out.

## Time delays

In the engine, the fuel is injected into the manifold, mixed with the air, and led into the cylinder where it is burned. It is the responsibility of the control system that exactly the right amount of fuel is available in the combustion chamber when the combustion begins. The fuel is not instantly available for combustion but is dependant on various time delays which will be stated below. These are defined analogue to the definition in [4].

- *Computation duration:* The time it takes the engine control unit to calculate all values necessary for proceeding to the next step in the control strategy. The ECU of the ecocar consist of different modules. The module which is taking care of all time-critical calculations is a *field programmable gate array* (FPGA). With this module the computation duration is found to be below 20  $\mu s$  and is therefore too low to be significant in the overall time delay.
- *Injection duration:* It takes the nozzle a certain time to inject the required amount of fuel into the manifold. As it will be shown in the experimental section, the injection time is between 5 and 7 ms.
- *Injection timing:* To obtain the best mixture of fuel and air it is important that as much fuel as possible is evaporated when entering the combustion chamber. By injecting the fuel

onto closed valves the high temperature of the valves and manifold walls helps to evaporate the fuel. On the other hand, if the fuel is injected onto open valves, one can avoid flushing unburned fuel directly through the combustion chamber and out the exhaust manifold; which is what can happen during the phase where both intake and outtake valve is open. In [4] it is however stated that more hydrocarbons are emitted when the fuel is injected on open valves. An increase in hydrocarbon emission means that more fuel is wasted, hence it is important that the fuel is injected onto closed valves. To ensure that as much fuel as possible is evaporated the fuel must be injected as early as possible which is just after the intake valve has closed. This means that there will be around 360 crank angles degrees from the time the fuel has been injected until it is fed into the combustion chamber. This equals  $\frac{360 \text{ CAD} \cdot 60 \text{ sec/min}}{360 \text{ CAD/rev} \cdot N} = 60 \text{ ms at 1000 RPM and 12 ms at 5000 RPM.}$

- *Transport delay:* This delay is the time it takes the fuel air mixture to travel through the combustion chamber. This delay is only relevant for the  $\lambda$ -sensor because this sensor is placed in the exhaust, hence the fuel-air mixture has to go through the combustion chamber and out the exhaust before the  $\lambda$ -sensor is able to measure whether or not the fuel-air mixture is of the right ratio.

The travel through the combustion chamber starts when the intake valves open and the fuel-air mixture is sucked into the chamber which takes half a revolution. Afterwards, the mixture is compressed, ignited, and expanded (one whole revolution) which means that it takes around  $1\frac{1}{2}$  revolutions before the first burned fuel-air mixture reaches the exhaust manifold. This is equivalent to 90 ms at 1000 RPM and 18 ms at 5000 RPM. The  $\lambda$ -sensor is placed around 100 mm downstream of the outtake valve which means that it will take even longer before the mixture reaches this sensor.

Summed up this means that the time delay for sensors placed in the inlet manifold will be:

Best case:  $(5+12)=17 \text{ ms}$

Worst case:  $(7+60)=67 \text{ ms}$

The time delay for the  $\lambda$ -sensor placed in the exhaust manifold will be:

Best case:  $(5+12+18)=35 \text{ ms}$

Worst case:  $(7+60+90)=157 \text{ ms (or more)}$

### Poor sensor response

Another time delay is the response time of the sensor used. This response is just as essential as the above mentioned delays. Therefore the response time of all relevant sensors must be identi-

fied which will be done in section 6

## 5.2 Problems concerning the application of the control system in a real car in contrast to a test stand

Another important requirement for the control system is its reliability. The ecocar is fully dependant on the control system thus it must work at all times, especially during the race when no adjustments can be made to the system. If the control system only had to work in a test stand, it would be easy to correct defects, apply modifications and conduct debugging. This is not the case with the ecocar, hence the value of simplicity is not to be underestimated and precautions that make the system robust and reliable are crucial. The robustness, simplicity and consistency of the control system including sensors will therefore be of high importance because of the systems employment and importance in a complex machine which (in contrast to an experimental setup) has to work reliably in practice on real roads, in different kinds of weather, and without the influence of anybody else other than the driver.

In conclusion, the key requirements to the control system are:

- The control system must respond well under transient conditions. This includes compensating for various phenomena that are present only during transient engine operation.
- The robustness, simplicity and consistency of the system is crucial
- From previous section it is found that the control system should keep the excess air ratio between 1.0 and 1.2

## 6 Sensors

Well-functioning sensors are essential for the control system to fulfil the required specifications. Because of the transient characteristics of the problem addressed in this report the response times of the relevant sensors are of primary importance. In the following, the most relevant sensors will be presented and discussed.

### 6.1 Lambda-sensor

There are two types of  $\lambda$ -sensors in common use called narrowband oxygen sensors (NBO<sub>2</sub>) and wideband oxygen sensors (WBO<sub>2</sub>). NBO<sub>2</sub> can only measure if  $\lambda$  is more or less than 1, while the WBO<sub>2</sub> (extended version of the NBO<sub>2</sub>) is able to measure the actual value of  $\lambda$  in the entire range of engine operation.

The concentrations of many combustion products are dependent on the excess air ratio. A NBO<sub>2</sub> utilises this by comparing the oxygen-concentration in the exhaust gas to its concentration in atmospheric air. A schematic representation of the NBO<sub>2</sub> can be seen on figure 7. The sensor

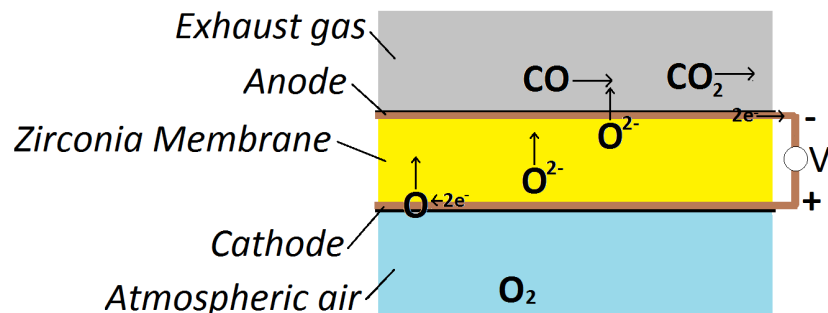


Figure 7: Narrowband oxygen sensor

consists of a heated ceramic membrane separating atmospheric air and exhaust gas. When there is a lack of oxygen in the exhaust gas, oxygen-ions diffuse from atmospheric air through the membrane to react with CO, hydrogen or unburned hydrocarbons. This diffusion is very temperature dependant and is only possible when the membrane is above 300 °C [13]. When the oxygen-ions react with the exhaust gas components, electrons are released creating a voltage-signal. If oxygen is already present in the exhaust gas there will be no diffusion through the membrane, hence no voltage-signal. If the condition in the exhaust gas is stoichiometric there will be a voltage-signal in between the high output and no output as seen on figure 8

The WBO<sub>2</sub> is built up the same way as an NBO<sub>2</sub>-sensor but has an extra membrane and a

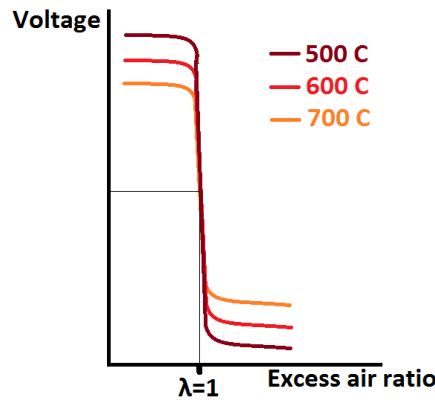


Figure 8: Sketch of the output of a narrowband oxygen sensor at different temperatures.

measurement chamber as seen on figure 9. The extra membrane, called the pump cell, has the

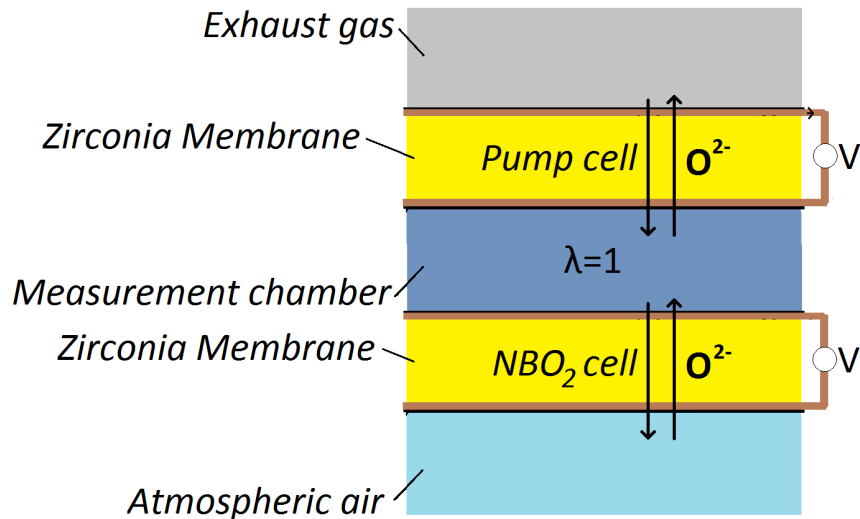


Figure 9: Wideband oxygen sensor

opposite function of the first membrane - instead of detecting a voltage signal it creates a voltage that makes oxygen diffuse in a certain direction. This way oxygen-ions are pumped in and out of the measurement chamber to maintain stoichiometric conditions in the chamber. The quantity of transported ions is dependant on the magnitude of the voltage. When the conditions in the measurement chamber are no longer stoichiometric, the  $\text{NBO}_2$  cell detects the change and the pump cell recreates stoichiometric conditions. The voltage needed for the pump cell to maintain

stoichiometric conditions in the measurement chamber is converted to an output indicating the  $\lambda$ -value of the exhaust gas [7, p. 117].

As previously described, the oxygen-ions also react with unburned hydrocarbons. One should be aware that this means, that both the NBO<sub>2</sub> and WBO<sub>2</sub> are not able to measure the fuel/air ratio of the *burned* components only, nor how well the fuel is burned. The sensors are only able to measure the total fuel/air ratio, unburned components included. In theory, one could lead a completely unburned, stoichiometric fuel/air mixture through the engine and obtain a  $\lambda$ -measurement of 1. The accuracy of a typical WBO<sub>2</sub> is between 1 and 6 % [4].

For the WBO<sub>2</sub> to react on a change in the  $\lambda$ -value of the exhaust gas, oxygen-ions must first travel across one membrane after which a signal is detected resulting in oxygen-ions being pumped across a second membrane. This results in a response time of WBO<sub>2</sub> in the range of 50-100 ms [4, table 1] [11] [20].

This, combined with the earlier mentioned time delay, results in a worst case response time of the WBO<sub>2</sub> of above; 100 ms + 157 ms = 275 ms. Because of the accuracy of the sensor, the  $\lambda$ -value used for control will also have to be an average of many measurements. All in all, this means that closed-loop  $\lambda$  control is not directly possible under transient conditions. This is confirmed in [25]. Here, the throttle angle was changed resulting in transient conditions. Afterwards the throttle angle was kept constant at its new position thereby making the flow rate return to a steady state. Thereby this test contained a step function. However, it still took up to 6 seconds for the fuel-air ratio to return to its desired value. A settle time of more than 6 seconds is completely unacceptable when the engine is only turned on for about 10 seconds at a time.

Because of the high response time of the WBO<sub>2</sub> this project will not deal with any control systems using ordinary closed-loop  $\lambda$  control. Instead, experiments will be carried out with a simplified closed-loop  $\lambda$  control system which is adapted to the performance specifications.

Finally, it must be noted that it is stated in [4, table 1] that the WBO<sub>2</sub>-sensor is subject to drift making frequent calibration important. - According to the owner's manual of the WBO<sub>2</sub> used in the ecocar, calibration should be performed every 2-3 days if the sensors are used for dynamometer tests [14].

## 6.2 Flow sensors

In modern cars a flow sensor is used to determine the air mass flow which is needed to determine the fuel-air ratio and the engine load.

In this report two different flow sensors will be discussed; the hot wire Mass Air Flow (MAF) sensor and a laminar flow meter.

### 6.2.1 Hot wire MAF sensor

The hot wire MAF sensor is the most common sensor used to measure the air flow in real cars [4] [9]. This sensor works by placing an electrically heated wire in the inlet manifold. The air flow through the inlet manifold cools the wire. Because the electrical resistance of the wire is temperature dependant, the flow cooling the wire can then be detected in the current to the hot wire.

Advantages in using this sensor:

- Takes up little space.
- Low cost compared to a laminar flow meter.
- Does not restrict the air flow much compared to a laminar flow meter.
- Is not dependant on other sensors in order to measure the mass air flow.

Disadvantages in using this sensor:

- Slow response time - between 50 and 500 ms [4].
- Unidirectional - not able to measure back-flow.
- It is inaccurate during fast transients [4].
- Over time, oil and dirt will get deposited on the hot wire making it inaccurate [9].

That this sensor is unidirectional is critical when working with a one-cylinder engine because the earlier mentioned large pressure pulsations will create large back-flows. This problem can however be eliminated, for example by using two hot wire sensors each with a back-flow preventer placed in the opposite direction of the other.

That this sensor is inaccurate during transients is contrary to the performance specification and is a strong argument for not using this sensor in the control system. Also it is a problem that the response time will in worst case be 500 ms plus the 67 ms time delay earlier mentioned. These are the main reasons for not choosing this sensor for the experiments carried out in this project.

### 6.2.2 Laminar flow meter

A laminar flow meter measures the pressure difference between two points in the air stream as seen on figure 10. To make the flow laminar, the casing contains a bundle of capillary tubes. If the air flow is laminar, the pressure difference across the bundle is proportional to the air volume flow as seen from equation (7.59) in [6]:

$$\dot{V}_{air} = \frac{\pi D^4}{128\mu L} \Delta p \quad (9)$$

where

$\dot{V}_{air}$  is the volume flow through one capillary,  
 $D$  is the hydraulic diameter of the capillary,  
 $\mu$  is the fluid dynamic viscosity,  
 $L$  is the tube length between the pressure tabs,  
 $\Delta p$  is the pressure difference across the capillary bundle.

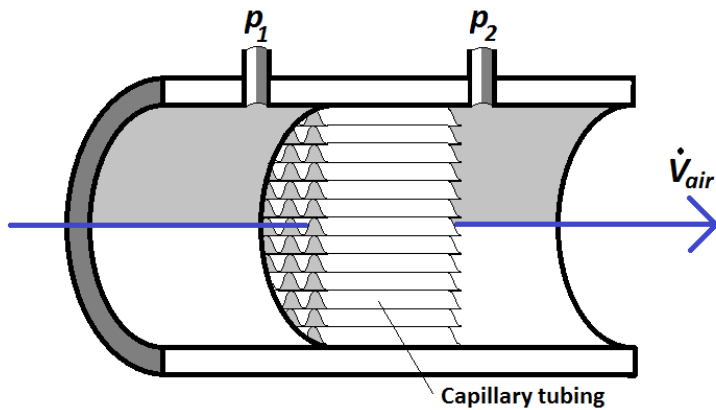


Figure 10: Laminar flow element. Combined with a differential pressure sensor it measures the air volume flow

Advantages in using this sensor:

- Linear relation between pressure drop and the volume flow rate. The capillary tubing makes this relation valid in a very wide range of volume flow.
- "Accurate measure of average flow rates in pulsating flow" [6].
- It is bidirectional, thus well suited for measuring back-flows.

- It has overall acceptable respond time - 16 ms for the laminar flow element [17] and less than 1 ms for the differential pressure sensor [10].

Disadvantages:

- High cost.
- It takes up a lot of space especially because the flow has to be laminar when it meets the first pressure tab. This makes high demands to the geometry of the inlet manifold.
- If the flow meter is used for a dirty gas, it will clog and thus become inaccurate.
- To be able to measure flow, a pressure loss is necessary. This loss will be included in the pumping loss of the engine.
- The measurement is dependent on a temperature sensor and a pressure sensor to convert volume flow to mass flow.

As it is seen, there are very relevant advantages in using this sensor in the ecocar because the flow will probably contain pulsations and back-flow. The transient conditions also require the response time to be low. There is however a serious disadvantage - if the pressure loss is significant the sensor will make the fuel economy worse. The purpose of the sensor is to improve the fuel economy, hence the pressure loss must be very low for the sensor to be useful. Also, the size of the sensor makes it potentially heavy thus it is important that the sensor does not become heavy enough to affect the rolling resistance of the car significantly. The advantages of this sensor do however make it a worthy candidate for fulfilling the given performance specifications, thus experiments will be carried out examining the applicability of this sensor.

### 6.3 Axle encoder

An accurate determination of the piston position at all times is crucial for proper engine control because the position determines injection time, spark timing, engine speed, etc. To measure the position of the piston, a rotary encoder must be placed on either the camshaft or crankshaft axle. The output of the sensor is three different pulses (A- B- and Z-pulse). The pulses change between high and low input when the axle is rotated in relation to the encoder. The A- and B-pulses change with a frequency of 720 pulses per revolution. For both these pulses the rising edge has the same duration as the falling edge as seen on figure 11. There is a phase shift between the two pulses that can be used to very accurately determine the piston position. The Z-pulse has one rising edge per revolution. This rising edge is half the length of the rising edge of the A- and B-pulses [5].

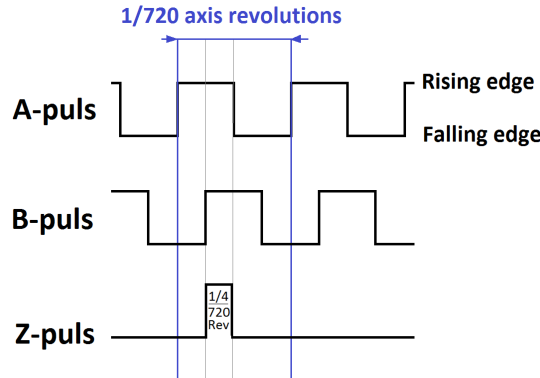


Figure 11: The 3 outputs of an axle encoder. The length of the A- and B-pulses rising edges are  $\frac{1}{720}$  of a revolution while the length of a Z-pulse rising edge is  $\frac{1}{4}$  of a revolution.

The axle encoder used in this project is a SCANCON incremental encoder type SCA50 with a resolution of up to 12500 pulses per revolution and a frequency response of up to 300 kHz [5]. In the 2013 DTU ecocar the encoder was placed on the camshaft axle. In 2012 it was placed on the crankshaft axle. The camshaft axle rotates with half the rotational speed of the crankshaft axle, thus when placing the encoder on the camshaft axle there will be 1 A-pulse for each CAD and 1 Z-pulse for each cycle.

## 7 Types of excess air ratio control systems

In this section different approaches to control of  $\lambda$  will be presented and discussed in relation to the requirement specification. Initially, the strategy used in today's auto-mobile industry will be presented followed by the strategy used at the Shell Eco Marathon 2012. Finally a new and alternative approach will be presented.

### 7.1 Conventional $\lambda$ -control

In modern cars the fuel injection length is determined by the engine control unit (ECU) on the basis of a so called engine map which is a multidimensional lookup table [9], [15], [16]. All values from this table have been found by having the engine thoroughly measured on a dynamometer. The backbone of the engine map is a table having fuel consumption as a function of engine load and engine speed. An example can be seen on figure 12.

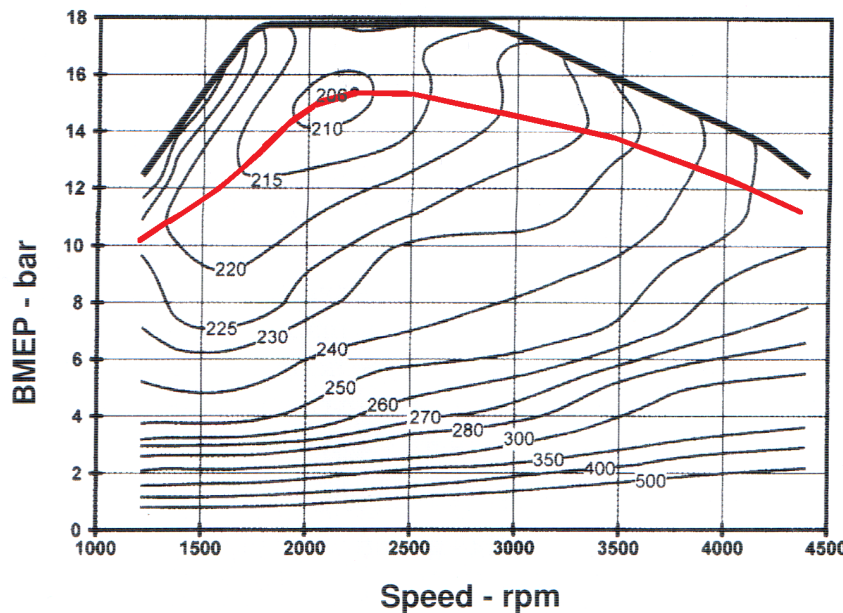


Figure 12: Example of the backbone of an engine map having the *BSFC* as a function of engine speed and *BMEP*. The contours indicate *BSFC*. The red line is added by the author of this paper and approximates the load curve at WOT and a fuel-air ratio corresponding to the lowest *BSFC*. The specific engine is a Mercedes-Benz, four-stroke three-cylinder turbocharged diesel engine. The graph is taken from [24, page 48]

On figure 12 the fuel consumption is given using brake specific fuel consumption defined as:

$BSFC \equiv \frac{\dot{m}_f}{BP}$ . The engine load is represented using  $BMEP$  which can be calculated using [24, equation (1.32)]:

$$BMEP = \eta_v \cdot \rho_{in} \cdot FA \cdot H_u \cdot \eta_e \quad (10)$$

$\eta_v$  is dependent on multiple parameters such as engine speed and absolute manifold pressure,  $p_{in}$  and is therefore also found using the lookup tables [9], [15].

$\rho_{in}$  is the air density of the air used for combustion. It is found by measuring  $p_{in}$  and the inlet manifold temperature,  $T_{in}$ , and then applying the ideal gas law:

$$\rho_{in} = \frac{p_{in}}{T_{in} \cdot R_{air}} \quad (11)$$

Where  $R_{air} = 287 \frac{\text{J}}{\text{kg} \cdot \text{K}}$ . This; however, gives the inlet manifold air density which is only equal to the cylinder air density at a certain operating point. When the intake valve is closed, there is no air flow and the inlet manifold pressure is approximately on average atmospheric pressure. When the intake valve is open the air flow makes the inlet manifold pressure lower than the relevant pressure. Therefore, when using a pressure sensor placed in the inlet manifold, the pressure must be measured only when the intake valve is open and the piston is just around bottom dead center (BDC) and there is no longer any air flow to decrease the pressure. This gives the best estimate of the cylinder air density.

The fuel-air ratio,  $FA$  is found by calculating the mass of injected fuel from the injection length and by measuring the air flow, typically using a hot wire MAF sensor.

The mechanical efficiency,  $\eta_m$  is a function of various parameters such as excess air ratio as earlier mentioned and is also found using the engine map [9], [15].

When  $BMEP$  is calculated and  $BSFC$  is found using the engine map, the appropriate fuel mass flow can be found using [24, equation (1.41)]:

$$\dot{m}_f = BSFC \cdot BP = BSFC \cdot \frac{BMEP \cdot V_d \cdot N}{60x} \quad (12)$$

The fuel mass flow can easily be converted to injection length using the engine speed and the characteristic relation between fuel mass flow and injection length for the specific injection nozzle used. For the nozzle used in the DTU ecocar, which has a 4 bar pressure in the fuel tank and a voltage supply to the nozzle equal to 12 V, the correlation between injected fuel mass and injection length is [12]:

$$m_f = 0.0008138 \frac{\text{mg}}{\mu\text{s}} \cdot \text{injection length} - 0.6695 \text{ mg} \quad (13)$$

Where the correlation between  $\dot{m}_f$  and  $m_f$  is:

$$\dot{m}_f = \dot{m}_f \cdot \frac{60 \text{ sek/min} \cdot 2 \frac{\text{revolutions}}{\text{injection}}}{N} \cdot 1000 \text{ mg/g} \quad (14)$$

The injection length which has been calculated is however only the *base* injection length. This value is then corrected by numerous calibration factors derived from the output of various sensors. Using lookup tables as seen on table 1 the ECU finds the calibration factors for the current sensor outputs. An example of a calibration factor is the coolant calibration factor which adjusts the injection length relative to the coolant temperature. Another example is a  $\lambda$  calibration factor which adjusts the injection length relative to the error in the excess air ratio in the exhaust. In practice, the ECU may use more than 100 calibration factors [15]. The final injection length is then found as the product of the base injection length and the relevant calibration factors:

Final injection length = Base injection length  $\times$  Coolant calibration factor  $\times \lambda$  calibration factor  $\times$  calibration factor 3 ...  $\times$  calibration factor  $n$ .

Coolant temperature [°C]	Coolant calibration factor
0	1.2
10	1.2
20	1.1
30	1.1
40	1.0
50	1.0

Excess air ratio	$\lambda$ calibration factor
0.8	0.9
0.9	1
1.0	1
1.1	1
1.2	1.1
1.3	1.1

Table 1: Hypothetical examples of lookup tables for adjusting the final injection length

The backbone of the engine map used to determine the base injection length is an example of feed forward control because the injection length is pre-defined without responding to the result of the combustion process. The  $\lambda$  calibration factor is an example of closed-loop feedback control because this factor adjusts the injection length based on the output of the combustion process. During acceleration there is no closed-loop control because the feedback response time is too slow to function during transients. Thus in modern cars there is only closed-loop  $\lambda$  control during steady-state operation while the control system is entirely based on feed forward control during acceleration [9] [16]. This means that conventional  $\lambda$  control is most accurate under steady-state conditions.

### 7.1.1 Conventional $\lambda$ control in relation to the requirement specification

As it is seen in the requirement specification (section 5), during the Shell Eco Marathon the engine will in practice only be used under transient conditions. This means that if a conventional  $\lambda$  control system is used it will be entirely feed forward controlled which might create inaccuracies resulting in unacceptable variations in  $\lambda$ . There are however also advantages in using conventional  $\lambda$  control. During the race the engine will only operate at WOT and the fuel-air ratio will sought to be kept constant at a ratio corresponding to  $\lambda = 1.1$ . This means that the engine map will be significantly simplified. If it is assumed that a  $\lambda$ -value at 1.1 corresponds to the lowest *BSFC*, the backbone of the engine map will be simplified as exemplified by the red line on figure 12 because the constant fuel-air ratio combined with an engine only running at WOT results in a constant load at constant engine speed. Because of the constant load it is no longer necessary to calculate the base injection length as a function of *BMEP*. Instead; one can, using dynamometer tests, create a fuel map where the base injection length is found directly from the engine speed. A sketch of this is seen on figure 13.

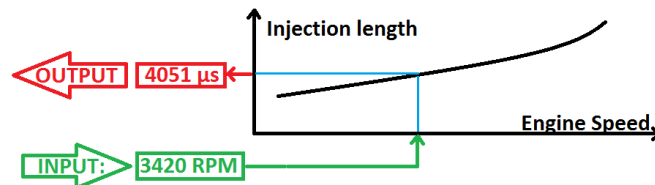


Figure 13: Sketch of the backbone of an engine map for full load and constant fuel-air ratio

The advantage of this base engine map is that it is a very simple method for finding the injection length. Also the injection length is only dependant on one very reliable sensor - the axle encoder. The base engine map does not take variations in the engine and the environment into account. However, the complexity and accuracy of the control system can be increased by adding calibration factors if required.

The main problem with engine mapping is that it is a very time consuming process. Even a simple engine map like the one sketched on figure 13 calls for numerous dynamometer tests. Also when it comes to the ecocar there is currently no dynamometer available that properly simulates real road acceleration, thus the car would have to go through numerous outdoor tests which is difficult when no track is available and thus the ecocar has to be tested on a real road among real cars. Another important aspect of the DTU ecocar is that it is constantly being modified

and improved making it temporarily unavailable for testing. Also, all modifications affecting the fuel economy will ultimately affect the engine map putting it in a potential risk of recalibration.

## 7.2 Control using the speed-density function

Instead of basing the determination of injection lengths upon lookup tables, one can rely entirely on algebraic equations. This is the idea behind the control system of the 2012 DTU ecocar. Here, the air mass flow is found using the speed-density function [3]:

$$\dot{m}_{air} = N \cdot \frac{V_d}{60x} \cdot \rho_{in} \cdot \eta_v \quad (15)$$

When the air mass flow is found, one can calculate the fuel mass flow using that  $\lambda = \frac{FA_s}{FA}$  and that  $FA_s \text{ ethanol} = 0.111$

The cylinder air density,  $\rho_{in}$  is found through  $T_{in}$  and  $p_{in}$  using the ideal gas law as earlier mentioned. The volumetric efficiency,  $\eta_v$  is estimated to have a constant value of 0.85. In [3] the author, C. F. Aquino points out that errors must be expected when using the speed-density function instead of actually measuring the air mass flow. In this case the estimation of  $\eta_v$  will contribute to this error because the volumetric efficiency cannot be expected to be constant. To compensate for the error, three calibration factors are used - a pressure calibration factor,  $k_{pressure}$  initially adjusting the pressure input, a temperature calibration factor,  $k_{temperature}$  initially adjusting the temperature input and a final calibration factor,  $k_{final}$  which adjusts the calculated injection length. These factors are found by testing the car on a dynamometer. An overall diagram of this control system can be seen on figure 14.



Figure 14: Diagram for a control system using the speed-density function. Three calibration factors called  $k_{temperature}$ ,  $k_{pressure}$  and  $k_{final}$  are used to compensate for errors.

### 7.2.1 Speed-density control in relation to the requirement specification

It is required of the control system to be able to work outdoors; therefore resulting in the air density varying with temperature and pressure. The advantage of this system is that by measuring the temperature and pressure the system will immediately adjust to the surroundings in

contrast to a system based on a lookup table created on a dynamometer in a different environment than the actual racing environment.

The disadvantage of the system is that it, in addition to the engine speed sensor, relies completely on a temperature and a pressure sensor which both must react fast and accurately. Also, as mentioned earlier an error is expected and it is uncertain if the calibration factors are sufficient compensation. To determine the error of this system one can evaluate the results of the Shell Eco Marathon 2012 where the system was applied. This is done in the results section (page 35).

### 7.3 Transient closed-loop $\lambda$ control

By now various arguments against closed-loop  $\lambda$  control of the ecocar have been mentioned:

- The engine will only run under transient conditions making engine parameters change constantly.
- According to the requirement specification the engine will run in intervals of around 10 seconds, hence the control system has very few seconds to adjust to changing operating conditions.
- The response time of a WBO<sub>2</sub>-sensor is slow - between 50-100 ms (excluding the time delay, which in worst case is above an additional 157 ms).
- In real cars there is no closed-loop  $\lambda$ -control during transients because of the time delay mentioned above.

It is however worth mentioning that the DTU ecocar has a much more specific purpose than a real car which has to be very versatile to meet the user's demands. From the requirement specification it can be seen that all laps at the Shell Eco Marathon are very much alike in regard to the velocity curve. This means that an evaluation of  $\lambda$ -measurements from one lap can be used to control  $\lambda$  in the following lap. The most simple version of this is to take the average of all  $\lambda$ -measurements from one lap and use this for adjustment in the next lap. Ideally, the result would look something like the top sketch on figure 15 where a  $\lambda$ -time curve can be seen for two laps. This simplified version of closed-loop  $\lambda$  control is only able to adjust the whole  $\lambda$ -curve up and down and is therefore more useful the more the  $\lambda$ -time curve for a lap is horizontal. Therefore, this closed-loop control system is dependant on a basic feed forward control system that ensures that the  $\lambda$ -time curve is a straight, horizontal curve. It is not important that the feed forward control system results in  $\lambda = 1.1$  constantly in time, as long as the result is any constant  $\lambda$ -value in time that the closed-loop system afterwards can adjust up and down. An

example of a bad feed forward system combined with a closed-loop system can be seen on the bottom sketch on figure 15. Here, the closed loop system is not able to compensate for the feed forward error.

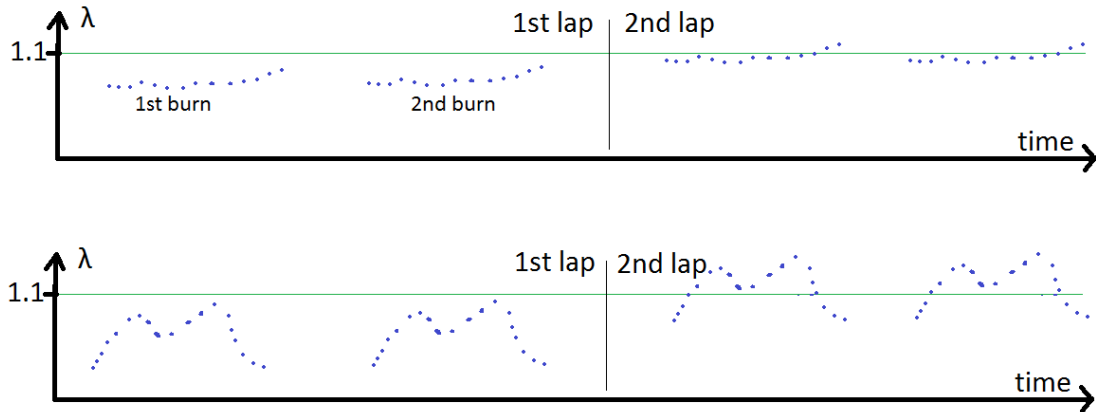


Figure 15: A simplified version of closed-loop  $\lambda$  control where the calibration factor is adjusted after each lap. The top sketch exemplifies the effect of this adjustment if the basic feed forward control system works appropriately. The bottom sketch shows the effect of the adjustment if the basic feed forward control is poor.

### 7.3.1 Transient closed-loop $\lambda$ control in relation to the requirement specification

Even though this version of closed-loop  $\lambda$  control is extremely simple it can be very useful because it can make adjustments for all parameters that do not change considerably from lap to lap. These are parameters such as atmospheric temperature and pressure, humidity and engine temperature. It is however, as mentioned earlier important to have a dependable feed forward control system as a foundation, if this closed-loop system is to function properly. An obvious feed forward system to use is the simple engine map from figure 13 because this system is what forms the backbone of control systems in real cars and it is functioning well under transient conditions. As mentioned earlier the weakness of this feed forward system is that it does not take variations in the engine and the environment into account. This is however exactly what the simple closed loop system is able to compensate for. It must also be noted that the combination of simple closed loop control and a simple engine map only relies on two sensors - the  $\lambda$ -sensor and the axle encoder.

As mentioned earlier, it is very resource-demanding to make even a simple engine map, especially for the ecocar because it is constantly being modified and no proper dynamometer or outdoor track is available for testing. Therefore, a feed forward solution avoiding these problems will also be proposed. For decades, laminar flow meters have been used in test stands to accurately determine the air mass flow into the engine. They are however not used in real cars because of their price and size. In regard to fuel economy it is also important to be aware of the pressure loss present in a laminar flow meter. Price, size and pressure loss are however parameters that can be minimised by designing a laminar flow meter specifically for its purpose in the ecocar. In this report a solution containing a customised laminar flow element will also be examined. The disadvantage of using a laminar flow meter instead of an engine map is that the control system becomes more complex and relies strongly on more sensors - a laminar flow sensor, a pressure sensor and a temperature sensor.

In conclusion, the advantages of simple closed-loop  $\lambda$  control combined with a simple engine map are that by combining the two they compensate for each other's flaws and the combined systems simplicity makes it reliable. The disadvantage is that it is a complex and comprehensive task to create an accurate engine map. This disadvantage can be eliminated by using a laminar flow meter which instead makes the system more complex thereby jeopardising its reliability and robustness.

## 8 Dynamometer testing of a speed-density function control system

### Purpose

The main purpose of this experiment is to evaluate the functionality of the new ECU program created for the Shell Eco Marathon 2013. This experiment examines if any flaws are to be found in the new program when the car is doing its first WOT acceleration.

The  $\lambda$  control system used in this experiment used the same principle as the one used at the Shell Eco Marathon 2012 which is the speed-density control system described in section 7.2. Therefore the purpose of this experiment is also to evaluate the speed-density control system by testing it in the ecocar.

### Experimental setup

#### General test-preparation of ecocar

Before every dynamometer or outdoor engine test run, air was injected into the pressure tank until the pressure was 5 bar. The fuel valve was opened after it was checked that enough fuel was present in the fuel tank. For dynamometer tests, it was also checked that the left rear tire was sufficiently fastened to the dynamometer and it was checked that the ventilation was turned on and that the suction tube was connected to the exhaust of the car. The atmospheric air temperature and humidity were measured and the atmospheric pressure was taken from the Danish Meteorological Institute at [www.dmi.dk](http://www.dmi.dk).

The car was then warmed up until the the coolant temperature was above 50 °C. This meant around 30 minutes at idle speed.

#### Test procedure of the current experiment

During the test the car was accelerated from idle speed to 16 km/h in first gear at WOT. Then quickly the engine was stopped, the gear was changed to second gear and the engine was started again. The car was then accelerated again.

The injection length was calculated in accordance with the speed-density method described in section 7.2. After warmup, the calibration factors were adjusted until it no longer seemed possible to obtain better  $\lambda$ -values when accelerating the car. Ultimately the calibration factors were set according to the values in table 2.

The  $\lambda$ -sensor used in the ecocar is a Bosch, model LSU4.2. The electronics for this sensor consist of a digital air/fuel ratio gauge of the model; MTX-L by Innovate Motorsports. Before

Calibration factor	Shell Eco Marathon 2012	Experiment 2013
$k_{temperature}$	1	1
$k_{pressure}$	0.860	0.7
$k_{final}$	0.867	1.2

Table 2: Calibration factors for speed-density control at Shell Eco Marathon 2012 and at first test run of the car in 2013. For explanation of calibration factors please see figure 14.

the experiment the MTX-L was calibrated and set to measure  $\lambda$  in the range of 0.5 to 1.5.

All measurements were logged using labview. Data was logged every 100 ms.

The relevant labview code for the speed-density control can be found in appendix G.1.

During the test it was observed that the engine was running undesirably unstable when accelerating. It sounded like sudden negative deviations in engine speed were occurring frequently. Also, when the car reached a certain speed, it was not capable of further acceleration. In the electronics of the car, a LED was flashing whenever a signal was sent to the nozzle to inject fuel. When the car was no longer capable of accelerating, it was observed that this LED was flashing with a lower frequency than usual.

After the experiment the oil in the crankcase was checked. It was concluded, by the looks and smell of the oil, that a large amount of ethanol was present in the oil. The engine was opened up, and all parts were inspected. No signs of defects were present.

## Results

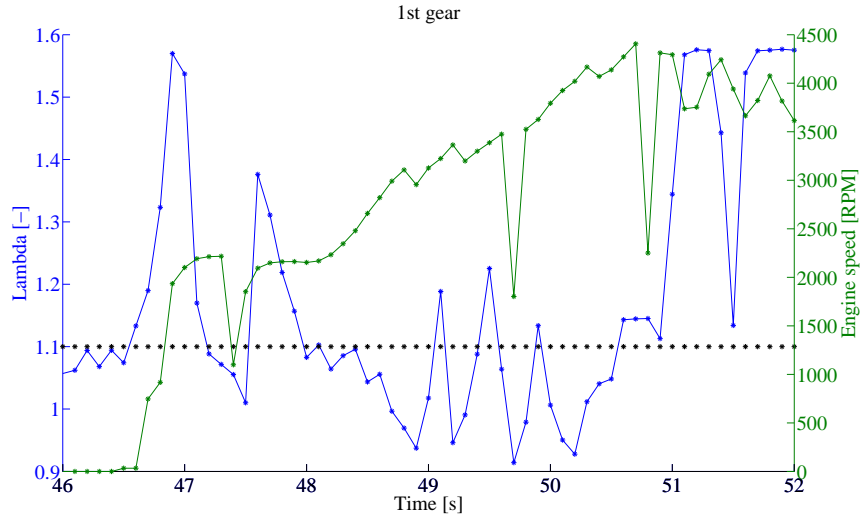


Figure 16: First test of the system in 1st gear. The desired  $\lambda$ -value of 1.1 is marked with black dots.

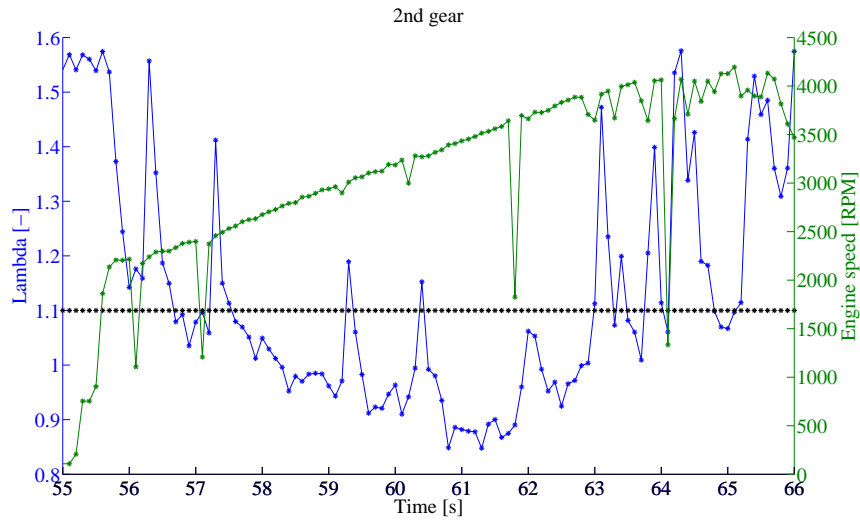


Figure 17: First test of the system in 2nd gear. The desired  $\lambda$ -value of 1.1 is marked with black dots.

## Discussion

On figures 16 and 17 a dynanometer test in first and second gear can be seen. This is the first test where the car was able to run somewhat consistently at WOT without stopping.

The injection length increases continuously from 5870  $\mu\text{s}$  at the beginning of acceleration to 5945  $\mu\text{s}$  at end of acceleration which is equivalent to a injected fuel mass of 4.09 mg to 4.15 mg. In the race in 2012 the engine was run with wasted spark, hence fuel was injected two times per combustion cycle. The injection length in 2012 did not exceed 2415  $\mu\text{s}$  which means that the injected fuel mass for one combustion cycle did not exceed:

$$(0.0008138 \frac{\text{mg}}{\mu\text{s}} \cdot 2415 \mu\text{s} - 0.6695 \text{ mg}) \cdot 2 \frac{\text{inj.}}{\text{cycle}} = \underline{2.6 \text{ mg}} \quad (16)$$

(From equation 13).

In first gear it is seen that  $\lambda$  rises to 1.5 (or higher) when acceleration is initiated. Afterwards it falls to around 1 and increases again to 1.5 before the gear is changed. In second gear the same trend is seen. It is immediately obvious that either the engine or the ECU is not functioning correctly when the amount of injected fuel is 1.4 times higher than in 2012 and the engine still runs, in general, very lean and the car is not able to accelerate above 4000 RPM.

Regarding engine speed it can be seen that there are significant negative fluctuations in speed each followed by a positive fluctuation in  $\lambda$ . When the speed reaches around 4000 RPM the car is no longer able to accelerate. These fluctuations support the observations made during the experiment. On the figure, each measurement is indicated with a point. Many of the fluctuations, especially the big ones, consist of only one measurement. This could lead one to think that the fluctuations are not actually fluctuations but just outliers coming from measurement errors. The fact that the fluctuations were auditorily observed and the fact that it seems like there is a correlation between the fluctuations in  $\lambda$  and engine speed makes it reasonable to conclude that the fluctuations are not just measurement errors. It is important that these fluctuations are eliminated. It is hard to explain why a negative fluctuation in speed creates a positive fluctuation in  $\lambda$ . A possible explanation could be found in that the  $\lambda$ -signal is delayed so that it actually is a positive fluctuation in excess air ratio in the engine that creates a decrease in engine speed. The combusted part of the air/fuel mixture becomes so lean that the mixture cannot ignite making the speed decrease. At around 4000 RPM the combustion becomes so lean that there is not enough brake power to further accelerate the car. An explanation is that there is not injected enough fuel or the fuel is not evaporated and mixed well enough with the air. This reason is supported by the fact that the only major difference between the ECU in this experiment and the ECU in Shell Eco Marathon 2012 is the number of injections per cycle. In 2012 the engine was driven with wasted spark resulting in 2 injections per cycle. In this experiment only 1 injection is used which is initiated 140 CAD before the inlet valve begins to open. At 4000 RPM this corresponds to 5.833 ms which means that the injection is still taking place when the fuel-air mixture is fed into the combustion chamber. As earlier discussed, the fuel should sit in the

inlet manifold for some time so that it can evaporate before being induced into the combustion chamber. A possible explanation could therefore be that the fuel is not mixed well enough with the air because it is inserted into the cylinder as droplets. A solution could then be to inject the fuel earlier. In the description of the WBO<sub>2</sub>-sensor it is however stated that the sensor does not measure only burned air/fuel mixture. The WBO<sub>2</sub>-sensor will include unburned fuel droplets in the  $\lambda$  measurements as well. Therefore, non-evaporated fuel can explain a bad combustion, hence a low BMEP at 4000 RPM because fuel is fed into the chamber as droplets which are not ignited. However, it can not explain the  $\lambda$ -value at 4000 RPM which is very high considering the high amount of fuel injected.

Even though the injection timing could not explain the problem, the injection timing was set according to the performance specification so that injection was initiated right after closing of the intake valve. This was done to ensure optimum evaporation and minimise the wall-wetting phenomenon.

Another possible explanation to the limit of 4000 RPM is that the piston is damaged resulting in a pronounced blow-by. This would explain the large amount of ethanol in the crankcase oil. It can however again not explain why the combustion is still lean even though the injected fuel amount is 1.4 times the 2012 amount. It is not possible to say if the large amount of ethanol in the oil is a trend that has not always been present. This is because the problem has not earlier been in focus. To examine if the piston was damaged a thorough mechanical inspection of the engine was conducted. No signs of mechanical defects were found and thus it cannot be concluded that a blow-by is the reason for the engine not running properly.

The main reason for the engine problems has to be found in the fact that the LED that is indicating the fuel injection signal was not flashing as supposed. This shows that the ECU is not sending the correct signal to the nozzle. It was found that the reason for this is that the engine speed encoder was not read properly by the program. The labview code for the control system is programmed so that a loop is constantly checking if the Z-pulse has a rising edge. If a rising edge is detected the program waits until it is time to inject fuel and then sends a signal to the nozzle to open. The computation time for the Z-pulse-checking-loop is also measured. It was measured that the time between each Z-pulse-check was 14  $\mu\text{s}$ . It is known from figure 11 that the duration of the rising edge of the Z-pulse is  $\frac{1}{720}$  camshaft revolutions or  $\frac{1}{360}$  crankshaft revolutions equal to 1/4 CAD. If the engine speed is 4000 RPM, the duration of the rising edge converted to a time-duration equals:

$$\frac{1/4 \text{ CAD}}{4000 \text{ RPM} \cdot \frac{1}{60} \frac{\text{min.}}{\text{s}} \cdot 360 \frac{\text{rev.}}{\text{min.}}} = \frac{10 \mu\text{s}}{} \quad (17)$$

This means that the rising edge of the Z-pulse will last  $10 \mu\text{s}$ . The ECU checks if the Z-pulse has a rising edge each  $14 \mu\text{s}$ , thus the program will inevitably overlook a portion of the Z-pulses. This will result in no fuel-injection thereby explaining why the LED is not flashing as supposed and explain why the BMEP is too low for the car to accelerate to above 4000 RPM. It can also explain the sudden speed fluctuations.

To eliminate the problem, the program was redesigned so that the computation time for the loop surveying the Z-pulse was decreased to  $1 \mu\text{s}$ . It was found that this removed the fluctuations and made the car capable of accelerating above 4000 RPM without problems. This was however done after this experiment was conducted. Because of a time pressure the speed-density control system was not further investigated experimentally. Instead of doing more experiments with the speed-density control system, the data from the Shell Eco Marathon 2012 was investigated. These data are very valuable because they describe the functionality of the speed-density control system during the Shell Eco Marathon. These data can therefore give a much better picture of the functionality of the speed-density control system than a dynamometer test is capable of. In the following subsection the relevant data from 2012 will be extracted and discussed.

### **Shell Eco Marathon 2012 results**

On figure 18 and figure 19 the results from the final and most fuel efficient race of 2012 can be seen. On figure 18,  $\lambda$  is plotted as a function of engine speed and on figure 19 the injecton length is plotted as a function of time. For a more detailed picture of the development of the injection length please see figure 45, 46, 47 in appendix A. The data has been processed in Matlab and the Matlab code can be found in appendix I on page 113.

From the requirement specifications,  $\lambda$  should be between 1 and 1.2. As seen on figure 18 these requirements are approximately met between 2500 RPM and 4250 except for a few outliers. From 2000 RPM to 2500 RPM and again from 4250 RPM to 5500 RPM the  $\lambda$ -value has a undisputed trend to be undesirably high. This shows that the three calibration factors are not enough to compensate for the error stemming from using the speed-density function and using a constant  $\eta_v$ . A further examination of the race data can be seen on figure 19. Here it is seen that the injection length slowly decreases from around  $2400 \mu\text{s}$  at the beginning of the race to  $2200 \mu\text{s}$  at the end of the race because of changes in manifold temperature and pressure. This shows that the system is able to compensate for the operating condition changes. - The pressure is slowly decreasing and the temperature is slowly increasing (figure 46) resulting in a decrease in density which means that the injection length has to be reduced according to equation 15.

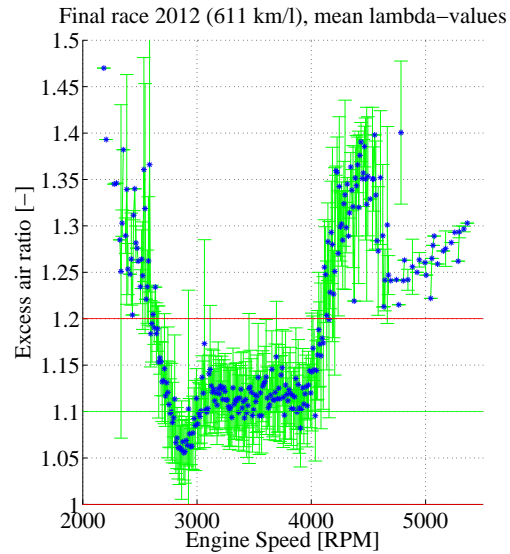


Figure 18: Shell Eco Marathon 2012,  $\lambda$  as a function of  $N$ . Each point is the mean of all lambda values in a range of 10 RPM. The green bars indicate 2 standard deviations.

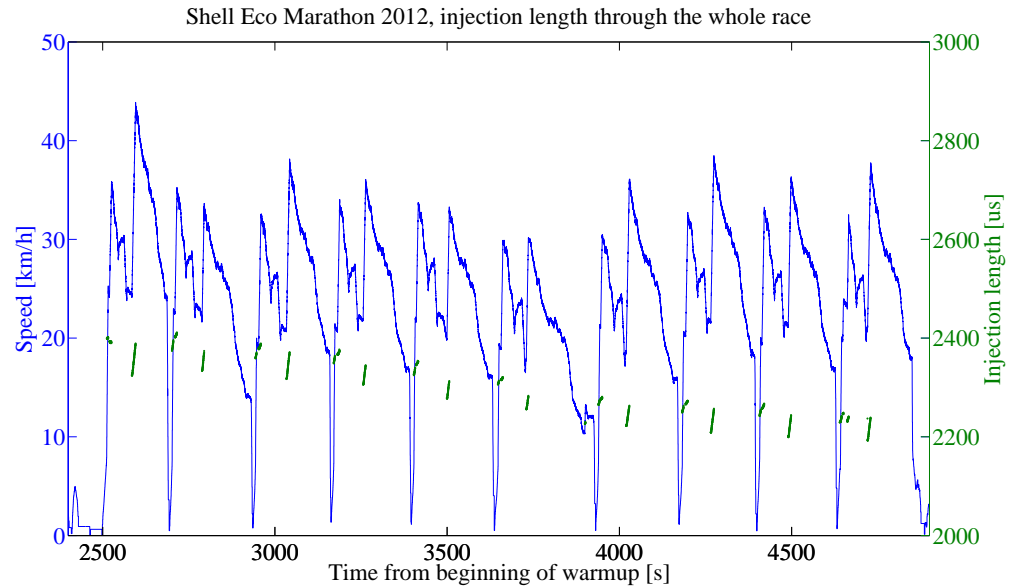


Figure 19: The injection length and the engine rotation speed during Shell Eco Marathon 2012.

On figure 19 (and also figure 45) the injection curves for each burn can also be seen. It is seen that the injection length is continually increasing during each burn. The difference between injection length at the beginning of the burn and the injection length at the end of the burn is highest on the second burn in 2nd gear in 1st lap (at around 2600 seconds after beginning of warmup). Here, the difference between start and end is around  $66 \mu s$ . In most of the burns it is much lower than  $66 \mu s$ . From the  $\lambda$ -values on figure 18 it is clear that shape and inclination of the injection curves of each burn are incorrect. In the following experiments it will also be shown that a difference in the shortest and longest injection lengths during one burn has to be around 10 times higher than  $66 \mu s$ .

In table 2 it is seen that both the pressure calibration and the final calibration are far from 1, meaning that the injection length is far from the speed-density-theoretically correct injection length. The values of the calibrations factors show that the speed-density control system is highly dependant on calibration tests to function properly.

Even though the control system is capable of compensating for the pressure and temperature changes occurring during the race, the system is as discussed, not capable of compensating for the changes in engine conditions happening during each burn. This shows that the system is not able to adjust the fuel amount when the rotation speed is changed. In section 5.1 different problems occurring during engine transient were discussed. It was described that pumping fluctuations make the volumetric efficiency change with changing engine speed. This correlation can be expected to be strong in the ecocar because it only has one cylinder. Therefore, a reasonable explanation for the poor  $\lambda$  control is that the system does not compensate for volumetric efficiency variations. Therefore, it is found that a control system using the speed density function and a constant  $\eta_v$  is not able to determine the injection time properly.

### Conclusion

To ensure optimum quality of the fuel/air mixture the injection timing has to be set so that the fuel has the longest possible time to evaporate before ignition, see for example the discussion of the injection timing in the performance specification (section 5.1).

It was found that a lot of ethanol was present in the crankcase oil which means that the crankcase oil has to be checked often and changed if necessary to obtain minimum friction. No mechanical defects were found in the engine and hence an explanation of the large amount of ethanol in the oil was not found.

The most critical error of the ECU was the high computation time of the Z-pulse-counting loop in the labview program. By re-designing the program, the computation time of this loop was decreased from  $14 \mu\text{s}$  to  $1 \mu\text{s}$  making the engine capable of running more stable.

From the data-processing of the 2012 race data it was found that the speed-density control system depends strongly on calibration and injects an amount of fuel which does not vary sufficiently with varying engine speed mainly because the volumetric efficiency is set to be constant. Therefore, speed-density control with constant  $\eta_v$  is not directly capable of meeting the performance requirements and has to be further improved to obtain acceptable  $\lambda$ -control.

## 9 Experimental tests concerning a closed-loop $\lambda$ control system

### Purpose

The closed-loop  $\lambda$  control system uses both feed-forward and feedback control. The feed-forward subsystem is a simple engine map and the feedback subsystem is simple closed-loop  $\lambda$  control as described in section 7.3. The closed-loop control system is, as mentioned earlier, highly dependant on the feed-forward system. Therefore, this experiment will focus strongly on the making and testing of the foundation of the closed-loop control; the simple engine map. This experiment aims to evaluate the level of difficulty of the creation of a simple engine map and the level of functionality of the simple engine map

Furthermore, the purpose of this experiment is to evaluate the functionality of the simple closed-loop  $\lambda$  subsystem. Through analysis of test-data it will be examined, whether the closed-loop  $\lambda$  control system is capable of meeting the requirements defined in the performance specification.

### Experimental setup

The creation of the engine map consisted of an initial making of the map followed by numerous calibrations carried out over a longer period of time. An engine map that was capable of making the engine run on the dynamometer in the range from 0 to 6000 RPM was created on the 28th of April 2013. An additional preliminary calibration test was carried out on the 30th of May. Afterwards, 8 calibration tests in the days from 11th-17th of May were carried out each consisting of a dynamometer- or outside driving test run followed by data-processing and adjustment of the injection values in the LabView program. After each of the official Shell Eco Marathon races carried out from the 17th-19th the engine map was also further adjusted.

The engine map was made of points indicating the injection length at 500 RPM, 1000 RPM and up to 6000 RPM in steps of 500 RPM. Between each point, the LabView program used linear interpolation to find the injection length. On the 14th of May the resolution of the map was doubled so that the injection length was indicated in steps of 250 RPM instead of 500 RPM.

Before all tests, the general test-preparation of the ecocar (described in section 8) was carried out. The relevant LabVIEW code for this experiment can be found in appendices G.3 and G.4.

*Preliminary dynamometer tests, 28th and 30th of May:*

The map was initially made by setting all values in the map to a constant value of 5900  $\mu$ s,

inspired by the speed-density experiment. In 2013 a centrifugal clutch was used in the car so that the car was not manually engaged. Instead, at just below 2000 RPM (depending on gearing ratio), the engine rotation speed remained constant until the wheel axle had the same rotation speed as the axle out of the gearbox. During the test the car was accelerated from complete stop to 16 km/h in first gear at WOT. Then quickly the engine was stopped, the gear was changed to second gear and the engine was started again and accelerated up to 35 km/h. While this was done, the  $\lambda$ -sensor and the engine rotation speed were both carefully observed. At a certain rotation speed the  $\lambda$ -value was noticed. Then, in the engine map at the given rotation speed, the injection length was adjusted up or down depending on the difference between the measured  $\lambda$ -value and 1.1. This procedure was repeated until  $\lambda$  was approximately 1.1 during the complete acceleration. Between each acceleration the brakes were put on the dynamometer to forcefully stop the wheels of the car. This meant that the coasting of the car was not simulated.

#### *Calibration tests 11th-17th of May*

As many of the calibration tests as possible were carried out on real outdoor road. In the first 3 test runs the car was driven as in the preliminary tests. In the rest of the tests the brakes were not used so that the car was coasting in between burns as in the real race. After each test,  $\lambda$  was plotted against the engine rotation speed. Because of a time pressure, these tests were not only used as calibration tests but were also used to optimise various parameters such as different gearing ratios. By changing the gearing ratio, the speed at which the gear was changed also had to be changed a little. In the tests, different race strategies - 2 or 3 burns - were also examined which meant that the maximum speed at which the engine was stopped was also varied a little. The tests were also used to analyse the closed-loop  $\lambda$  subsystem.

#### *Official Shell Eco Marathon races 17th-19 of May*

Before each race the car underwent a thorough mechanical check where all bolts and screws were tightened, the wheel alignment was checked and the oil was checked and changed if necessary. The car was warmed up until the axle encoder was no longer able to function which was when the crankcase oil temperature was around 70 °C and the coolant temperature was around 90 °C. In around 10 minutes up to the race the engine was not allowed to be turned on. This meant that if the warm-up was timed perfectly, the oil temperature was just below 60 °C when the race began. Before the last race the passive cooler of the axle encoder was replaced with a fan so that overheating of the encoder was no longer a problem and the oil temperature during the race was optimised. It was however very hard to time the warm-up perfectly because it was never known when one was able to go from the queue and onto the race track. Therefore, the oil temperature was around 55 °C in the beginning of most of the races.

In all races, each lap consisted of 3 burns in contrast to 2012 where each lap consisted of 2 burns. After the first race no adjustments were made to the engine map. After the second race

the map was further calibrated by changing the injection length at 4000 RPM from 5580  $\mu\text{s}$  to 6063  $\mu\text{s}$ . After the fourth race the injection length at 2750 RPM was changed from 4600  $\mu\text{s}$  to 4714  $\mu\text{s}$  and the injection length at 3250 RPM was changed from 4950  $\mu\text{s}$  to 5137  $\mu\text{s}$ .

### **Method used for extraction of data and for calibration of the engine map**

On figure 20, 23, 21 and 22,  $\lambda$  can be seen as a function of the engine rotation speed. Each blue point is the average of  $\lambda$ -values in an interval of 10 rpm. The standard deviation of the same  $\lambda$ -values is also calculated. The green bar indicates 2 standard deviations. The  $\lambda$ -values used for these calculations are all values that were logged in LabVIEW except for values above 1.5 and below 0.5 which are excluded. Values that are measured at a throttle angle below 80 degrees are also excluded. All data is processed in Matlab and the Matlab code can be found in appendix J on page 117.

After each calibration test run,  $\lambda$  was plotted as a function of engine speed using the method mentioned above. At locations where the average  $\lambda$  deviated from 1.1 the injected fuel mass was adjusted using the following formula:

$$m_{f \text{ new}} = m_{f \text{ old}} \cdot \frac{\lambda_{\text{measured}}}{1.1} \quad (18)$$

The motivation for using this simple formula can be found in appendix C.

### **Method used for the closed-loop $\lambda$ control subsystem**

On figure 24 the closed loop calibration factor is plotted against time. An average of the  $\lambda$ -values is also plotted. This average is calculated by the ECU. It is done by adding all  $\lambda$ -values measured in 2nd gear in the interval between 2000 and 5000 RPM. Whenever the gear is changed from 2nd and down to 1st gear this sum is divided by the number of measurements used to obtain an average  $\lambda$ -value. The ECU then starts over and sums up measurements until the gear is changed from 2nd to 1st again.

The calculated average is divided by 1.1 to obtain the calibration factor for the given lap:

$$\text{1-lap calibration factor} = \frac{\lambda_{\text{avg}}}{1.1} \quad (19)$$

This factor is however not the final factor. The final calibration factor is the 1-lap-calibration factor multiplied by the old final calibration factor. For example:

After the first lap, the average of the  $\lambda$ -values is 1.17 resulting in a 1-lap-calibration factor of  $\frac{1.17}{1.1} = 1.06$ . This is the first lap thus no old final calibration factor exists. Therefore, the new

final calibration factor immediately becomes 1.05. The average of the  $\lambda$ -values in the second lap is 1.08 resulting in a 1-lap-calibration factor of  $\frac{1.08}{1.1} = 0.98$ . The new final calibration factor thus becomes:  $1.06 \cdot 0.98 = 1.04$ .

## Results

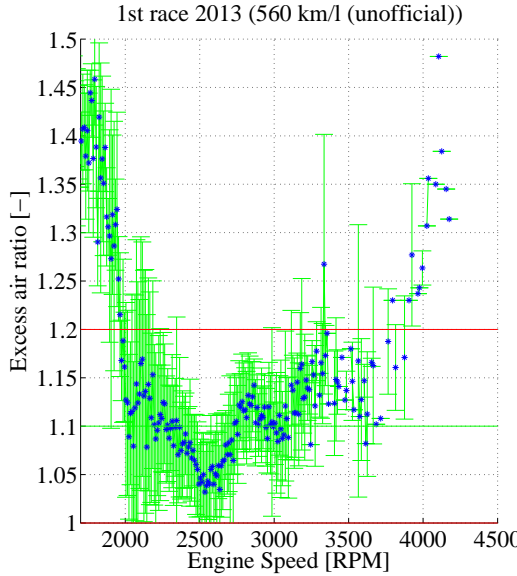


Figure 20:  $\lambda$  as a function of engine speed. 1st race 2013. Gearing=22/65. Underdamped closed-loop control.

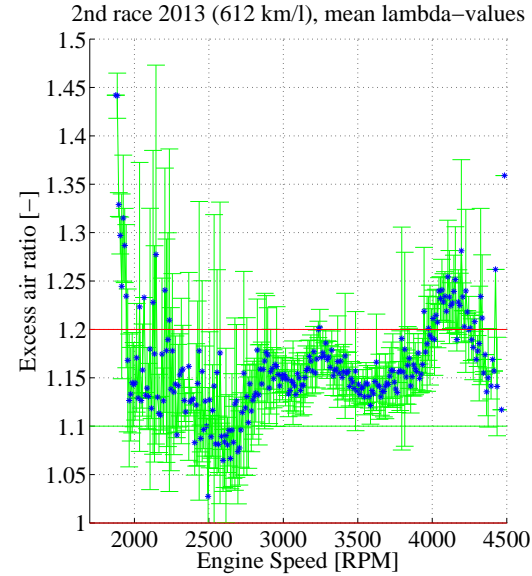


Figure 22:  $\lambda$  as a function of engine speed. 2nd race 2013. Gearing=17/70. No closed-loop control

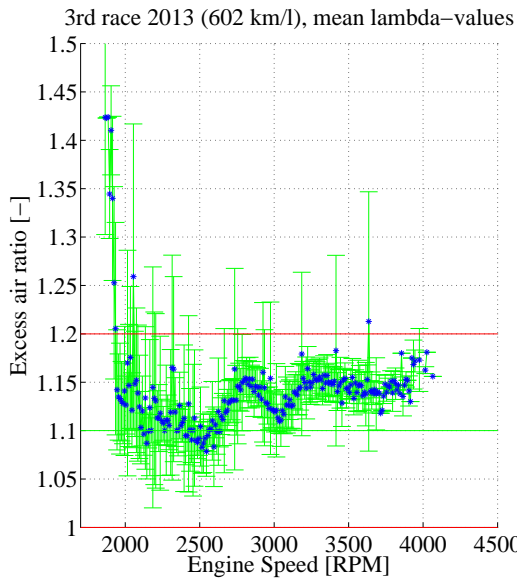


Figure 21:  $\lambda$  as a function of engine speed. 3rd race 2013. Gearing=19/68. Damped closed-loop control

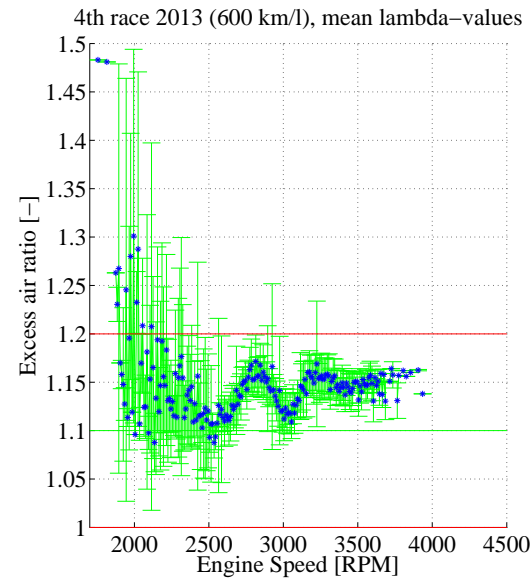


Figure 23:  $\lambda$  as a function of engine speed. 4th race 2013. Gearing=19/68. Damped closed-loop control

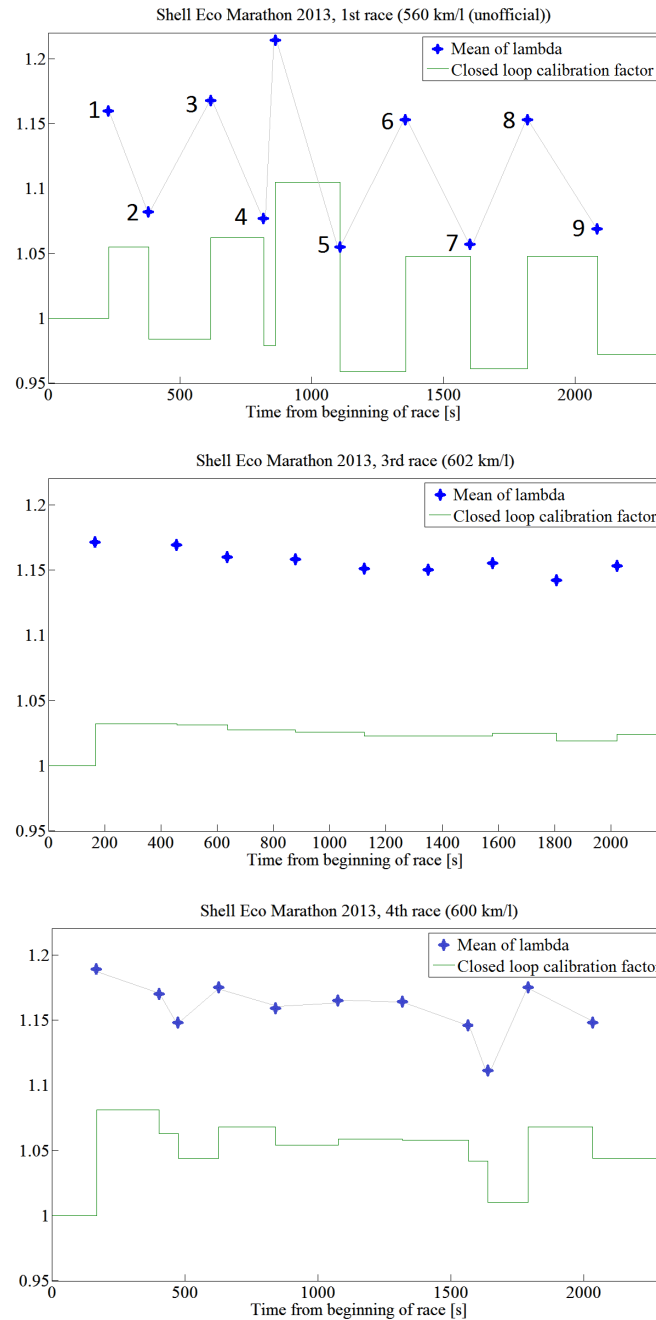


Figure 24: Average of  $\lambda$ -values for each lap, race 1, 3 and 4. The resulting closed-loop calibration factors are also plotted.

## Discussion

On figure 20, the  $\lambda$ -averages of the first race can be seen. To see all logged values for this race instead of averages, please see figure 50 in appendix B.

From 2000 RPM until 3750 RPM the average  $\lambda$  is between 1.0 and 1.2. Before and after,  $\lambda$  is in general too high. The centrifugal clutch is engaging around 2050 RPM. which means that it is hard to obtain proper  $\lambda$ -control below and around 2050 RPM. This does however not change the fact that the curve is at no time a straight horizontal line as required for proper simple closed-loop control and the twisting of the curve results in too many  $\lambda$  measurements outside of the required interval. The result is however better than in 2012.

Apart from the many bends and twists of the curve, the averages are also fluctuating considerably and the standard deviations are much higher than in the other races. The explanation of this can be found on the top graph of figure 24. Here, the average of  $\lambda$  for 1 lap (if the driver changes gear as supposed) is shown together with the resulting calibration factor. In first lap the average of  $\lambda$  is around 1.16. This results in a calibration factor of around 1.05 for the 2nd lap. This factor is however a little too high, resulting in an average of  $\lambda$  being 1.08 in 2nd lap. This makes the calibration factor lower than 1 which makes the average of  $\lambda$  for lap 3 further above 1.1 than in lap 1. The average of  $\lambda$  keeps oscillating around 1.1 and the calibration factor keeps oscillating around 1. The oscillations do not decrease through the race. When further investigating the calibration factors, it is found that the closed-loop calibration factor is at all times equal to the 1-lap-calibration factor instead of being equal to the old closed-loop calibration factor multiplied by the latest 1-lap calibration factor. If the system would have worked as intended, the final calibration factor after 2nd lap would not have been below 1. Instead it would have been 1.04 as seen in the example in section 9. Looking at the graph, a calibration factor of 1.04 would have been a good estimate for obtaining an average of  $\lambda$  of 1.1. Instead the system is highly overcompensating and not improving during the race. It is only adjusting to the directly preceding lap creating undesirably large oscillations resulting in high deviations among the  $\lambda$ -measurements. A solution to this problem had to be found. The reason why the final calibration factor was equal to the 1-lap-calibration factor was not found for the 2nd race and thus the closed-loop subsystem was turned off. Before 3rd race, an explanation to the problem was still not found and the closed-loop subsystem was redesigned so that it was damped in the following way:

$$\text{Closed-loop calibration factor} = \frac{1 \text{ lap calibration factor} + 1}{2} \quad (20)$$

In race 3 and 4 this subsystem was implemented in the ECU.

On figure 22, the  $\lambda$ -averages of the second race can be seen. To see all logged values for this race instead of averages, please see figure 52 in appendix B.

Here, it is seen that the curve is very wavy. At 3250 RPM the averages of  $\lambda$  is close to the performance specification limit of 1.2. From 4000 to 4250 RPM the averages go above 1.2. That  $\lambda$  in both the 1st and 2nd race exceeds the limits from the performance specification shows that 2 preliminary calibration tests followed by 8 calibration tests is not enough to obtain an acceptable simple engine map. This is problematic because it is a comprehensive task to do calibration tests because no one else has access to the car while it is being tested. It is a time consuming process, especially because there is usually some debugging which needs to be done. To obtain a better engine map at the Shell Eco Marathon next year, either more tests are needed or a better calibration method is needed. Even though the  $\lambda$ -values do not fall within the required limits it is important to note another item of the performance specification which has been met - the robustness and consistency of the simple engine map is impeccable. The control system was in contrast to many other mechanical and electronic systems of the car able to perform at all times through the competition which was crucial for the outcome of the competition.

In race 3 and 4 (figure 21 and 23) it is seen that the change in gear ratio makes the engine not exceed 4000 RPM thus avoiding the critical interval from 4000 to 4250 RPM where  $\lambda$  exceeded 1.2 in race 2. When comparing race 2 and 3 (figure 22 and 21) it can be seen that the curve has smaller fluctuations in race 3 as in race 2 and that the averages in  $\lambda$  is not at any time getting as close to 1.2 in race 3 as in race 2 (the engagement phase is not taken into account). Also, the standard deviations are in general smaller and much less fluctuations in the  $\lambda$ -averages are present, making the curve much more defined. The same trend is present in race 4 (figure 23) although the curve is not as defined from 2500 RPM and down as in race 3. It can be concluded that the control system is working better in race 3 and 4 than in race 2. Two changes in the control system were made between race 2 and 3. The engine map was adjusted and the damped closed-loop system was turned on. The engine map was only adjusted at 4000 RPM and thus this adjustment does not have any affect. Therefore, it is shown that the damped closed-loop subsystem has a positive effect on the fuel/air ratio.

When looking at the middle and bottom graph on figure 24 the behaviour and effect of the closed-loop system can be further investigated. In 3rd race the oscillations seen in race 1 are eliminated. It is seen that the average  $\lambda$ -values are between 1.15 and 1.17 resulting in calibration factors around 1.03. When the  $\lambda$ -average decreases the calibration factor is also decreasing as expected. The calibration factor is not effective enough to lower the  $\lambda$ -average to 1.1. This shows that the system is highly overdamped. In race 4 the same trend is shown - the high  $\lambda$ -values results in large calibration factors. In this race the calibration factor has a maximum

of 1.08. That the system is highly overdamped makes the effect of the closed-loop calibration undesirably small. Also, the fact that the calibration factor still only takes the preceding lap into account makes the system less efficient. However, the system works better when it is highly overdamped compared to underdamped and a calibration factor of 1.03 and up to 1.08 can be a strong improvement compared to no calibration considering the high  $\lambda$ -values. To improve the control system, one could experiment with damping the system less, although the most efficient improvement would be to make the system able to take the old calibration factor into account when calculating the new factor.

Even though it is clear to see an improvement in fuel/air ratio from race 2 to race 3 the fuel economy is best in race 2. This is because of the variation of numerous other parameters such as the weather, traffic on the track, gear ratio and oil temperature. It must also be noted that the strength of the conclusions deducted from this experiment are weakened by the bad control of variables. - Numerous parameters other than the parameters examined were changed between races potentially affecting the results of the  $\lambda$ -measurements.

The results of the last race are strongly affected by the numerous changes made before the race such as implementation of a kinetic energy recovery system, change of cylinder head and change of gear ratio. The results are therefore not as usable as the other results. They can however be found in appendix B, figure 54 and 55.

### Conclusion

Even though calibration tests are a comprehensive task, it is seen that 2 preliminary tests and 8 calibration tests were not enough to meet the requirements. It is however enough to make a simple engine map capable of improving the air/fuel ratio compared to last year's Shell Eco Marathon. Also, the system was robust and consistent and did not fail at any time.

By combining the simple engine map with a simple closed-loop control system, a gear ratio of 19/68 and 3 burns on each lap, it was found that the requirements of the performance specification could be met.

The closed-loop subsystem is still not fully functioning because it only takes the preceding lap into account. A big improvement to the closed-loop system could be to fix this problem.

## 10 Laminar flow meter experiment

### Purpose

This experiment examines the possibilities of using a custom built laminar flow meter to determine the air mass flow into the engine which is used to determine the amount of injected fuel into the engine. This is done in four phases: Firstly, a preliminary calibration test will be conducted to test how well an already constructed laminar flow element would be suited for application in the ecocar. Secondly, a laminar flow meter which is improved for the application will be constructed and calibrated. On the basis of the calibration, an improved laminar flow meter is constructed and calibrated. This procedure is repeated until a well suited flow meter with the proper dimensions for the ecocar has been constructed. Thirdly, this flow meter will be tested on the engine used in the ecocar on a test stand. Fourthly, the laminar flow meter will be tested outside in the ecocar.

### Calculations

The calibration of laminar flow meters is carried out using a pre-calibrated commercially available laminar flow meter of the type; Meriam Laminar Flow Element Model 50MC2-2F. This element has not been calibrated since april 1999 and it has been observed that a few of the lamellae of the capillary tubing are damaged. By having the same mass flow going through the two laminar flow meters and measuring the output from both meters (figure 25), a calibration curve for the new laminar flow meter can be made.

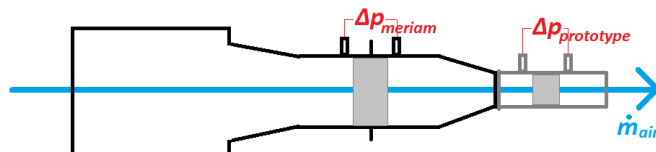


Figure 25: Sketch of laminar flow meter calibration

To calculate the mass flow from the differential pressure of the Meriam laminar flow element the following formula obtained from the calibration certificate (appendix L) is used:

$$\dot{V}_{LPM} = (14.6054 \cdot \Delta p_{mmH2O} + (-0.00406571 \cdot \Delta p_{mmH2O}^2) \cdot \left( \frac{\mu_{std}}{\mu_{wet-air}} \right) \left( \frac{T_{std}}{T_f} \right) \left( \frac{P_f}{P_{std}} \right) \left( \frac{\rho_{wet}}{\rho_{dry}} \right)) \quad (21)$$

where  $\dot{V}_{LPM}$  is the standard volumetric flow in litres per minute,  $\Delta p_{mmH2O}$  is the pressure difference in mm H<sub>2</sub>O and  $\left( \frac{\mu_{std}}{\mu_{wet-air}} \right)$ ,  $\left( \frac{T_{std}}{T_f} \right)$ ,  $\left( \frac{P_f}{P_{std}} \right)$  and  $\left( \frac{\rho_{wet}}{\rho_{dry}} \right)$  are all correction factors normalising

the volume flow to reference conditions. Tables with these correction factors can be found in appendix M.

To calculate the mass air flow one can use:

$$\dot{m}_{air} = \frac{\dot{V}_{LPM}}{60\text{s}/\text{min}} \cdot \rho_{air} \cdot \frac{1000 \text{ g/kg}}{1000 \text{ litre/m}^3} \quad (22)$$

$\rho_{air}$  is found using the ideal gas law (equation 11).

The laminar flow meter constructed has to be designed to fit the range of air mass flow of the engine. To estimate the maximum air mass flow of the engine the speed-density function (equation 15) is used. The volumetric efficiency is set to 1. This is unrealistically high and ensures that the estimated range is not smaller than the actual range. The temperature and pressure are set to standard conditions:

$$\dot{m}_{air} = \frac{V_d \cdot p_{in}}{120 \cdot R \cdot T_{in}} \cdot \eta_v \cdot N = \frac{0.000049334 \text{ m}^3}{120 \cdot 287.058 \frac{\text{Pa}\cdot\text{m}^3}{\text{kg}\cdot\text{K}}} \cdot \frac{100000 \text{ Pa}}{298.15 \text{ K}} \cdot 1 \cdot N = 0.0026 \frac{\text{kg}\cdot\text{min}}{\text{s}} \cdot N \quad (23)$$

From the performance specification it is seen that the maximum engine revolution speed is around 5500 RPM:

$$\dot{m}_{air\ max} = 0.0026 \frac{\text{kg}\cdot\text{min}}{\text{s}} \cdot 5500 \text{ min}^{-1} \cdot 4 = 11 \text{ g/s} \quad (24)$$

The value is multiplied by 4 because the air flow only occurs in the intake phase which is 1 out of the 4 phases in the four-stroke cycle. The estimated required range of the laminar flow element is therefore 0 - 11 g/s.

It is also important that it is ensured that the pressure loss in the laminar flow meter will not have a significant impact on the pumping losses. By having the maximum pressure loss in the laminar flow meter relative to the inlet manifold pressure of 0.65 bar, one can get an idea of the impact of the laminar flow meter pressure loss.

### Experimental setup

The laminar flow elements measures the volume flow. Therefore, to obtain the mass flow, the atmospheric pressure, temperature and humidity must be measured before every laminar flow meter test.

The results of the preliminary test of the pre-constructed laminar flow element were used together with the dimensions of the pre-constructed laminar flow element to design prototype 1. Afterwards, prototype 1 was tested and the results were evaluated together with the earlier results obtained . From this evaluation the dimensions could be improved and a new prototype was constructed. This process was repeated until the proper dimensions were found. By proper dimensions is meant dimensions resulting in optimal measure-range combined with minimum pressure drop and optimum measurement reliability.

### Setup of the calibration experiment

The preliminary test was carried out by setting up the pre-constructed laminar flow meter in a serial connection with the Meriam flow meter as seen on figure 26.

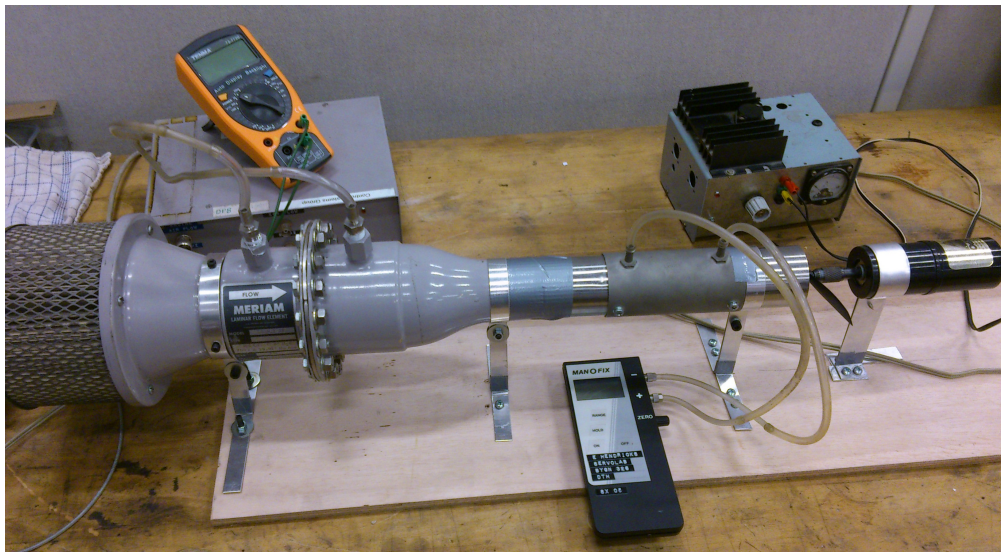


Figure 26: Experimental setup of the preliminary test

An air flow was established using the propeller seen on the right side of the figure. The motor of the propeller was connected to an adjustable voltage source.

Three different devices were available for measuring the differential pressure; One differential pressure meter with a sensitivity of 1 Pa, a preamplifier having a voltage output (the box below the voltmeter on figure 26) and smaller preamplified pressure sensor also having a voltage output. This preamplified pressure sensor was of the Honeywell 160PC-series (model 164PC01D37) and

will be similar to the sensor used in the final flow meter used in the car.

Before measurements could be taken the big pre-amplifier had to be turned on for 1 hour because it took a while before it stopped drifting. After 1 hour the propeller was turned on and the pressure loss over the Meriam flow element was measured using the big preamplifier in combination with a voltmeter. Simultaneously the pressure loss over the pre-constructed flow element was measured using the differential pressure meter. The speed of the propeller and thereby the air flow was varied randomly to avoid extraneous factors possibly affecting the result. The result of the preliminary calibration test can be seen of figure 36.

The calibration tests of the laminar flow meter constructed later was carried out by the same procedure as above except for a few changes:

- In most of the calibration tests the differential pressure in the laminar flow meter constructed was measured using the 160PC sensor instead of the differential pressure meter.
- Instead of establishing an air flow by the use of a propeller, an industrial vacuum cleaner was used. The flow could be adjusted by opening a vent in the tube of the vacuum cleaner (figure 56). To scale down the air flow, the vacuum cleaner was not connected air tight to the flow meter. Instead a small gap was present between the vacuum cleaner hose and flow meter as seen on figure 27.

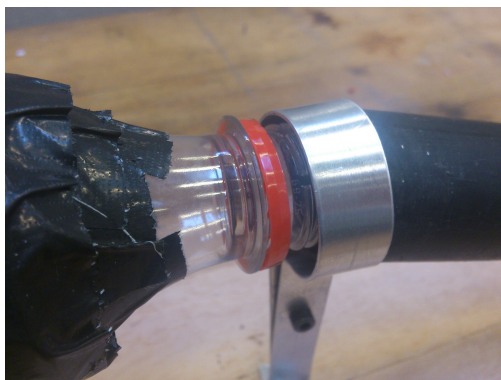


Figure 27: The air flow of the powerful vacuum cleaner was scaled down by making a gap between flow meter and vacuum cleaner hose.

For the calibration tests of prototypes 4 and 5 the small pressure sensor was replaced with the electronic component used in the final laminar flow meter. This component also consisted of

the same preamplified 164PC01D37 pressure sensor which was later modified so that the offset in voltage was changed and the sensor was changed to the less sensitive 143PC03D sensor. The calibration test of prototype 4 can be seen on figure 56.

### Construction of laminar flow elements

The first three laminar flow elements were constructed using aluminium pipes. The fourth element was made using a polymer pipe because no aluminium pipe was available with the required diameter. The fifth element was made using a 3D-printed construction made of ABS. The capillary tubing was made of foil (as on figure 10). The capillary tubing was constructed using aluminium foil for prototype 1 and brass foil for all other prototypes. The tubing was produced by coiling crimped foil together with straight foil into a spiral as seen on figure 28. Firstly two pieces of straight foil were cut into the right dimensions as seen on figure 29. One of these pieces was corrugated using the tool seen on figure 31 while the other piece was straightened. When comparing the corrugated foil made of aluminium and of brass it was observed that the corrugation of the brass foil was much more successful than the corrugation of aluminium foil which was not very effective. The preconstructed laminar flow meter was also made with brass foil. It was however observed that the foil in the preconstructed flow meter had a much higher corrugation depth than the brass foil corrugated for this experiment. This resulted in smaller capillaries of the laminar flow meters made for this experiment and thus a lower hydraulic diameter than in the preconstructed flow meter.

Afterwards, the foil was coiled into a spiral as seen on figure 31. The capillary tubing was then inserted into the aluminium pipe. A cross brace made of 1 mm thick welding wire was used in each end of the tubing to keep it fixed as seen on figure 32. The welding wire was fastened using epoxy glue. It was ensured that the holes in which the wire was placed were afterwards air tightened using the epoxy glue. Also, the hole in the middle of the capillary tubing was covered using epoxy. Finally, brass nipples were screwed and glued using PVC glue into holes in the aluminium pipe as seen on figure 33. The brass nipples were made on a lathe from 8 mm screws. Down through the screws, a 1.5 mm hole was drilled so that the pressure in the aluminium pipe could be measured through the nipples. For the construction of the laminar flow elements all work using epoxy and PVC glue was carried out in a fume cupboard using gloves.

The core dimensions of the constructed laminar flow elements can be seen in appendix E. Sketches of the final laminar flow element (prototype 5) can be seen in appendix F.

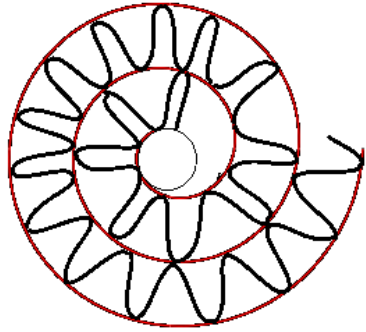


Figure 28: Sketch of capillary tubing used for the prototypes. The tubing consists of a layer of corrugated foil (black) and a layer straight foil (red). Because of the tool used, a hole will be present in the middle of the capillary tubing.

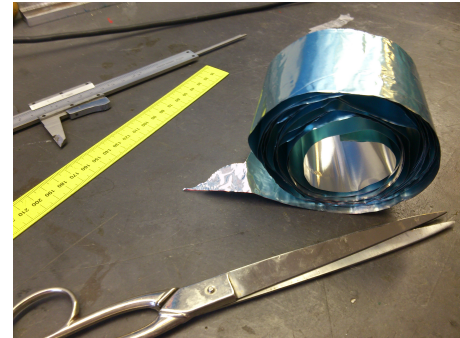


Figure 29: Aluminium foil is cut into the right dimensions before being corrugated and coiled into a spiral.

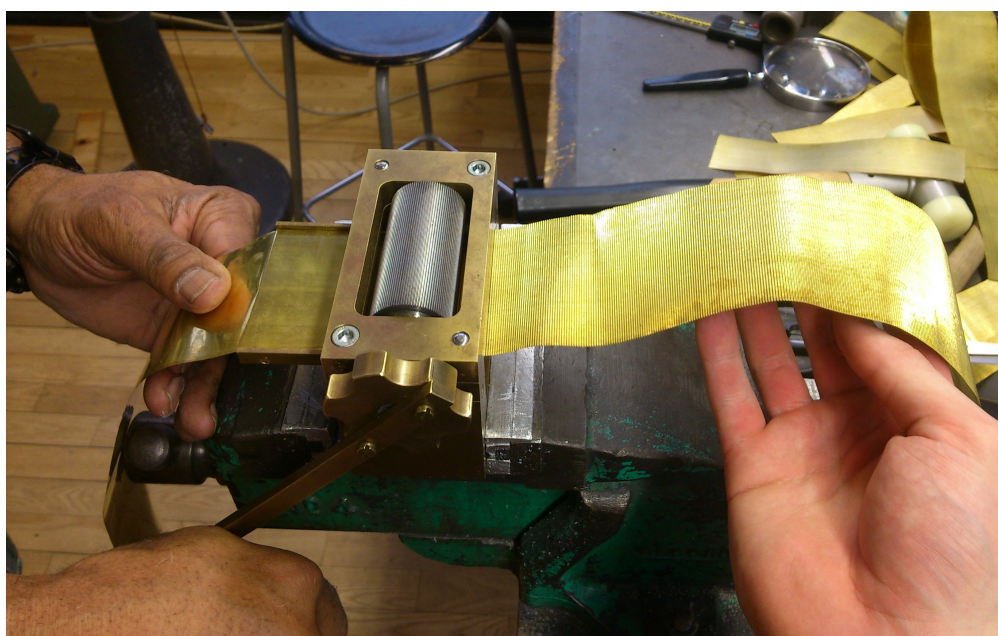


Figure 30: Corrugation of foil



Figure 31: Coiling of the two foil layers into a spiral.

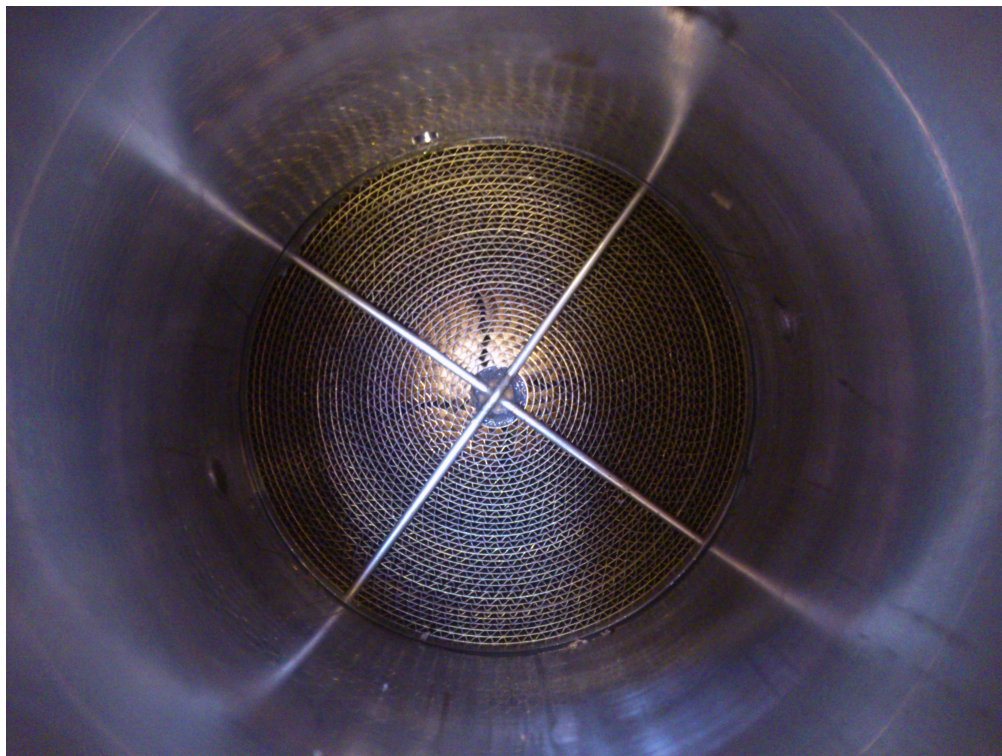


Figure 32: The inside of a laminar flow element. The crossed welding wires were fastened with epoxy. The hole present in the middle of the capillary tubing is covered by epoxy.



Figure 33: Laminar flow element, prototype 1. The nipples are hollow so that the pressure at each end of the capillary bundle can be measured through them. The small holes seen in the aluminium cylinder are made for the welding wire. Care was taken that the holes were sealed with epoxy after the wire brackets were inserted.

### Laminar flow meter experiment in testing stand

The laminar flow meter, prototype 3 was mounted on the testing stand in the intake manifold downstream of the air filter. To reduce pressure pulsations a plenum chamber was mounted downstream of the laminar flow element as seen on figure 34. The experiment was carried out both with and without a plenum chamber. The laminar flow meter was mounted using foam to reduce vibrations.

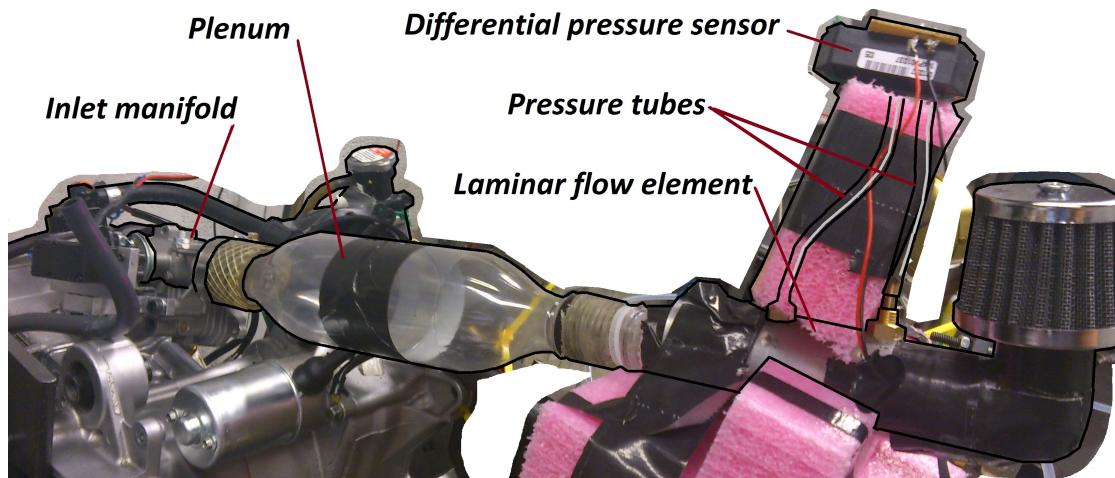


Figure 34: Experimental setup of laminar, prototype 3 flow meter in testing stand.

After the laminar flow element was mounted, the measurements could begin. During the test, the piston was driven by a servo motor mounted on the crankshaft axle. That is - the engine was at no point driven by combustion. The servo motor was used instead of combustion because it resulted in more consistent results with less unknown variables. It was also less time consuming.

Measurements were carried out using an oscilloscope to measure the signal coming from the differential pressure sensor. Data was obtained for the engine running at constant speed levels. Without the plenum chamber, data was obtained for 500 RPM and up to 2500 RPM with a step size of 500 RPM. With plenum chamber, data was obtained for 500 RPM up to 5000 RPM also with a step size of 500 RPM.

### Laminar flow meter test using the ecocar

For this experiment the final laminar flow meter (prototype 5) was used. The flow meter was mounted on top of the gear casing as seen on figure 35. The differential pressure sensor elec-

tronics were connected to the electronics of the ecocar through an ethernet cable. Using a NI Compact Rio and a program written in LabVIEW, the signal from the laminar flow meter was measured and logged. The LabVIEW code can me found in appendix G.2

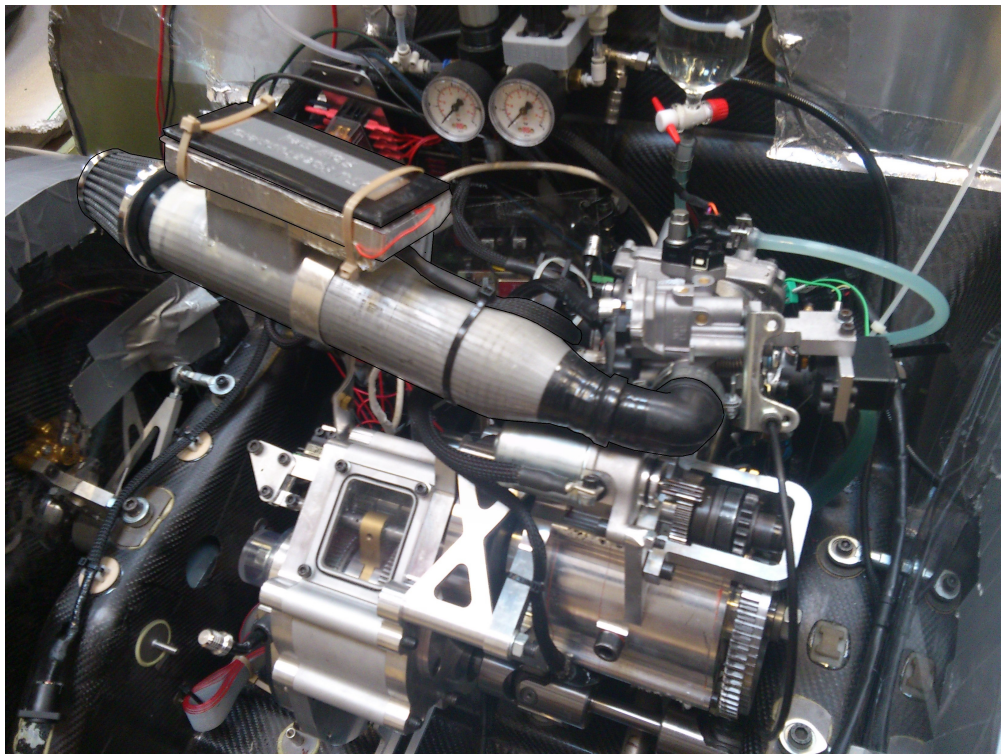


Figure 35: Laminar flow meter prototype 5 mounted in the car.

The experiment was carried out the 12th of May. Before the test the car was prepared according to the general test preparation procedure described in section 8. After the car had been warmed up it was accelerated with WOT from 0 to around 35 km/h - a burn strategy similar to the one described in the performance specification. This acceleration was repeated 10 times and the data was afterwards processed in matlab. During the test, the fuel injection length was determined using the simple engine map. That is, the laminar flow meter was not used in the control system. It was only in the car so that its measurements could be evaluated afterwards.

## Results

### Laminar flow meter calibration test results

On the following figures the most relevant calibration results can be seen. Other calibration results can be found in appendix D. On the figures, the differential pressure measured using the Meriam flow meter has been converted to mass flow using equations 21 and 22.

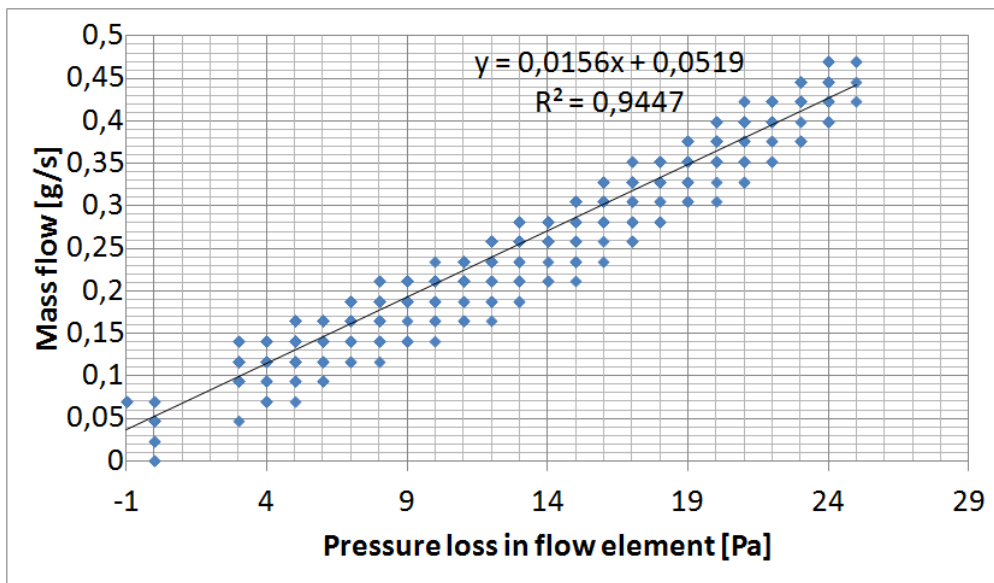


Figure 36: Preliminary laminar flow meter test using a flow element made by Elbert Hendricks. The differential pressure of the preconstructed flow meter was measured using the differential pressure meter with a sensitivity of 1 Pa. The differential pressure of the Meriam flow meter was measured using the large preamplifier.

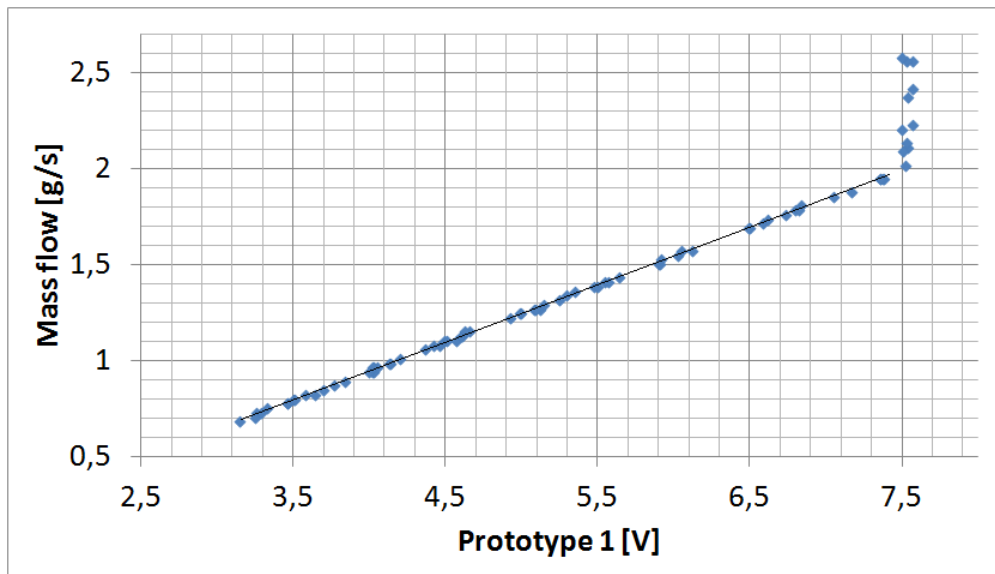


Figure 37: Test of laminar flow meter prototype 1. The equation of the trendline is  $y = 0.2994 \cdot x - 0.2537$  and the  $R^2$ -value is 0.9996 (measurements above 7.45 volts have been excluded). A 9 V battery was used as power source. The initial voltage of the battery was 9.07, the final voltage was 8.98. Atmospheric pressure was 1012 hPa and the temperature was 24°C.

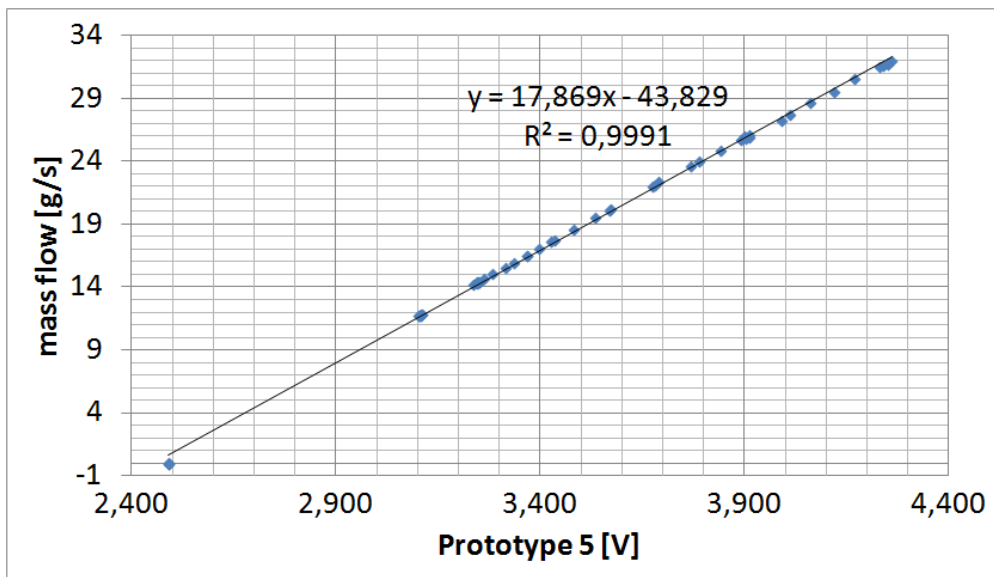


Figure 38: Test of laminar flow meter prototype 5. For this test the final electronic component seen on figure 56 was used. The electronic component is designed so that the input can be between 10 and 14 V without affecting the output. The output is between 0 and 5 V. The weight of the prototype 5 was 350 g. During the test, the atmospheric pressure was 1013 hPa and the temperature was 24 °C. Instead of using the linear correlation for the trend line seen on the graph, a  $R^2$  value of 0.9999 can be obtained by using the 2nd order polynomial correlation;  $\dot{m}_f = -1.0364 \cdot (voltage - 2.5)^2 + 19.949 \cdot (voltage - 2.5)$ .

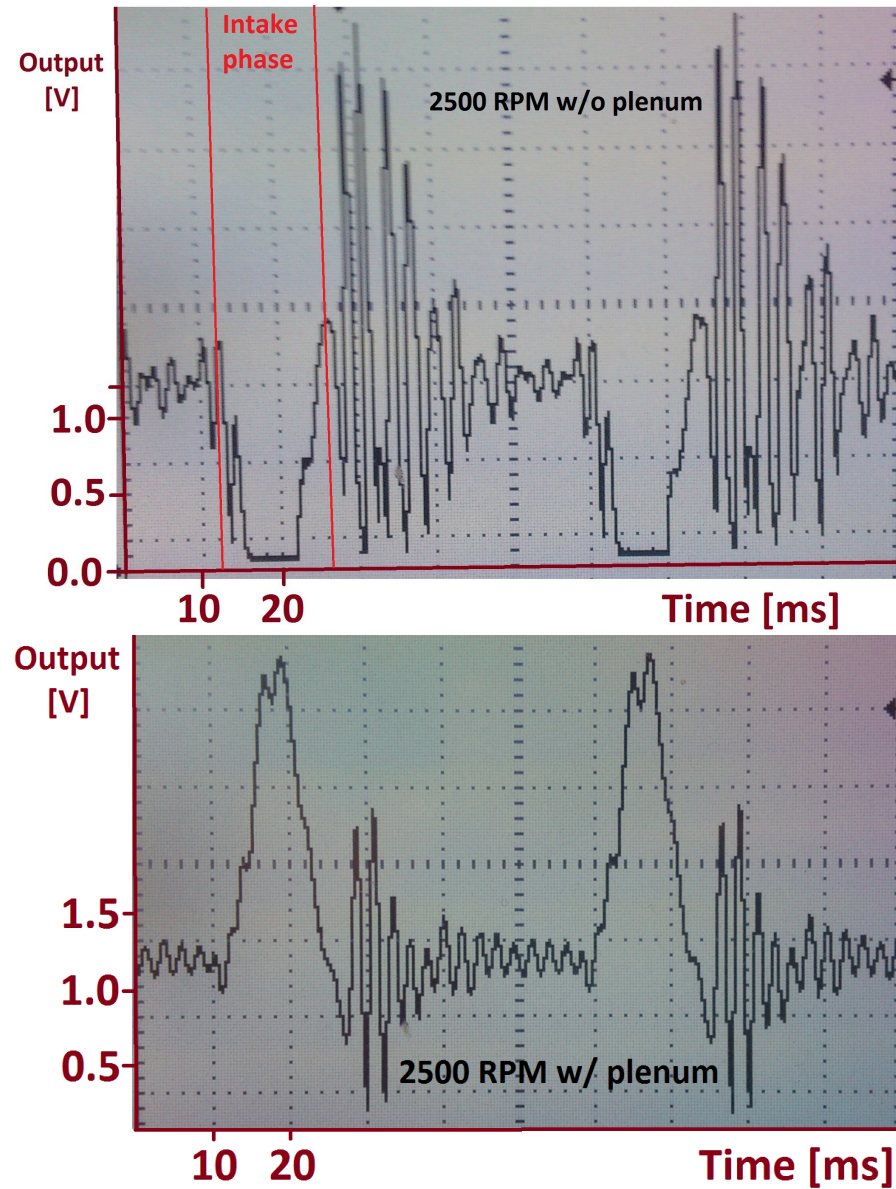


Figure 39: Pressure oscillations at 2500 RPM measured using prototype 3, with and without plenum. The D.C. offset of the sensor is 1.2 V.

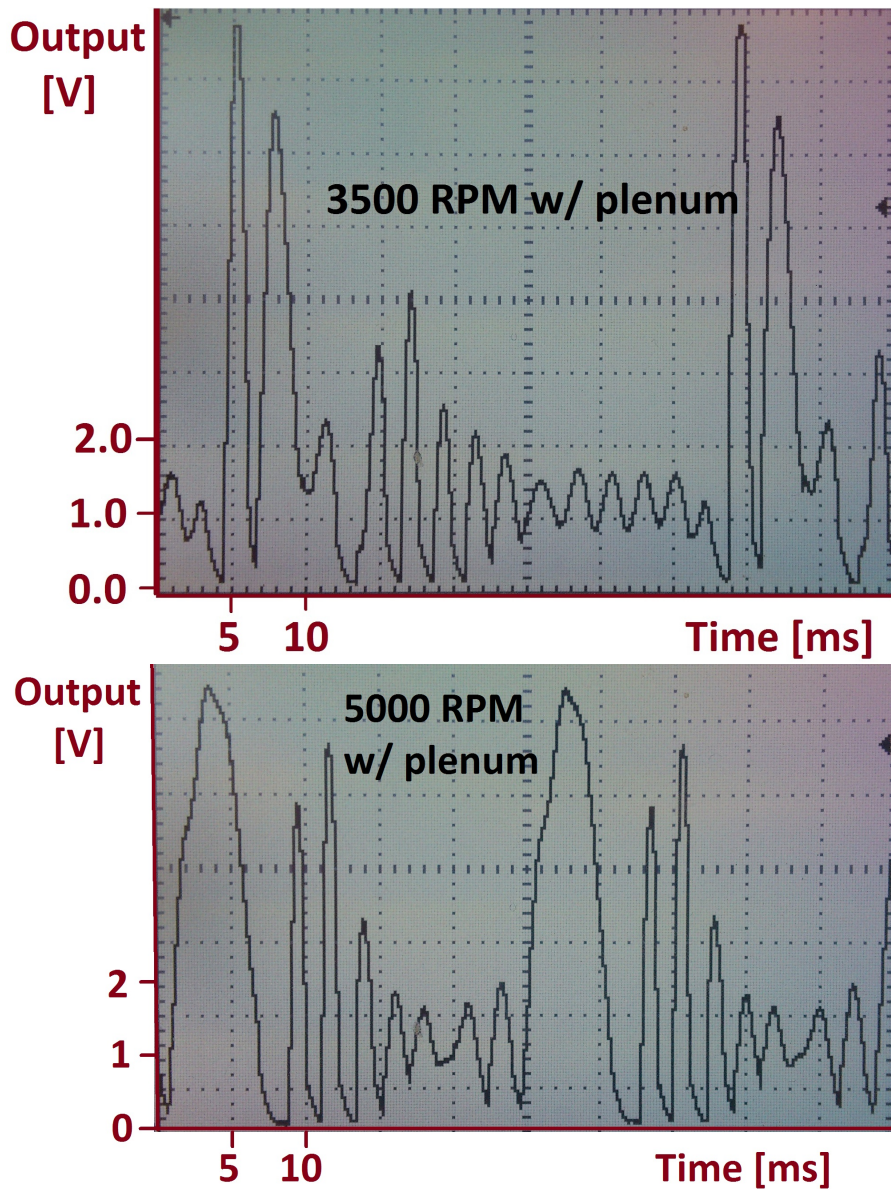


Figure 40: Pressure oscillations measured using prototype 3 with plenum. The D.C offset of the sensor is 1.2 V.

#### Result from laminar flow meter application in ecocar

In the following, the most relevant results of the laminar flow meter measurements are graphically presented. On figure 42 and 43 the voltage signal has been converted to the corresponding fuel

mass using the following equation (from figure 38);

$$\dot{m}_f = -1.0364 \cdot (voltage - 2.5)^2 + 19.949 \cdot (voltage - 2.5) \quad (25)$$

and that  $\lambda = \frac{FA_s}{FA}$  and that  $FA_s$  ethanol = 0.111. The voltage signal used for these calculations are the average of measurements executed each 50  $\mu s$  during one combustion cycle (as seen in appendix G.2).

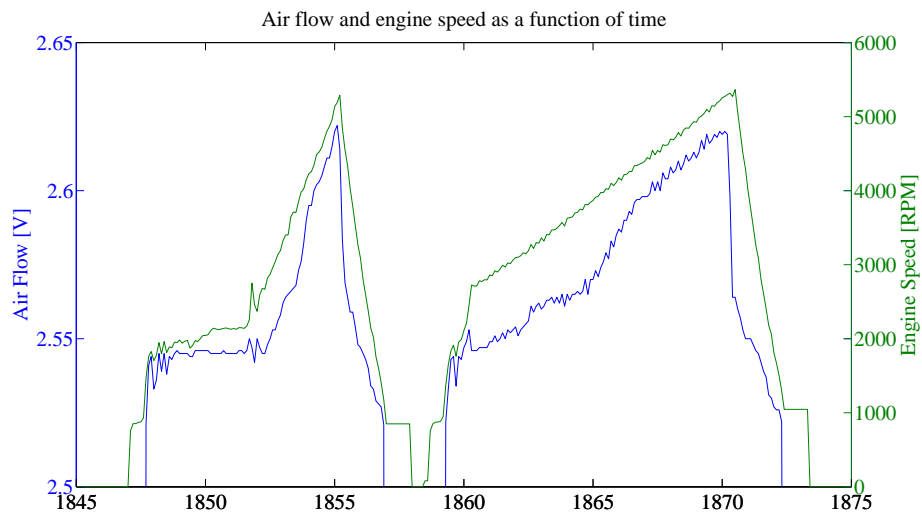


Figure 41: Outside test of ecocar with the laminar flow meter. Engine rotation speed and laminar flow meter output are plotted against time during 1 burn. The outdoor temperature and pressure were 12.5 °C and 1011 hPa.

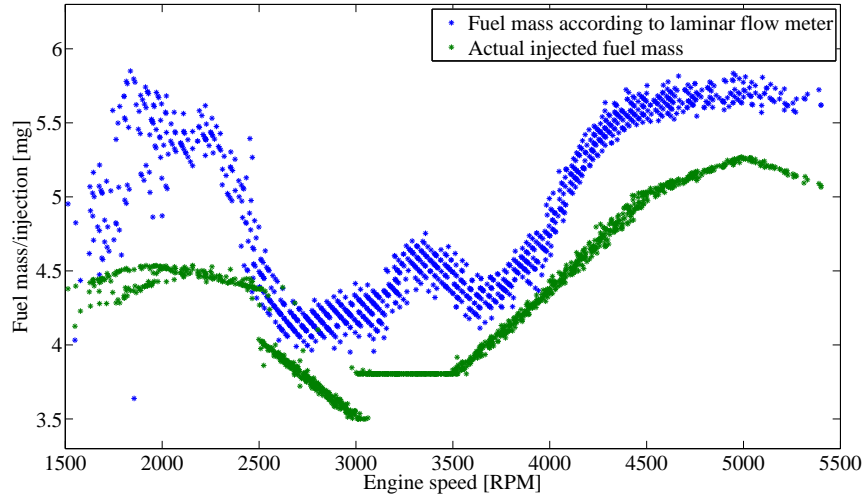


Figure 42: Fuel mass determined from laminar flow meter compared to the actual injected fuel mass

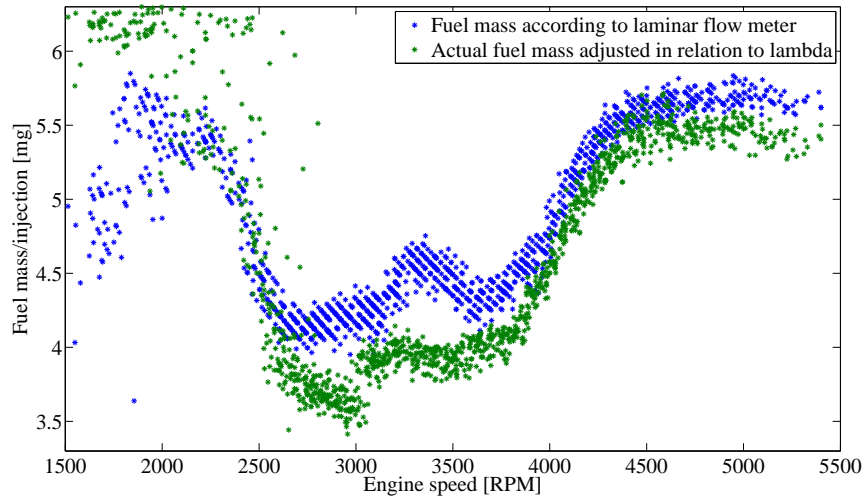


Figure 43: Fuel mass determined from laminar flow meter compared to the actual injected fuel mass adjusted to  $\lambda$  (adjusted mass = actual mass  $\cdot \frac{\lambda_{measured}}{1.1}$ ).

### Discussion

To confirm that the laminar flow elements do in fact create a laminar flow, the linearity of the calibrations results can be evaluated. The results of the preliminary calibration test can be seen

on figure 36. The  $R^2$ -value is far from 1 and the measurements are not placed on a straight line. This is due to bad measurements. - The sensors are too insensitive to measure values that are accurate enough for the given range in pressure loss. It is seen that the range in air flow is 0 - 0.45 g/s. The air mass flow range of the engine is 0 - 11 g/s. To test the laminar flow meter in a more relevant range in regard to the engine, the experimental setup was improved by replacing the propeller with a vacuum cleaner. This way, the air flow through the flow meters was increased significantly. The increase in air flow results in an increase in pressure loss high enough for the sensitivity of the sensors to be sufficient for examination of the linearity of the flow elements.

The 164PC01D37 sensor is more suitable than the differential pressure meter for application in the car, hence it must be ensured that the 164PC01D37 sensor is capable of measuring the flow in a suitable range. From the data sheet of the 164PC01D37 sensor it is seen that the pressure range is 0 - 10 inches  $H_2O$ , equivalent to 0 - 2490 Pa. Using the equation for the trendline seen on figure 36 it is found that a differential pressure of 2490 Pa corresponds to a air mass flow of 38.9 g/s. This means that the range of the preconstructed laminar flow meter is too wide because the range should be 0 - 11 g/s. Therefore, it can be concluded from the preliminary test that the dimensions of the laminar flow meter can be changed so that the range is smaller and thus more suitable for the application in the engine. This is done by increasing the pressure loss through the laminar flow element by decreasing the cross-section area. The diameter of the laminar flow meter was changed from 48.6 mm on the preconstructed flowmeter to 37.9 mm on prototype 1. All other core dimensions were kept the same.

On figure 37 the calibration measurements of prototype 1 can be seen. Here, it is seen that all measurements are approximately on a straight line and the  $R^2$  - value is close to 1. Also, the measurement's small deviations from the trendline are random - no trend is seen in the residuals. This means that the air flow is laminar and thus the capillary tubing is functioning properly. The unit of the x-axis is changed from pascal to volts because the 164PC01D37 sensor is used instead of the differential pressure meter. At 7.45 volts the sensor reached its limit which results in the vertical line of measurements. As it is seen, the range of prototype 1 is -0.25 - 2 g/s. This is too narrow for application in the engine. The reason why the range has become so narrow when the cross-section area is not even halved is that the ductility of the aluminium foil made the foil very difficult to corrugate. As a consequence, the hydraulic diameter of the capillaries became much smaller than expected and the pressure loss became too big.

To obtain a wider range than 0 - 2 g/s, prototype 2 was made using brass foil so that the corrugation would be more successful. All dimensions were equal to prototype 1. The range of prototype 2 was -1.2 - 7 g/s (from figure 57 in appendix D). From this it can be concluded that the hydraulic diameter of the capillaries had increased resulting in a lower pressure loss and thus

a wider range of mass flow. However, the range was still too narrow. This is because of the unexpected observed difference in hydraulic diameter between the brass foil prototypes and the preconstructed laminar flow meter. To further increase the mass air flow range, prototype 3 was made with a tube length between the pressure tabs of 35 mm instead of 65 mm. The pressure loss is proportionally dependant on the tube length (equation 9), hence this reduction would theoretically increase the range to  $((-1.2, 7) \text{ g/s} \cdot \frac{65}{35}) = -2.2 - 13 \text{ g/s}$  which would be the proper range. All other dimensions were kept the same as prototype 2.

The range of prototype 3 was -2.2 - 12 g/s (figure 58, appendix D) which is 7 % from the expected range. This deviation is acceptable and is caused by the inconsistency in the manual manufacturing process used by the author of this report. A process which he did not have any previous experience with.

A range of -2.2 - 12 g/s should be sufficient to cover the whole range of the engine operation. The measurements of the calibration test are approximately located on a straight line, with no serious trends among the residuals, and the  $R^2$  value of 0.9994 is sufficiently close to 1 to conclude that the flow in the sensor is laminar and the sensor is capable of measuring the volume flow. Therefore, the experiment was taken to the next step; Volume flow measurements in a testing stand.

The results without a plenum can be seen on figure 39 and on figure 62 in appendix D. On figure 39, the volume flow occurring in the intake phase can be seen as a definite decrease in the voltage signal. The pressure pulsations due to pumping fluctuations can also be seen as damped oscillations occurring after the intake phase. It can be seen on the graphs in figure 62 that the pressure pulsations are smaller in amplitude than the intake volume flow until the engine revolution speed reaches 2000 RPM. Here, the pulsations have just as big of an amplitude as the intake volume flow, hence it is no longer the volume flow of the engine that dictates the range of the laminar flow meter. Especially because the pressure pulsations create just as big of a back flow as a forward flow in contrast to the intake volume flow which only goes in one direction. This means that the amplitude of the pressure pulsations is just as big in the positive y-direction as in the negative y-direction. At 2500 RPM (figure 39) it is seen that volume flow in the intake phase is significantly decreasing the voltage signal to below 0 volts which is the limit of the range of the sensor. If the pressure tubes had been interchanged the volume flow of the intake phase would have increased the voltage signal instead of decreasing it and thus the sensor would not have reached its limit during the intake phase. It would however still have reached its limit after the intake phase because the pressure pulsations have a higher amplitude than the intake volume flow when the engine rotation speed is 2500 RPM. At 2500 RPM the experiment was discontinued to prevent damaging the 164PC01D37 sensor.

From the measurements it can be concluded that a range of -2.2 - 12 g/s is still not enough because of the large pressure pulsations. Either the range has to be increased or the pulsations through the sensor have to be damped. To damp the pulsations, a plenum was installed between the sensor and the engine. On figure 39, the volume flow at 2500 RPM with and without a plenum can be seen. It is seen that the plenum is effectively reducing the amplitude of the pulsations. Therefore, it was now possible to test the laminar flow meter at higher engine speeds.

The frequency of the pressure pulsations is around 27 kHz and the period is around 2.2 ms. These values are found by counting pulsations in a given period of time on figure 39, 40, and 62. The frequency is important when designing the LabVIEW code for calculating the air flow in the ecocar. The final output of the laminar flow meter when implemented in the ecocar is an average of laminar flow meter measurements for a whole combustion cycle. Now, when the frequency is known, the time between measurements can be determined so that it is ensured that enough measurements are used to obtain the correct average in air flow. This is critical because the pressure pulsations have a high frequency, hence the LabVIEW program might not be capable of doing enough measurements in each pressure pulsation period. The time is set to 50  $\mu$ s which results in ( $\frac{2200 \mu\text{s}}{50 \mu\text{s}} =$ ) 44 measurements in each pressure pulsation period which is sufficient to obtain a precise enough average in air flow signal for a whole combustion cycle.

Because of resonance in the intake pipe, the signal peaks around 3500 RPM as seen on figure 40. Here, the limit of 0 V and the limit of 7.5 V are both reached. It is seen, that during resonance, at a certain time during the intake phase, the pressure pulsations create a backflow powerful enough to completely even out the intake air flow. This results in an intake air flow of 0 g/s at a certain point in the intake phase. That no air is being pumped into the engine at a certain point in the intake phase is of course very critical for the volumetric efficiency and thus critical for IMEP and thus ultimately the fuel conversion efficiency. In contrast to the filling dynamics at 3500 RPM, is the filling dynamics at 5000 RPM where it is seen that the volume of air pumped into the engine (the area below the curve in the intake phase) is much higher resulting in a higher volumetric efficiency.

When the engine speed goes higher than 3500 RPM, the maximum peak decreases. However, the peaks of the pressure pulsations keep on increasing as the engine speed increases. At 5000 RPM the amplitude of the pressure pulsations is almost as big as the amplitude of the intake air flow signal. The amplitude from the pressure pulsations is however, in contrast to the intake air flow amplitude, just as big in the positive y-axis direction as in the negative y-axis direction. This means that the range is still not wide enough or the pressure pulsations need to be further damped. Because of the inconvenience in a bigger plenum and because the pumping loss is

lowered if the pressure loss is lowered, the cross-section area of the laminar flow element was changed from 37.9 mm to 52.0 mm without changing the corrugation depth.

This resulted in a range of prototype 4 of -3.2 - 25 g/s (figure 59). This would be the ideal range if the range was symmetric around the offset - if the range was just as high for back flow as for forward flow (which means around -12.5 - 12.5 g/s). This was not the case as the offset was 1.2 V out of 7.5 V. This problem was however solved by changing the differential pressure sensor from the 164PC01D37 model to a 164PC01D36 model. Unfortunately this sensor was not available, hence a 143PC03D model had to be used instead. This sensor was about half as sensitive and thus the range was doubled. This means that the pressure loss of the laminar flow element should be doubled again to obtain the more suitable range of around -12.5 - 12.5 g/s. However, from the experiment in the testing stand it was seen that no noise problems were present, hence a decrease in sensitivity was not a problem. Also, because of the plenum, the dimensions of the laminar flow meter made the diameter of 52.0 mm a natural choice. According to the performance specification it is also desirable to keep the pressure loss as low as possible. Therefore, it was decided not to change the dimensions of the laminar flow meter even though the sensor was replaced. The range with the new sensor can be seen on figure 60.

Now, it had to be tested whether prototype 4 had a range suitable for the ecocar engine or the range was too big resulting in imprecise measurement with too much noise. However, prototype 4 was a fragile construction, subject to measurement errors when used in a vibrating environment such as the real car. Especially vibrations of the pressure tubes would be undesirable because this would change the pressure inside of the tubes. To make a more robust solution, in agreement with the performance specification, a laminar flow element with the same core dimensions as the prototype 4 was constructed using rapid prototyping, where the pressure tubes were replaced with rigid canals and an integrated part of the laminar flow element was a box for the electronic components. A sketch of the prototype 5 can be seen on figures 68, 69, and 70 in appendix F.

The calibration test of prototype 5 can be seen on figure 38. It is seen that all measurements are approximately placed on a straight line and that the  $R^2$  value is acceptably close to 1. A vague trend among the residuals is seen - at high and low voltage the measurements in general lie below the trend line while the measurements around 3.4 V lie above the trendline. This trend is not good and indicates that the correlation is not completely linear. Possible explanations are that the construction is not completely gas impermeable or the flow is not completely laminar. Even though the correlation is not completely linear, the linearity is still acceptable and the experiment was taken to the last phase; testing in the ecocar.

On figure 41, the final output of the laminar flow meter can be seen together with the engine

rotation speed. It is seen that the output increases with increasing engine speed as expected. One can get an indication of the response time of the laminar flow meter by looking at the fluctuations in engine speed occurring at 1848 s og 1852 s. Here, the fluctuations in engine speed result in an instant fluctuation in voltage signal, hence the response time of the laminar flow meter is fast. From the figure it is also seen that the maximum air flow for a combustion cycle corresponds to a signal of 2.62 V. Using the trendlines of figure 38 it is found that this corresponds to a mass flow of 2.38 g/s. Because the intake phase is only 1 out of 4 phases, this means that the maximum air flow is  $2.38 \cdot 4 = 9.52$  g/s. This corresponds well to the estimated required range of 0 - 11 g/s, especially when noting that the estimated required range was calculated using a volumetric efficiency of 1 to ensure that the actual range was not wider than the estimated. Using the trendline of figure 61 it is seen that a mass flow of 9.52 g/s corresponds to a pressure loss of 755 Pa. This means that the maximum pressure loss (not the average pressure loss which of course is lower) is 1.16 % of the pressure in the inlet manifold of (at least) 65000 Pa. This is a small percentage, however, it is not insignificant, hence it clarifies that the laminar flow meter is only useful when it shows significant improvements of the fuel/air ratio.

On figure 42, all laminar flow meter measurements converted to the corresponding fuel mass are plotted together with the actual injected fuel mass. It is seen that the fuel mass according to the laminar flow meter is consistent - at a certain engine speed the deviation in fuel mass is small and there are no outliers. This indicates that the laminar flow meter is reliable.

It is seen that the injected fuel mass is highly dependant on the engine rotation speed. This confirms that the pumping fluctuations are strongly affecting the volumetric efficiency which also was the conclusion of the results from the experiments carried out in the test stand. The volumetric efficiency as a function of engine rotation speed can be seen on figure 66 on page 91.

This test of the ecocar was carried out when the fuel map was still not very well developed. To get an indication of how useful the laminar flow meter is, the fuel mass according to the laminar flow meter is compared to the actual fuel mass adjusted to the measured  $\lambda$ -values. This comparison can be seen on figure 43. The fuel mass according to the laminar flow meter is in general higher than the adjusted actual fuel mass. An explanation could be that the laminar flow meter method still does not take into account all the problems of transient engine control, for example the wall wetting phenomenon. The response time and the time constant involved in the evaporation of the fuel film are however expected to be insignificant because the fuel is sprayed directly on the intake valves which are warm during the whole test run. Thus the wall-wetting phenomenon cannot explain the difference in fuel masses.

Another explanation could be manifold filling phenomenon. The intake manifold filling dy-

namics is dependant mainly on the plenum volume and the engine speed. Because of the plenum volume of prototype 5, a time delay between the flow into the manifold (where the laminar flow meter is placed) and the flow out of the manifold (the combustion chamber) can occur. This does however not seem to be a problem because the laminar flow meter curve is displaced in the vertical direction (the fuel mass according to the laminar flow meter is in general higher than the adjusted actual fuel mass) instead of the horizontal direction which would be expected if the displacement was due to a time delay.

It must be noted that the adjusted actual fuel mass is only an approximation to the fuel mass required for the optimal air/fuel ratio. If this approximation was the correct fuel mass it would not have required 2 preliminary calibration tests and 8 calibration tests to create the final engine map (which still did not provide perfect fuel/air ratio). This is an explanation as to why the adjusted actual fuel mass and the fuel mass according to the laminar flow meter do not match perfectly.

Even though the adjusted actual fuel mass and the fuel mass according to the laminar flow meter are not coincident, they closely follow the same trend which, combined with the fact that the adjusted actual fuel mass does not correspond to perfect fuel/air ratio control, indicates that the laminar flow meter provides a reliable estimate of the required amount of injected fuel. Therefore, it should be possible to obtain proper  $\lambda$  control using the laminar flow meter constructed in this project. Unfortunately,  $\lambda$  control was not the only thing which needed to be optimised in the car, hence the possibilities of testing the car were limited because the car had to be constructed and afterwards modified prior to and after the testing of the  $\lambda$  control system. This combined with the many technical difficulties encountered when working with and modifying such a complex machine as the ecocar resulted in that the  $\lambda$  control using the laminar flow meter was not tested further because of a time pressure. Therefore, final implementation of the laminar flow meter for  $\lambda$  control will be subject to further work.

Another possibility than directly implementing the laminar flow meter to control the injection pulse length is to create the fuel map using the laminar flow meter. This way, the control system is not dependant on laminar flow meter during execution. Instead the creation of the engine map can be carried out more efficiently because the shape of the engine map can be quickly unravelled as seen on figure 42 using the laminar flow meter.

The laminar flow meter experiment did however give useful results. Other than showing that the flow meter provides a reliable estimate of the required fuel mass, the measurements have shown that the pressure pulsations make the volumetric efficiency depend highly on the engine rotation speed. On figure 42 and figure 66, it is found that the volumetric efficiency is low at a engine rotation speed from 2500 RPM to 4000 RPM. This explains why the speed-density control system used in 2012 did not work properly. In this system, the injected fuel mass was almost

constant as a function of engine rotation speed. Therefore, the  $\lambda$ -value became too high when the engine speed was below 2500 RPM and above 4000 RPM. Here, the volumetric efficiency rose and a lot of air was pumped into the engine.

In 2013 the gear ratio of the car has also sought to be improved. By making the car have a high speed and a low engine rotation speed, the friction losses are reduced (for example, the power consumption due to friction in a journal bearing is dependant of the square of the rotation speed [24, equation (9.5)]). In this project it is seen that one should take care when changing the gear ratio to reduce engine rotation speed because low engine rotation speed results in a lower volumetric efficiency and thus ultimately a lower fuel conversion efficiency of the engine. To be able to obtain a higher volumetric efficiency at low engine speed the filling dynamics of the engine have to be modified, for example by changing the camshaft of the engine so that the duration and timing of the valve openings are optimised.

### Conclusion

In this experiment a laminar flow meter with the proper dimensions for application in the ecocar has been designed, constructed, and tested. From this experiment the following observations were made:

- For the best result with the capillary tubing, brass foil should be used instead of aluminium foil because aluminium is too ductile.
- The core dimensions of a suitable laminar flow meter were an inner diameter of 52.0 mm and a tube length between pressure tabs of 35 mm.
- The maximum pressure loss of the laminar flow meter was 755 Pa which was 1.16 % of the minimum pressure in the intake manifold. The mass of the laminar flow meter was 350g.
- Because the engine only had one cylinder, large pressure pulsations were present in the intake pipe. The frequency of the pulsations was around 27 kHz. By having the LabVIEW program measure the air flow signal each 50  $\mu$ s a sufficient number of measurements were obtained for accurate calculations of the average.
- A small plenum was effective in reducing the amplitude of the pressure pulsations.
- The pressure pulsations make the volumetric efficiency strongly dependent on the engine rotation speed. Between 2500 RPM and 4000 RPM, the volumetric efficiency is low, affecting the fuel conversion efficiency negatively.
- The output of the final laminar flow meter was reliable and with a fast response time.

- By comparing the fuel mass according to the laminar flow meter with the adjusted actual fuel mass it was found that the laminar flow meter provided realistic fuel mass proposals for proper  $\lambda$  control.
- It is found that the laminar flow meter also can be used to facilitate the creation of the engine fuel map.

It was never tested if the laminar flow meter was actually capable of proper  $\lambda$  control, hence it cannot be finally concluded whether or not a control system using the laminar flow meter will be able to comply with the given performance specifications. From the above it can however be concluded that it is strongly indicated that a  $\lambda$  control system based on the laminar flow meter would be accurate and reliable.

## 11 Further work

As it is seen from the results of the Shell Eco Marathon 2013, there is still work to be done before the  $\lambda$ -value is 1.1 at all times. The simple engine map combined with simple  $\lambda$  control proved to be a good solution. To obtain better  $\lambda$ -values, the simple engine map should be further calibrated. The results of the laminar flow meter experiments show that the air flow measurements from the flow meter should be used in this calibration process to make the process less time demanding and more accurate. Also, as mentioned earlier, the LabVIEW code for the simple closed-loop  $\lambda$  control has to be redesigned so that it works as intended.

From the description of the Shell Eco Marathon 2013 it is also seen that the oil temperature at the beginning of the race was normally 55 °C because it was not possible to heat the oil in around 10 minutes up to the race. The oil temperature for optimum performance is 70 °C [19], hence a method for heating the oil in the last 10 minutes prior to the race should be found.

A control system based on the laminar flow meter showed promising results. However, the solution was never implemented, thus a control system where the fuel injection length is determined by laminar flow meter measurements has to be tested. It is also worthy of noticing that the pressure loss in the laminar flow meter can, in worst case, reach 1.16% of the pressure available in the inlet manifold. Therefore, an experimental comparison of the fuel usage of the DTU ecocar when using an engine map control system and using a laminar flow meter control system would be useful to determine which control system is gives the best fuel economy.

Experimental comparison of the two different control systems is not the only test which would produce valuable results. In 2013 the DTU ecocar was not completely finished until the night before the Shell Eco Marathon. Therefore, not much time for testing was available, hence too many variables had to be tested at once and the amount of tests were insufficient. Therefore, a more stable and fuel economic performance of the car can be obtained by gathering more knowledge by testing.

The pressure loss in the laminar flow meter can also be minimised further. In the final laminar flow meter the most sensitive pressure sensor was not used. By using a more sensitive sensor and simultaneously reduce the pressure loss across the capillary tubing (by increasing the cross-section diameter or decreasing the tube length), the same measure range can be obtained as in prototype 5, yet with a lower pressure loss.

Another important field for further work is optimisation of the volumetric efficiency. As seen from the results, the volumetric efficiency is low at an engine rotation speed between 2500 RPM and 4000 RPM. This is the interval in which the engine is operating, thus it is important that the volumetric efficiency is large in this interval. The volumetric efficiency could be optimised for example by modification of the camshaft axle.

## 12 Final conclusion

Different approaches for electronic control of the air/fuel ratio has been discussed and evaluated through experiments.

It was found that the speed-density control system used at the Shell Eco Marathon 2012 was highly dependant on calibration and was not capable of meeting the requirements from the performance specification. This was mainly because this control system was using a constant volumetric efficiency. From the laminar flow meter experiment it was shown that the volumetric efficiency is highly dependant on the engine rotation speed.

The transient driving strategy of the ecocar combined with a slow response time of the WBO<sub>2</sub> resulted in that normal closed-loop  $\lambda$  control was not tested. Instead a modified version of closed-loop  $\lambda$  control was tested together with a simple engine map. It was found that the creation of the engine map was time demanding. It was also found the simple closed-loop  $\lambda$  control did not work as planned. However, the control system consisting of a simple engine map and simple closed-loop control was capable of meeting the requirements from the performance specification. This entails that the system was capable of responding well under transient conditions and capable of making the  $\lambda$  value be within the interval of 1.0 - 1.2. Also, it entails that the system was robust and consistent and was always able to perform during the races. Therefore, it can be concluded that this control system is a good choice for accurate air/fuel ratio control in a single-cylinder combustion engine when performing similar accelerations repeatedly as in the Shell Eco Marathon. By programming the closed-loop system so that it works as intended and by further calibration of the engine map, the system can be further improved.

Another way of further improving the system is by implementation of a laminar flow meter. This conclusion is based on the laminar flow experiment which showed that a laminar flow meter designed for the ecocar was measuring reliably, with a fast response time, and provided a realistic proposal for the required fuel mass for proper  $\lambda$  control. It was also found that the laminar flow meter can be used to facilitate the creation of the engine map. Instead of using numerous calibration tests to define the shape of the injection length curve, the laminar flow meter measurements of the air flow can be used.

## References

- [1] International Energy Agency. *TRANSPORT, ENERGY AND CO<sub>2</sub>: Moving Toward Sustainability*. International Energy Agency, 2009.
- [2] International Energy Agency. *CO<sub>2</sub> EMISSIONS FROM FUEL COMBUSTION - HIGH-LIGHTS*. International Energy Agency, 2012.
- [3] C. F. Aquino. Transient a/f control characteristics of the 5 liter central fuel injection engine. *SAE Technical Paper*, 810494, 1981.
- [4] Alain Chevalier, Christian Winge Vigild, and Elbert Hendricks. Predicting the port air mass flow of si engines in air/fuel ratio control applications. *SAE Technical Paper*, 2000-01-0260, 2000.
- [5] Scancon Industrial Encoders Denmark. Specifications, type sca50. <http://www.scancon.dk/specifications/SCA50-specifications.pdf>, Visited: June 26th 2013.
- [6] Ernest O. Doebelin. *Measurement systems application and design, 4th edition*. McGRAW-HILL INTERNATIONAL EDITIONS, 1990.
- [7] Horst Bauer et al. *BOSCH Automotive Handbook 5th edition*. SAE society of Automotive Engineers, September 30th 2000.
- [8] Lino Guzzella. Automobiles of the future and the role of automatic control in those systems. *Annual Reviews in Control*, 33(1):1–10, 2009.
- [9] Elbert Hendricks. *Associate Professor, DTU*. personal communication, March 2013.
- [10] Honeywell International Inc. *Environmental condition sensors, Catalog 15*. Honeywell, September 1998.
- [11] Mike Kojima. Air-fuel meter shootout. [http://www.2gnt.com/documents/teklein\\_Wideband\\_Shootout.pdf](http://www.2gnt.com/documents/teklein_Wideband_Shootout.pdf), Visited: May 31st 2013.
- [12] Jacob Mac Rygaard. Optimization of the fuel/air ratio in an si engine. Technical report, DTU, June 31st 2012.
- [13] Innovate Motorsports. How wideband sensors work. <http://www.innovatemotorsports.com/resources/news3.php>, Visited: May 31st 2013.
- [14] Innovate Motorsports. Mtx-l digital air/fuel ratio gauge user manial. [http://www.innovatemotorsports.com/support/manual/MTX-L\\_Manual\\_1.1.pdf](http://www.innovatemotorsports.com/support/manual/MTX-L_Manual_1.1.pdf), Visited: May 31st 2013.

- [15] Karim Nice. Engine controls and performance chips. <http://auto.howstuffworks.com/fuel-injection5.htm>, Visited: May 5th 2013.
- [16] Keld Grønne Nielsen. *Consultant at Danish Technological Intitute, Employee at Peugeot from 1987 to 2008.* personal communication, May 1st 2013.
- [17] Meriam Instruments Cleveland Ohio. Meriam laminar flow elements. <http://meriam.com/assets/lfedatasheet.pdf>, Visited: June 6th 2013 September 12th 2011.
- [18] Bjarke Ove Andersen and A. Mathies Hjort Jensen. Udvikling og optimering af ethanolmotor. Bachelor project, DTU, July 22nd 2011.
- [19] Hannibal Christian Overgaard. Forbedring af virkningsgrad for firtakts økobilmotor. Final project, DTU, May 2013.
- [20] Prosport Performance. Bosch wideband 5-wire o2 sensor. <http://prosportgauges.com/bosch-wideband-5-wire-o2-sensor.aspx>, Visited: May 31st 2013.
- [21] J A Robison and W. M. Brehob. The influence of improved mixture quality on engine exhaust emissions and performance. *Journal of the Air Pollution Control Association*, 17(7):446–453, 1967.
- [22] Maibrit S. Andersen, Marina Ejlertsen, Nils Refstrup, and Morten Bæk. Motorstyring til økobil 2013. Technical report, DTU, June 28th 2013.
- [23] Shell. Shell eco-marathon europe 2013 - official rules, chapter 2. <http://s09.static-shell.com/content/dam/shell-new/local/corporate/ecomarathon/downloads/pdf/europe/sem-europe-official-rules-chapter-2-180413.pdf>, April 18th 2013.
- [24] Professor Spencer C. Sorensen. *Engine Principles and Vehicles.* Department of Mechanical Engineering, 2008.
- [25] Hongming Xu. Control of a/f ratio during engine transients. *SAE Technical Paper*, 1999-01-1484, May 3-6, 1999.

## A Additional plots concerning the Shell Eco Marathon 2012 final race

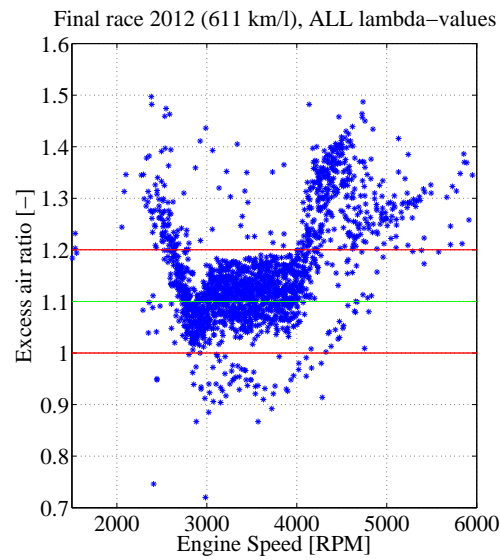


Figure 44: Shell Eco Marathon 2012,  $\lambda$  as a function of  $N$ . All measures  $\lambda$  values are plotted.

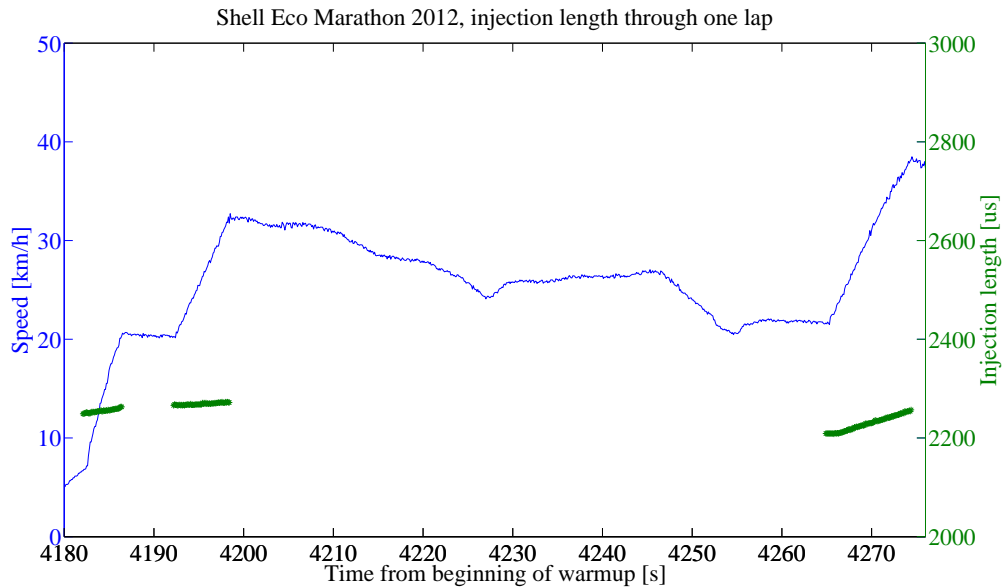


Figure 45: Injection length during one burn 2012.

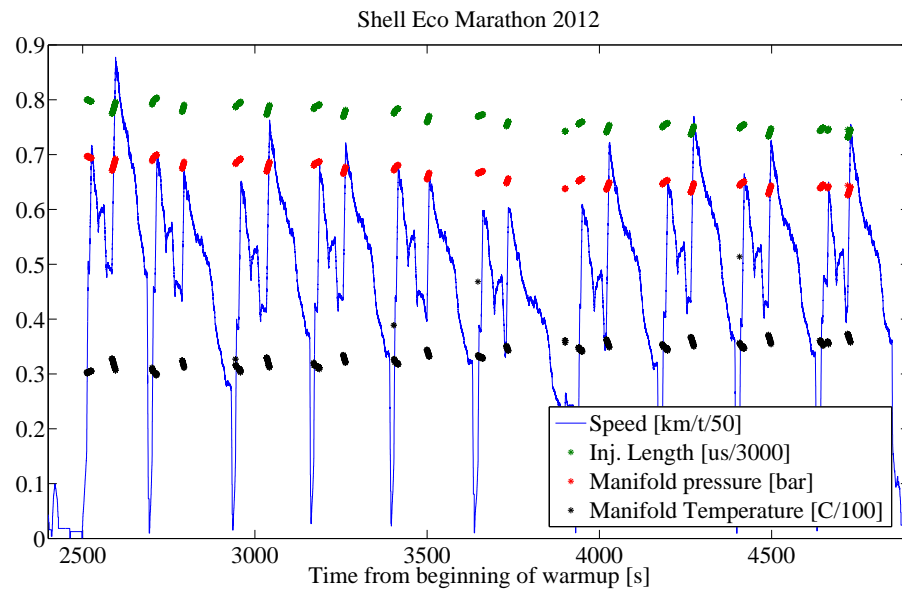


Figure 46: Different values during whole race 2012.

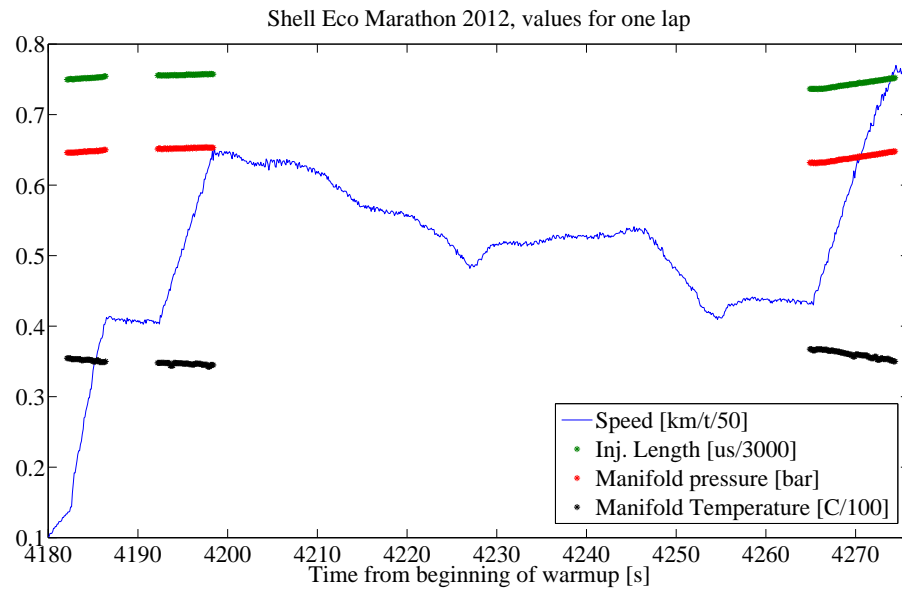


Figure 47: Various values during one burn 2012.

## B Additional plots concerning Shell Eco Marathon 2013

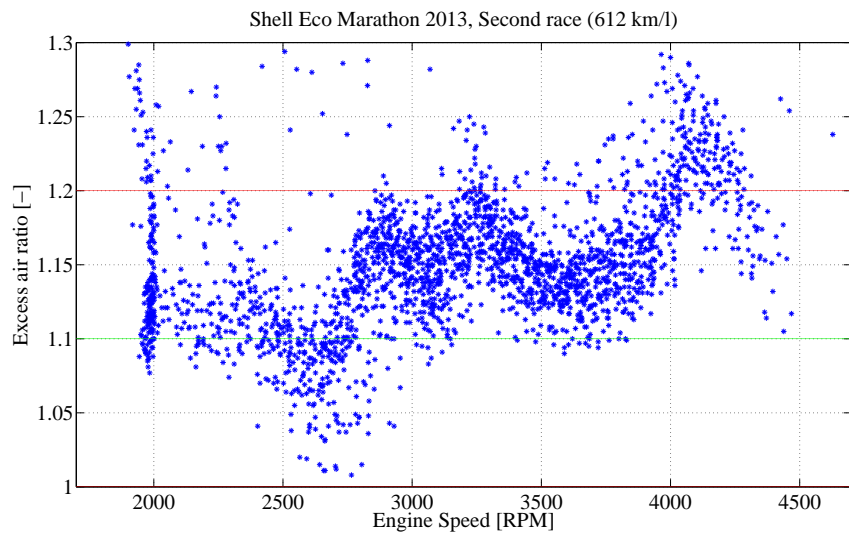


Figure 48:  $\lambda(N)$  2nd race 2013, zoomed plot. All measured  $\lambda$ -values are plotted.

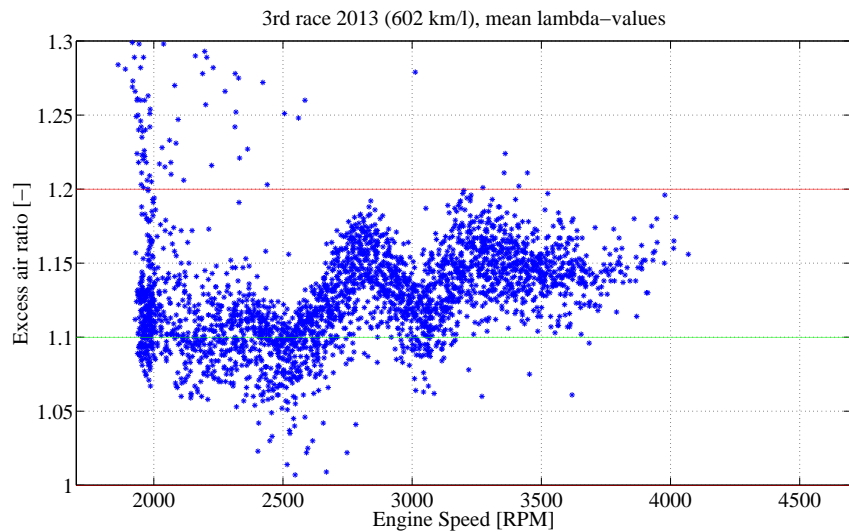


Figure 49:  $\lambda(N)$  3rd race 2013, zoomed plot. All measured  $\lambda$ -values are plotted.

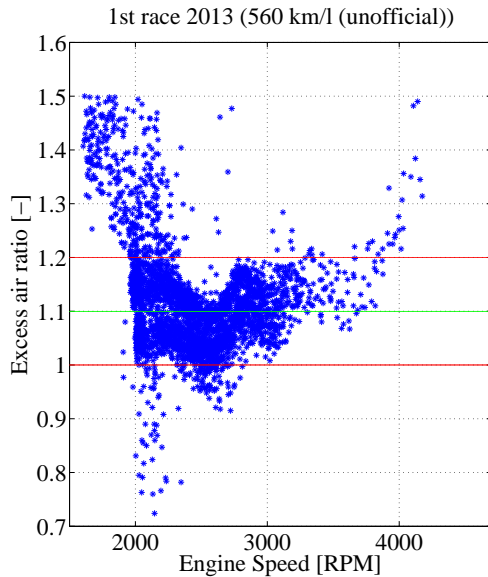


Figure 50:  $\lambda$  as a function of engine speed. 1st race 2013, all values

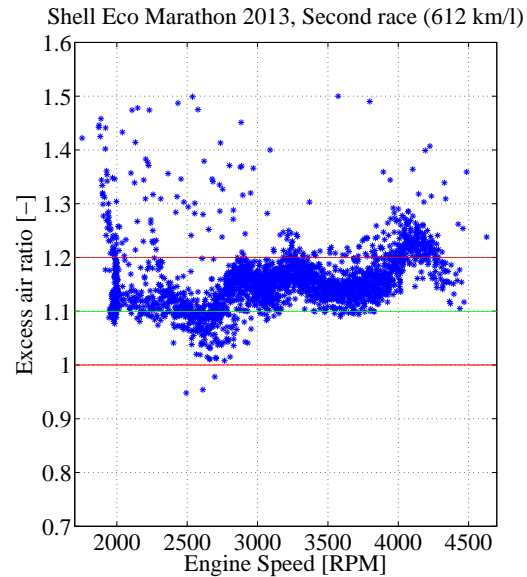


Figure 52:  $\lambda$  as a function of engine speed. 2nd race 2013, all values

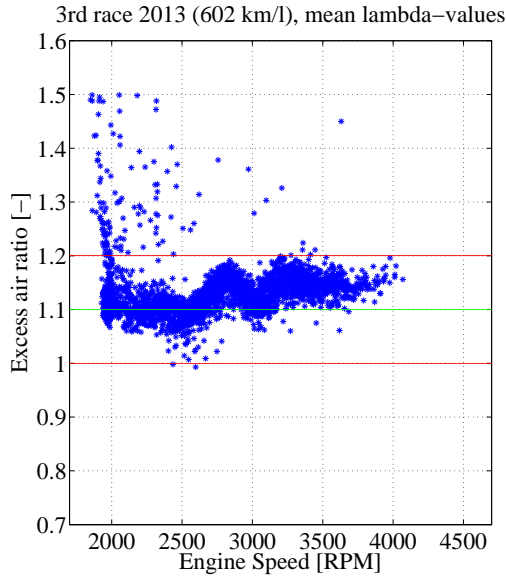


Figure 51:  $\lambda$  as a function of engine speed. 3rd race 2013, all values

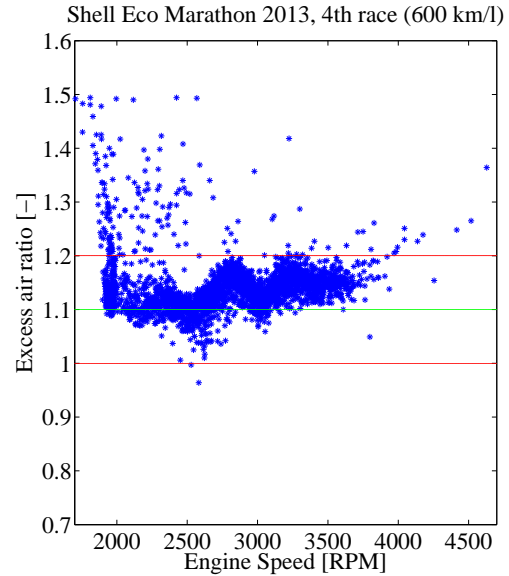


Figure 53:  $\lambda$  as a function of engine speed. 4th race 2013, all values

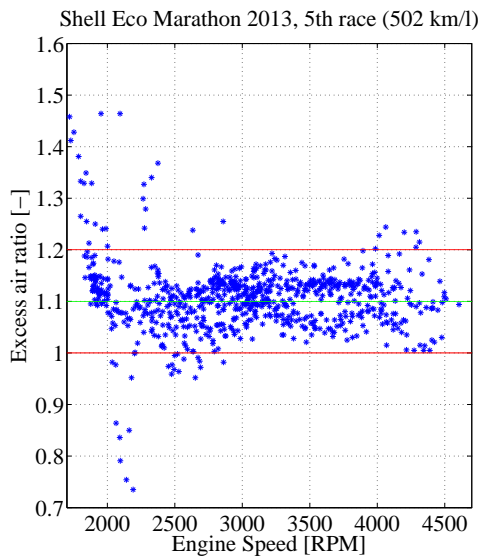


Figure 54:  $\lambda(N)$  5th race 2013. All measured  $\lambda$ -values are plotted.

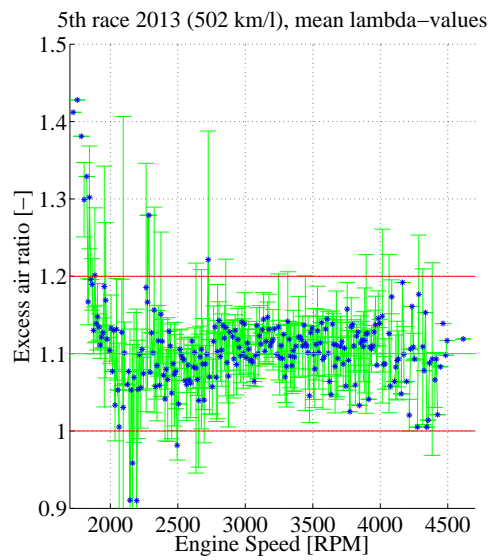


Figure 55:  $\lambda(N)$  5th race 2013. Each point is an average of all  $\lambda$ -values in a range of 10 rpm. The green bar is 2 standard deviations.

## C Deduction of calibration formula

By measuring  $\lambda$  and knowing the fuel mass we can calculate the air mass using:

$$\begin{aligned} \lambda_{measured} &= \frac{FA_s}{FA} \Leftrightarrow FA = \frac{\dot{m}_{f\ measured}}{\dot{m}_{air}} = \frac{FA_s}{\lambda_{measured}} \\ &\quad \Updownarrow \\ \dot{m}_{air} &= \dot{m}_{f\ measured} \cdot \frac{\lambda_{measured}}{FA_s} \Leftrightarrow m_{air} = m_{f\ measured} \cdot \frac{\lambda_{measured}}{FA_s} \end{aligned}$$

The target  $\lambda$ -value is 1.1:

$$\lambda_{target} = 1.1 = \frac{FA_s}{FA} \Leftrightarrow FA = \frac{\dot{m}_f}{\dot{m}_{air}} = \frac{FA_s}{1.1} \Leftrightarrow \dot{m}_f = \dot{m}_{air} \cdot \frac{FA_s}{1.1} \Leftrightarrow m_f = m_{air} \cdot \frac{FA_s}{1.1}$$

Put together we have:

$$m_f = m_{air} \cdot \frac{FA_s}{1.1} = m_{f\ measured} \cdot \frac{\lambda_{measured}}{FA_s} \cdot \frac{FA_s}{1.1} = \underline{m_{f\ measured} \cdot \frac{\lambda_{measured}}{1.1}}$$

## D Additional figures concerning the laminar flow meter experiment

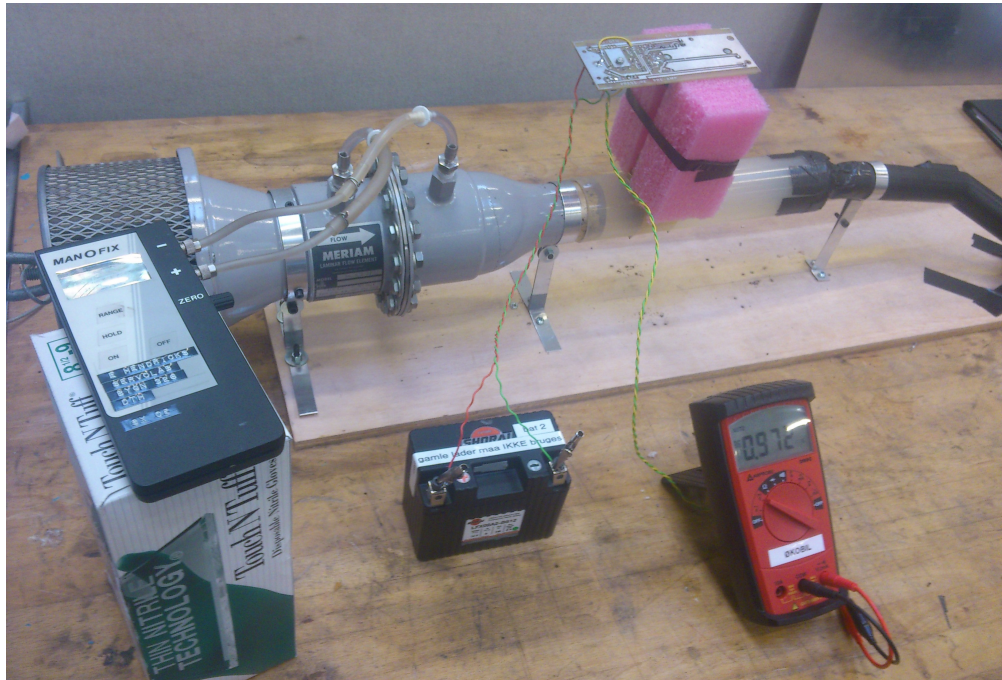


Figure 56: Experimental setup of the calibration test of laminar flow meter prototype 4. The same setup was used for the other prototypes. On this picture it can be seen that no gap is present between flow meter and vacuum cleaner. To obtain an air flow in an appropriate range a gap was made as seen on figure 27.

### Results from the testing stand

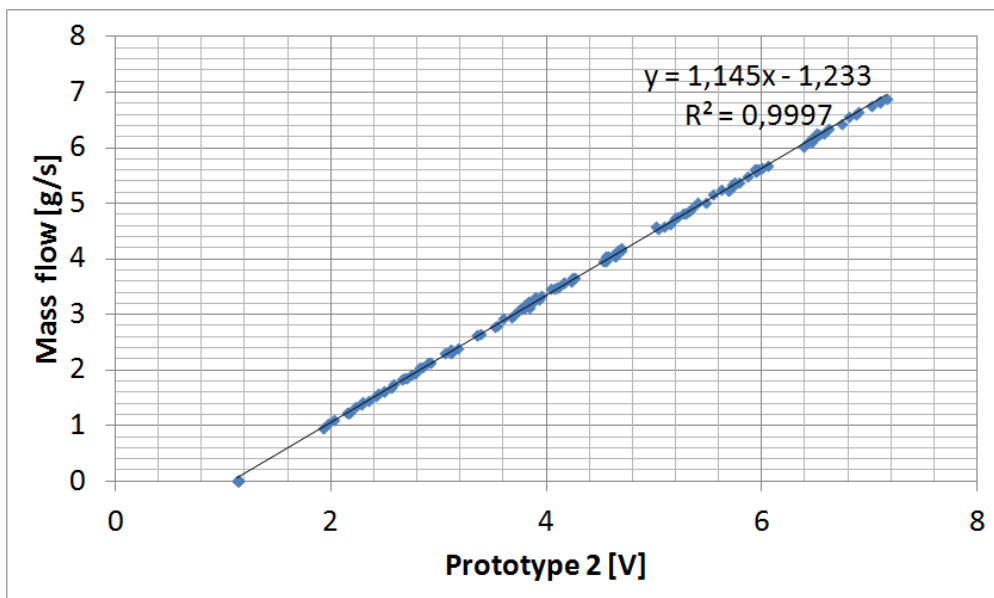


Figure 57: Test of laminar flow meter prototype 2. A 9 V battery was used as power source. The initial voltage of the battery was 8.94, the final voltage was 8.81. The pressure was 1014 hPa and the temperature was 24 °C.

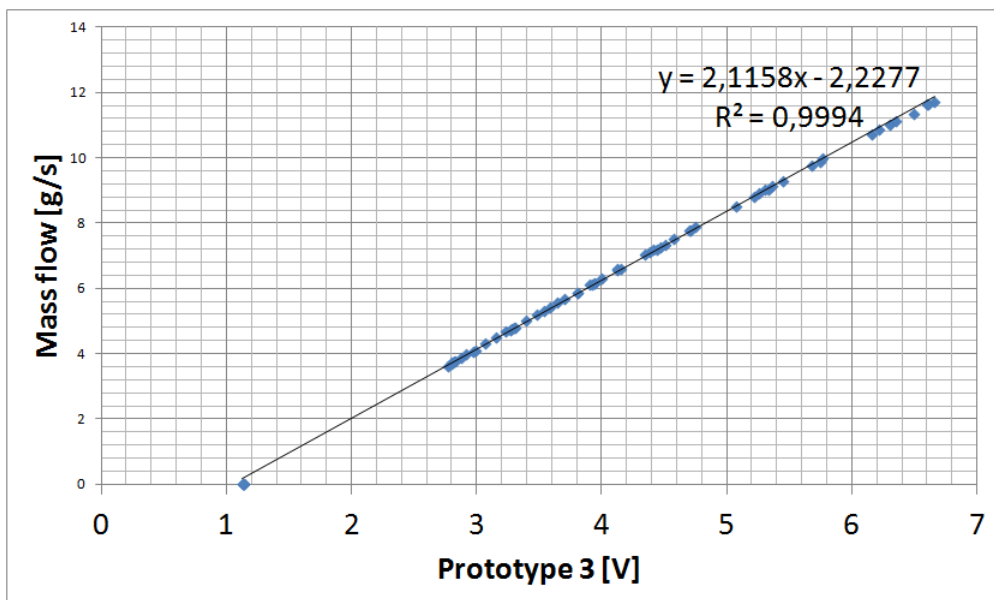


Figure 58: Test of laminar flow meter prototype 3. A 9 V battery was used as power source. The initial voltage of the battery was 8.96, the final voltage was 8.85. The pressure was 1019 hPa and the temperature was 23 °C.

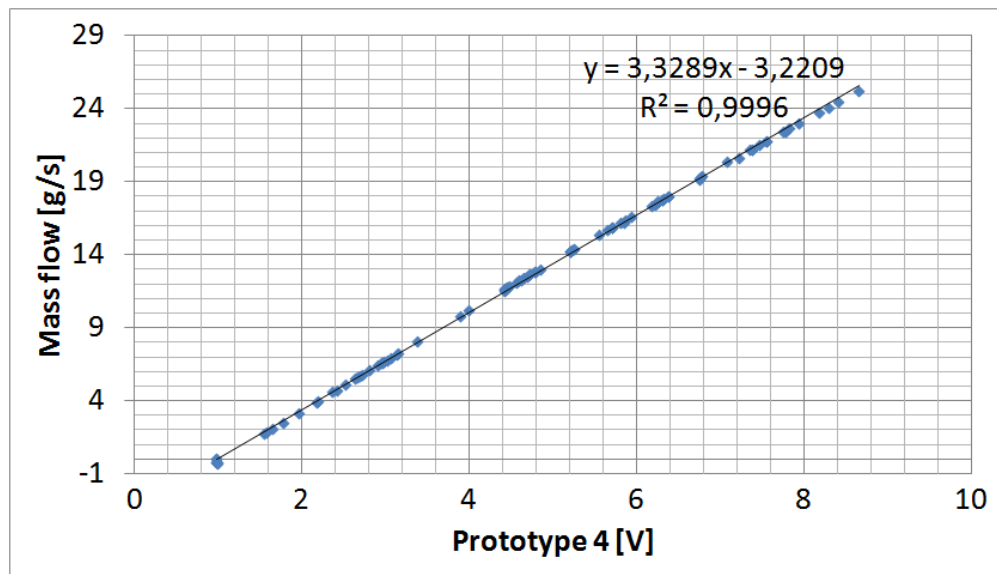


Figure 59: Test of laminar flow meter prototype 4. For this test the final electronic component seen on figure 56 was used. The electronic component was not completely finished, hence the large output voltages. A 12 V battery was used as power source. The pressure was 1011 hPa and the temperature was 25 °C.

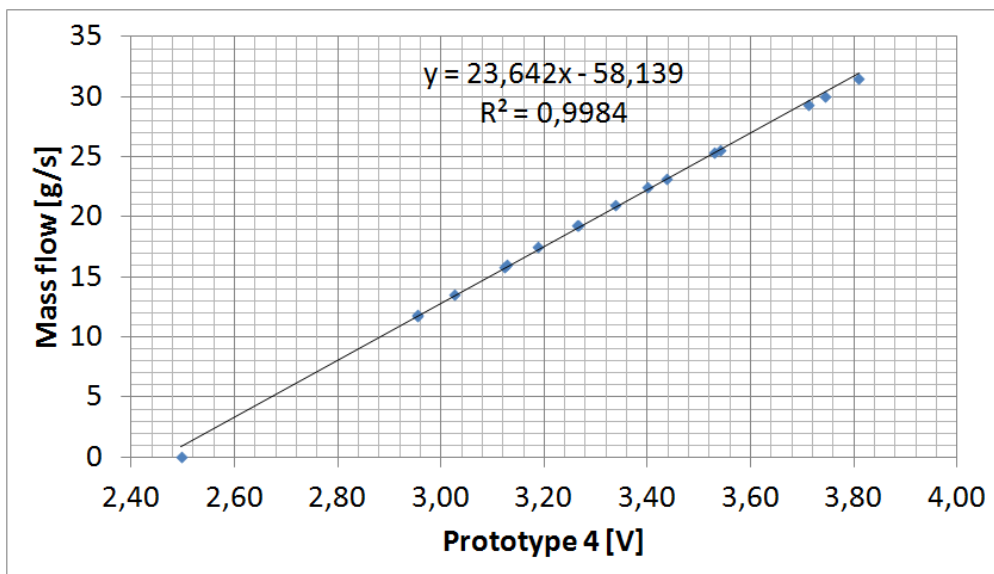


Figure 60: Test of laminar flow meter prototype 4 with a less sensitive differential pressure sensor. For this test the final electronic component seen on figure 56 was used. The electronic component is designed so that the input can be between 10 and 14 V without affecting the output. The output is between 0 and 5 V. A 12 V battery was used as power source. The pressure was 1011 hPa and the temperature was 25 °C.

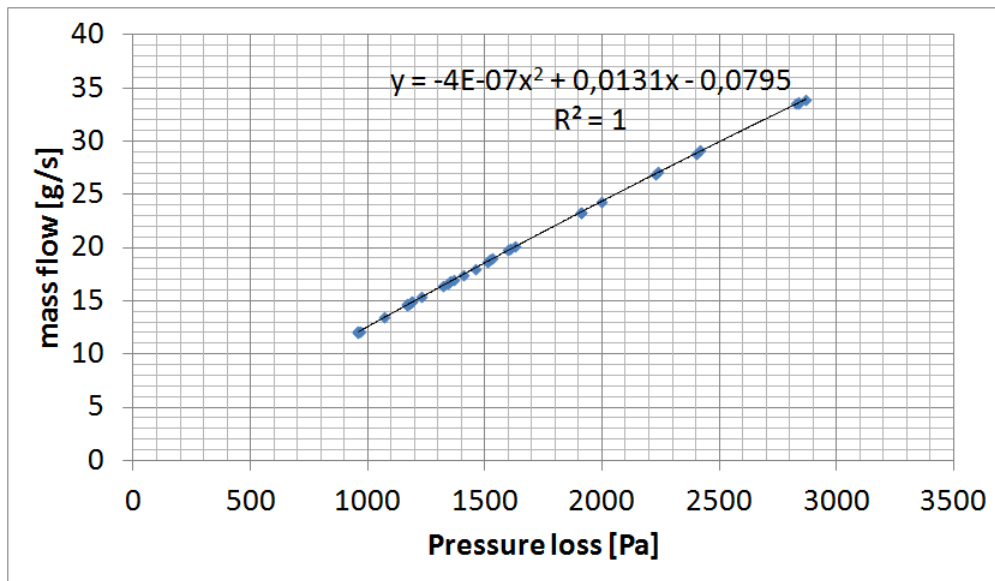


Figure 61: Test of laminar flow meter prototype 5 using a differential pressure meter. The pressure was 1012 hPa and the temperature was 25 °C. The  $R^2$  value of a linear correlation between pressure loss and mass flow was 0.9996.

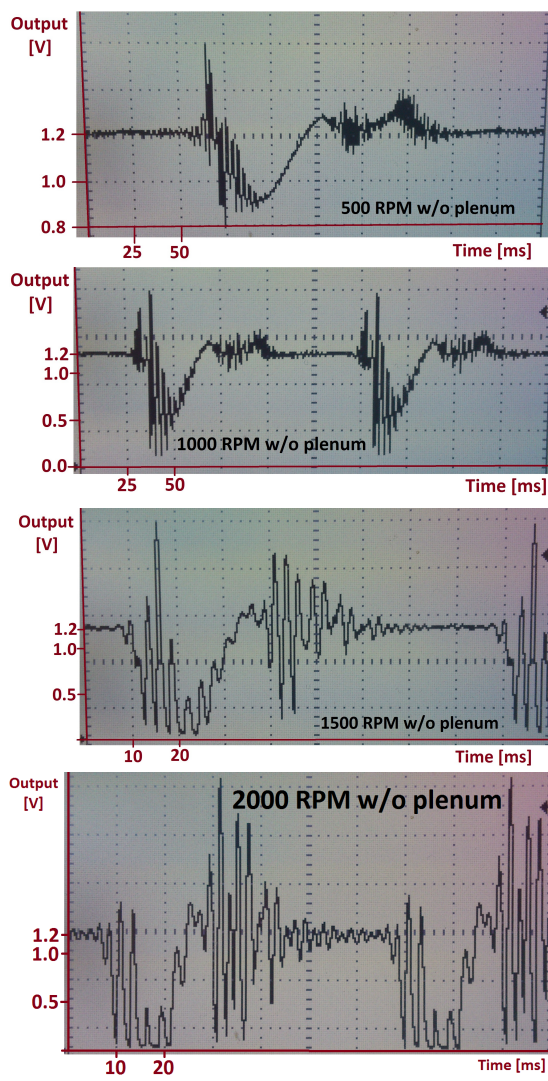


Figure 62: Pressure oscillations measured using prototype 3 without plenum. The offset of the sensor is 1.2 V.

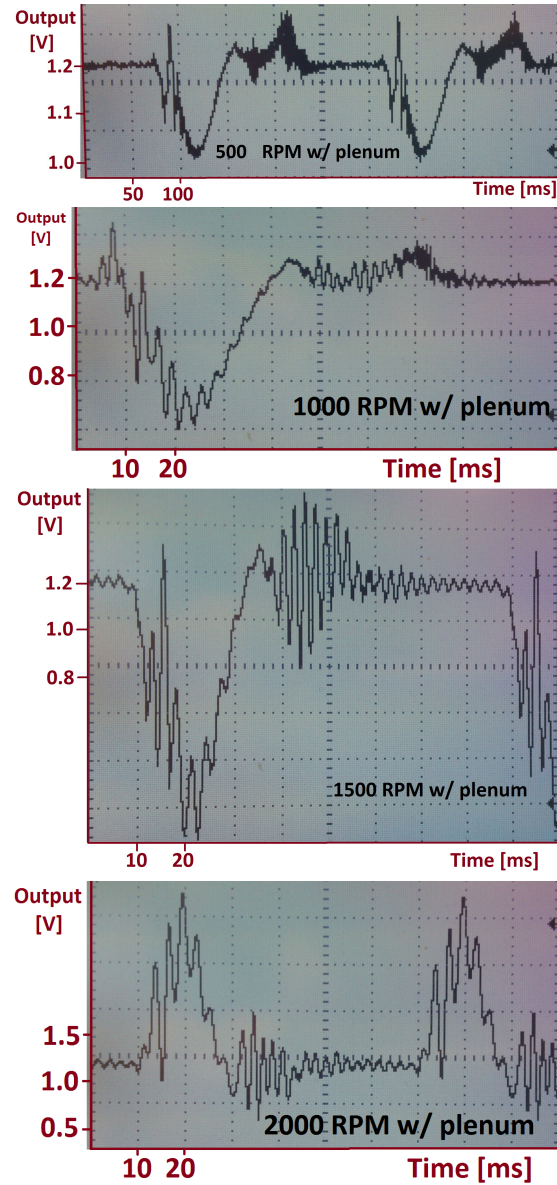


Figure 63: Pressure oscillations measured using prototype 3 with plenum. Between the test at 2000 RPM and the test at 2500 RPM the tubes of the differential pressure sensor was interchanged so that the full range of the sensor was used. The offset of the sensor is 1.2 V.

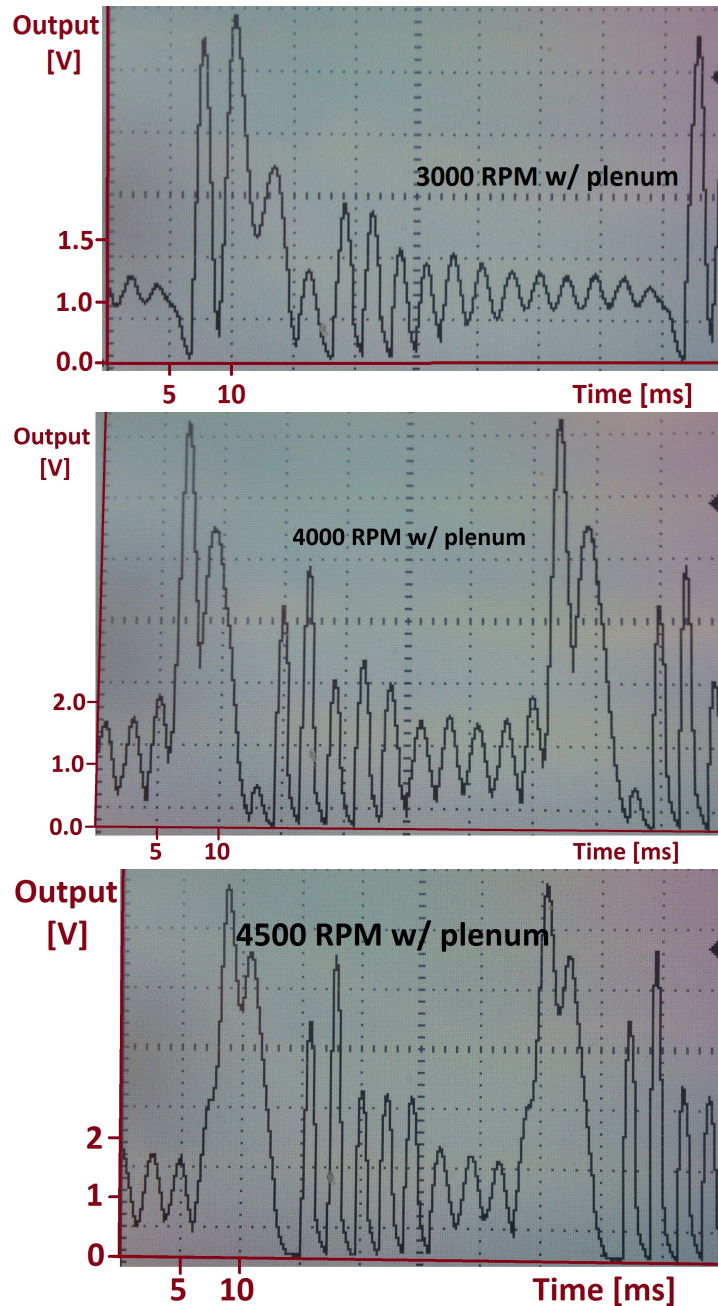


Figure 64: Pressure oscillations measured using prototype 3 with plenum. The offset of the sensor is 1.2 V.

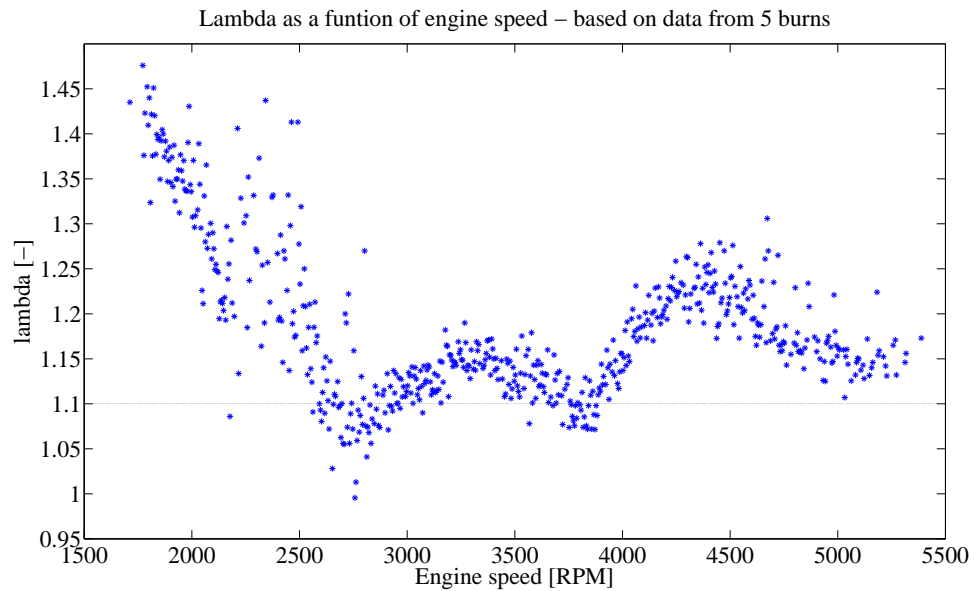


Figure 65:  $\lambda$ -values at outdoor test of laminar flow meter prototype 5.

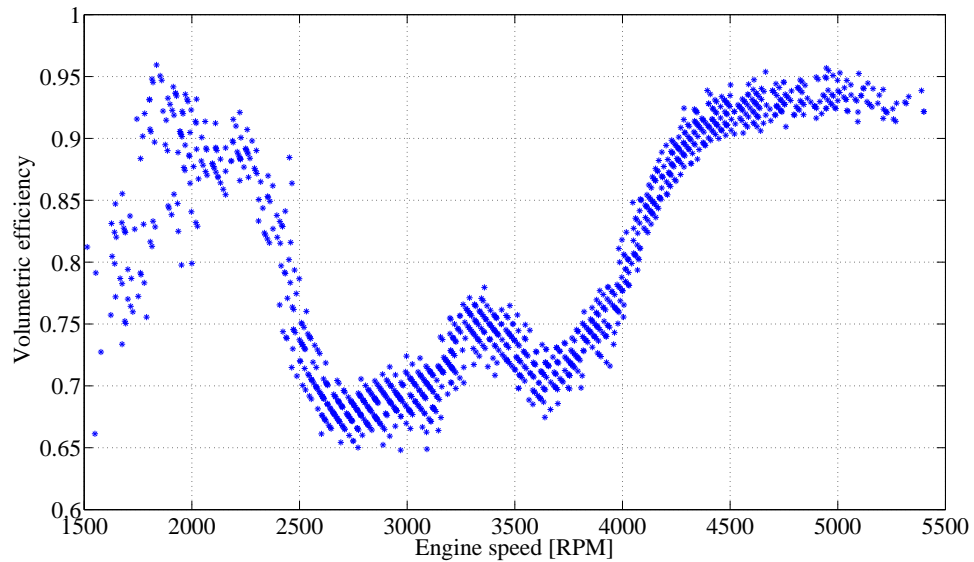


Figure 66: Volumetric efficiency of ecocar engine.

## E Core dimensions of the prototypes

In table 3 the dimensions of the prototypes can be seen. For further details on prototype 5, please see appendix F.

	$\emptyset$	L	A	B	C
<b>Prototype 1</b>	37.9	65	14.25	74	14.25
<b>Prototype 2</b>	37.9	65	14.25	74	14.25
<b>Prototype 3</b>	37.9	35	29.25	44	29.25
<b>Prototype 4</b>	52.5	35	50.5	43.02	146
<b>Prototype 5</b>	52.5	35	50.5	43.02	135.74

Table 3: Core dimensions of prototypes. All values are in millimetres. An explanation of the dimensions can be found in figure 67

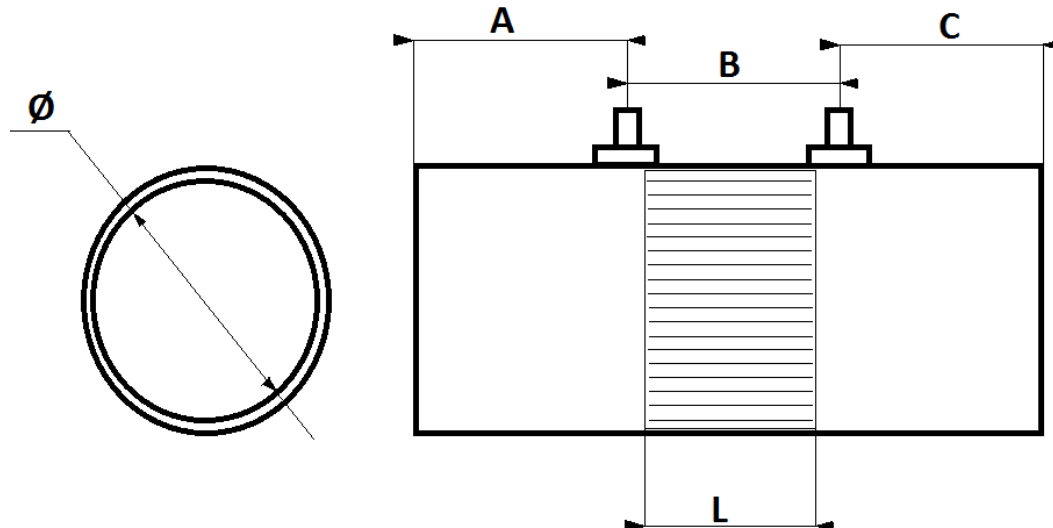


Figure 67: Sketch of prototype with core dimensions

## F Prototype 5 drawings and dimensions

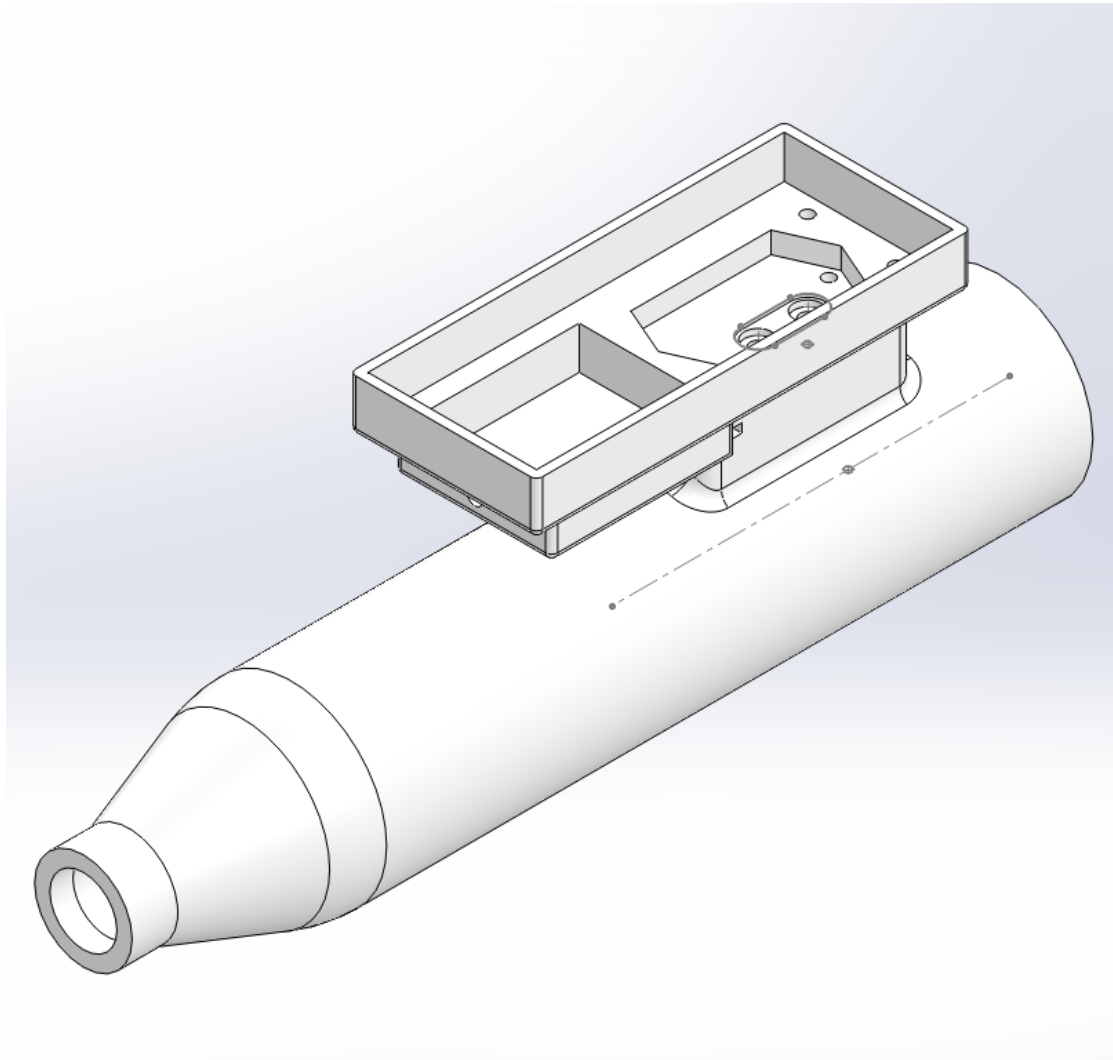


Figure 68: Drawing of laminar flow meter prototype 5

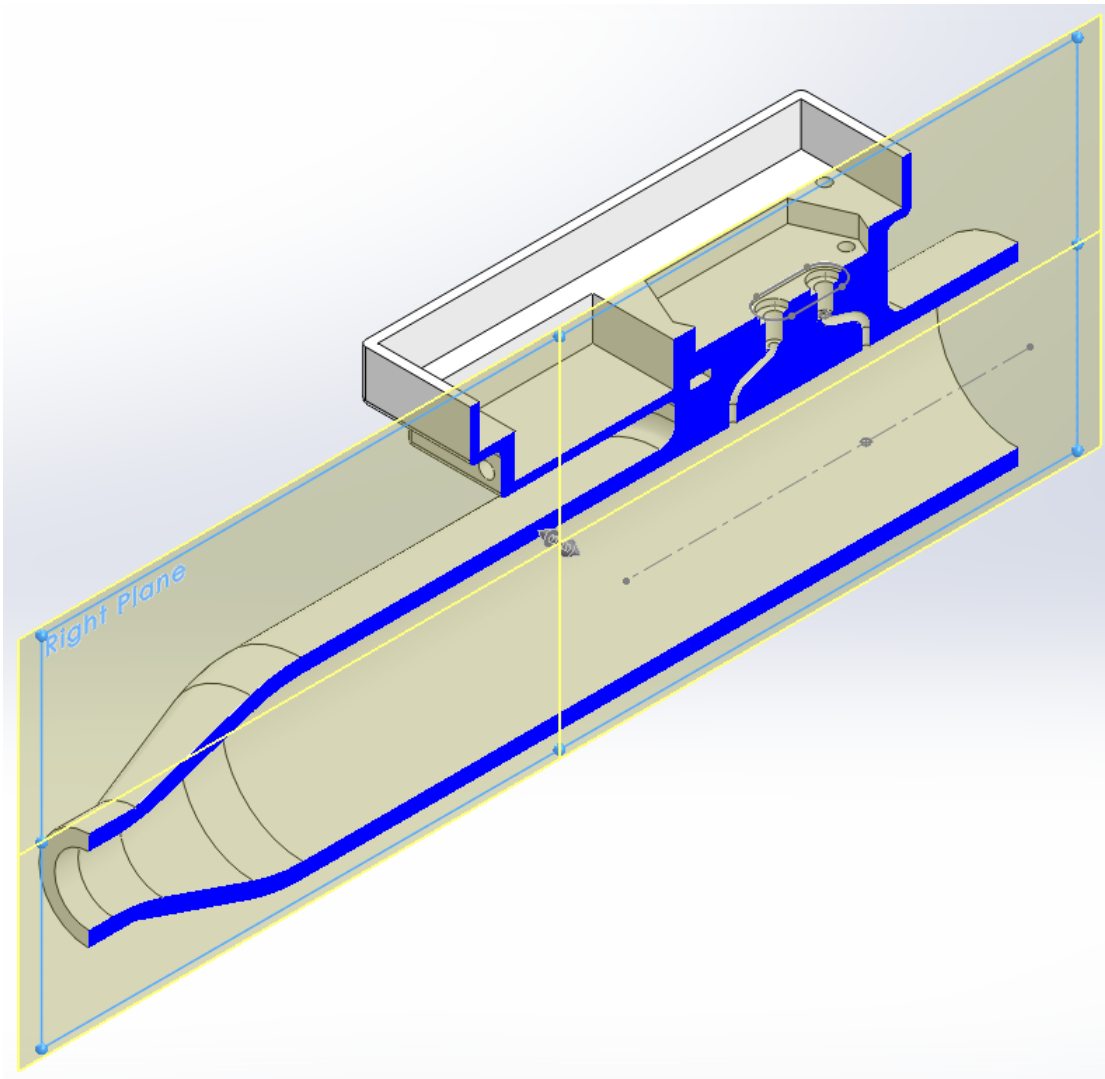


Figure 69: Drawing of laminar flow meter prototype 5 with intersection

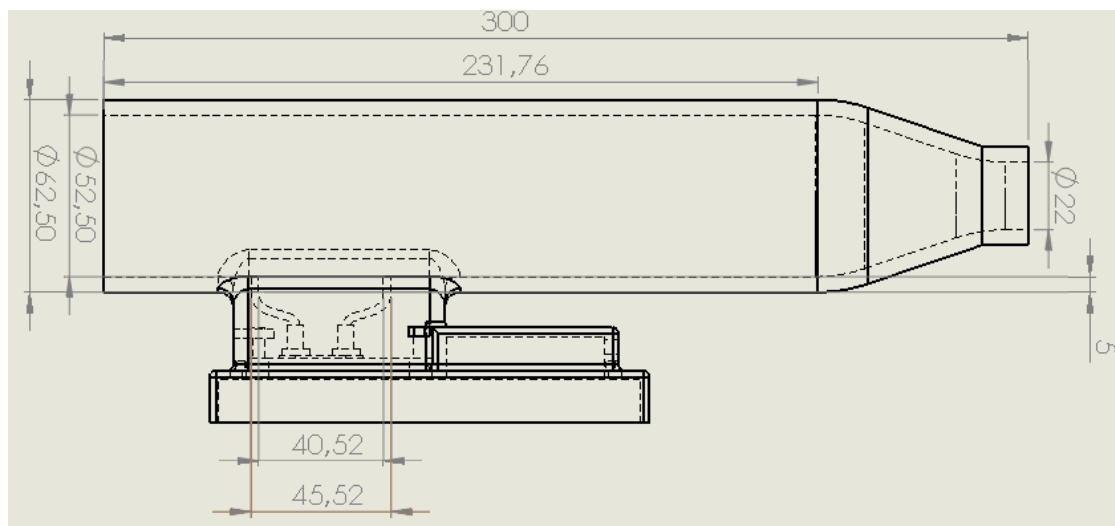


Figure 70: 2-dimensional drawing of laminar flow meter prototype 5 with core dimensions

## G LabVIEW code

In this appendix the relevant LabVIEW code used for control of the engine during the experiments will be presented. All code presented here is sub-code of the complete ECU LabVIEW code. For further information on the complete ECU code please see [22].

### G.1 Speed-density control system

On figures 72 and 71, the LabVIEW code for determination of the injection length using the speed-density method can be seen. When the case structure is true (at wide open throttle), the injection length is calculated using the cylinder pressure and the temperature pressure as described in section 7.2. The values used for this calculation is deducted in the following way:

$$\begin{aligned}\lambda &= 1.1 \\ FA_s &= 0.111 \\ \eta_v &= 0.85 \\ R_{air} &= 287.058 \text{ J/kg} - \text{K} \\ B &= 0.038 \text{ m} \\ S &= 0.0435 \text{ m} \\ \varepsilon &= 12 \\ V_d &= \pi/4 \cdot B^2 \cdot S\end{aligned}$$

From [12]:

$$\begin{aligned}T_{inlet} &= \frac{T_{signal} - 3.877}{-0.03} + 273.15 \\ p_{inlet} &= 1/4 \cdot p_{signal} \cdot 10^5\end{aligned}$$

From the ideal gas law:

$$\rho_{in} = \frac{p_{inlet}}{R_{air} \cdot T_{inlet}}$$

From [24, eq. 1.25]

$$\dot{m}_{air} = \rho_{in} \cdot \eta_v \cdot V_d \cdot N/120$$

$$\dot{m}_{fuel} = \dot{m}_{air} \cdot \frac{FA_s}{\lambda}$$

And finally, mass of fuel per injection in milligrams:

$$m_{fuel} = \dot{m}_{fuel} \cdot 120 \cdot 1000000/N = \frac{457794 \cdot p_{signal}}{-25.64 \cdot T_{signal} + 372.56} + 786.71$$

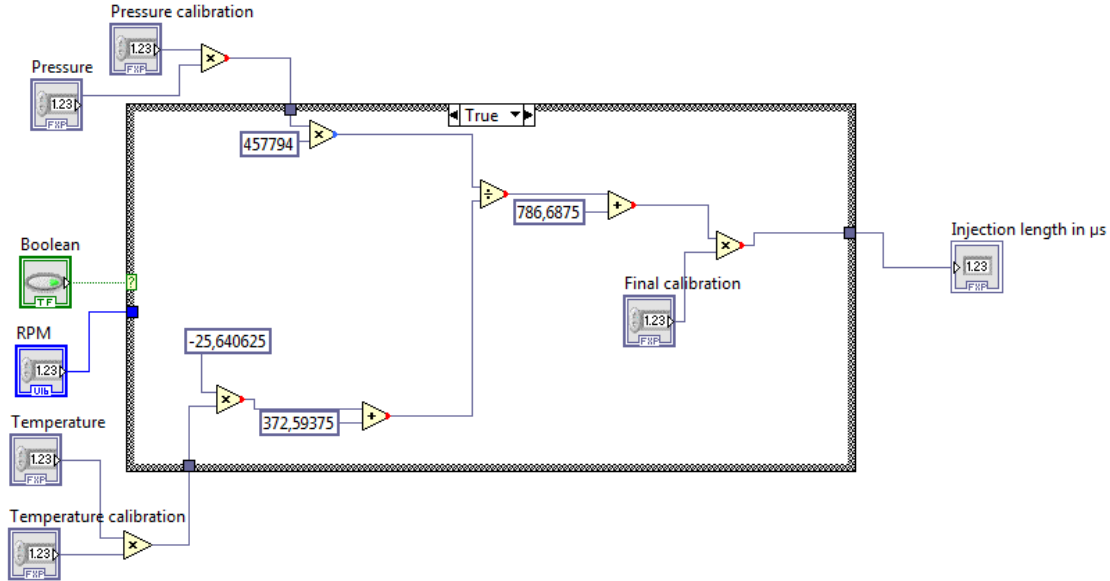


Figure 71: LabVIEW - Speed-density control, true

If the case is false and the engine speed is below 1000 RPM, the injection length is calculated using an input from a potentiometer. Otherwise, if the case is false, the injection length is calculated using the engine speed.

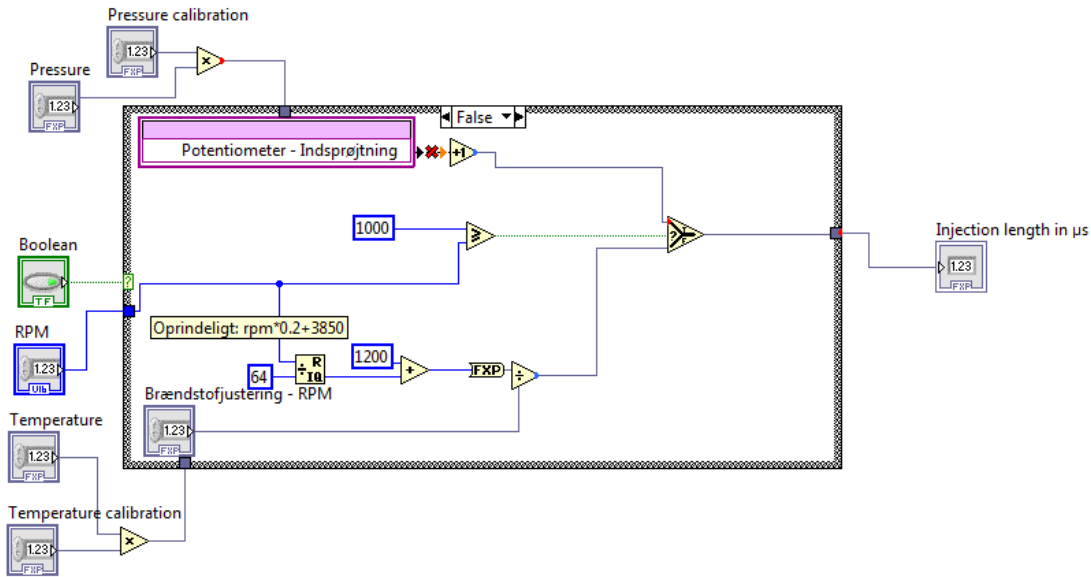


Figure 72: LabVIEW - Speed-density control, false

## G.2 Flow measurements

On figures 73 and 74, the loop for measuring of the average flow meter signal of a whole combustion cycle can be seen. The thick grey box is a while-loop. It is seen that a blue string is connected to the while loop without being used. This value is sent to the loop to ensure that the loop does not start execution before an initial loop is executed once. For more information on the initial loop please see [22]. In the bottom right corner of the while-loop, the condition for execution of the while-loop can be seen - the while-loop is always executing because the stop signal is set to false constantly. In the bottom left corner, the time between executions of the loop can be set. This value is set to  $50 \mu\text{s}$ . The pink square in the middle of the loop with the text 'Gearpotentiometer' is an analogue input. This is the input from which the signal from the laminar flow meter is received. This input is called 'Gearpotentiometer' because it was originally the input for the gear potentiometer. This input is sent to a case structure (the small framed box). The case structure is true when the encoder A-pulse value is smaller than the value for the last execution (this corresponds to that the camshaft axle has begun a new revolution and thus a new combustion cycle). Inside of the case structure it can be seen that:

- If the case is false, the signal from the laminar flow meter ('Gearpotentiometer' input) is added to the sum of previous signal values. Below this sum in the same case structure, a

counter is increased with 1.

- If the case is true, the sum of flow signals is divided by the quantity of flow signals to obtain the average in flow measurements of one combustion cycle. It is seen in the right side of the case-box, that the sum of input signals and the counter are then reset.

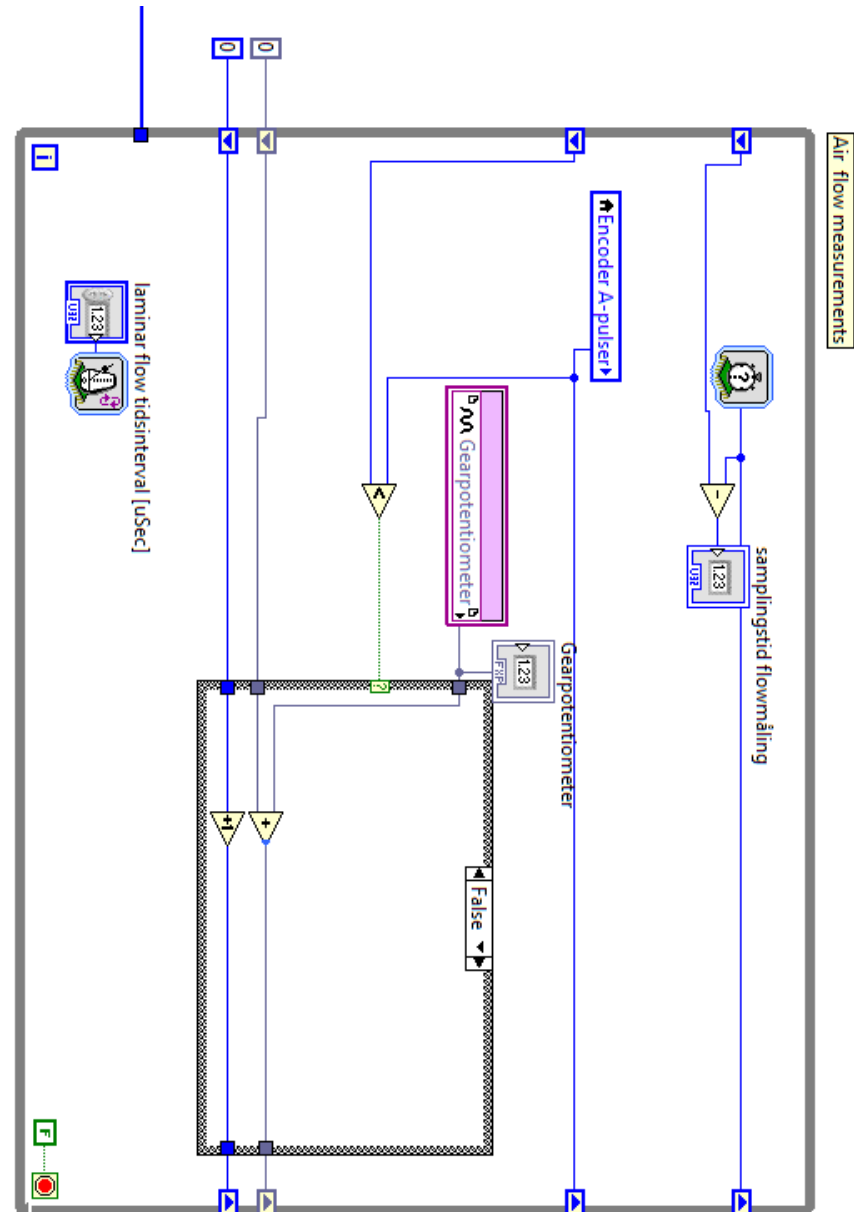


Figure 73: LabVIEW - flow measurements, case is false

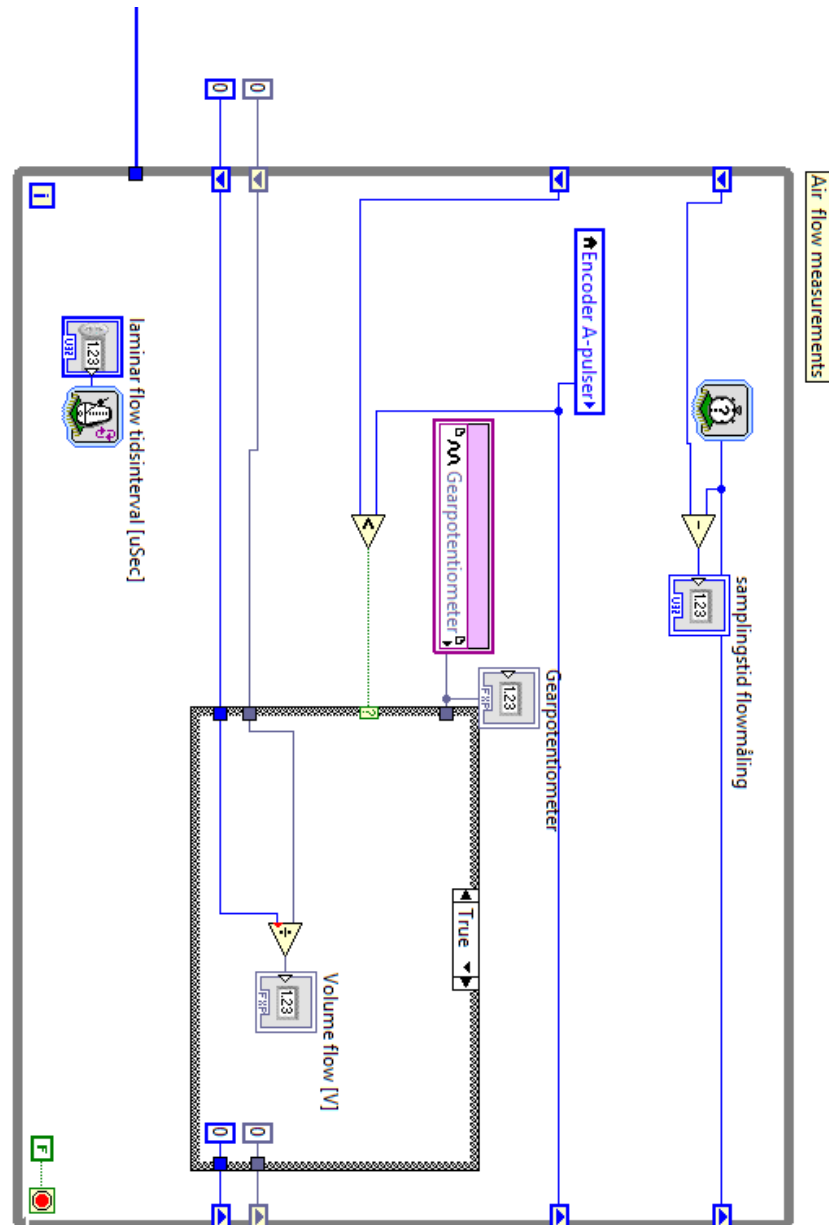


Figure 74: LabVIEW - flow measurements, case is true

### G.3 Control of injection

On figure 75 the system of control of injection is seen. Please note that this figure consists of 4 consecutive LabVIEW diagrams. The thick grey box is a while-loop. It is seen that a blue string is connected to the while loop without being used. This value is sent to the loop to ensure that the loop does not start execution before an initial loop is executed once. For more information on the initial loop please see [22]. Inside of the while-loop a 'movie-strip' is seen. This is a sequence of steps, where one step will not be executed before the previous step has finished execution. In each of the steps, the following actions are made:

- 1 The output signal to the injection nozzle ('dyse') is set to false to ensure that the nozzle is closed. The occurrence-symbol ( ) ensures that this step will not finish execution before it has received a signal from another loop indicating that a new combustion cycle has begun.
- 2 In this step the injection length is calculated. The struct called 'FPGA Input - Injection lengths ( $\mu\text{s}$ )' is the engine map. The final values of this struct can be seen on figure 78 on page 112. The struct is used to calculate the injection length for the given engine rotation speed using linear interpolation. The result of this linear interpolation is multiplied by an injection length calibration factor. This value is then sent on to a selector ( ). Here, the value is chosen only if the throttle angle is above 7 degrees (corresponding to a voltage signal of 0.9 (angle = (voltage signal - 0.64) · 25.7)). If the throttle angle is below 7 degrees and the starter motor is turned on, the injection length is a constant value of 2100  $\mu\text{s}$ , else it is a constant value of 1600  $\mu\text{s}$ .

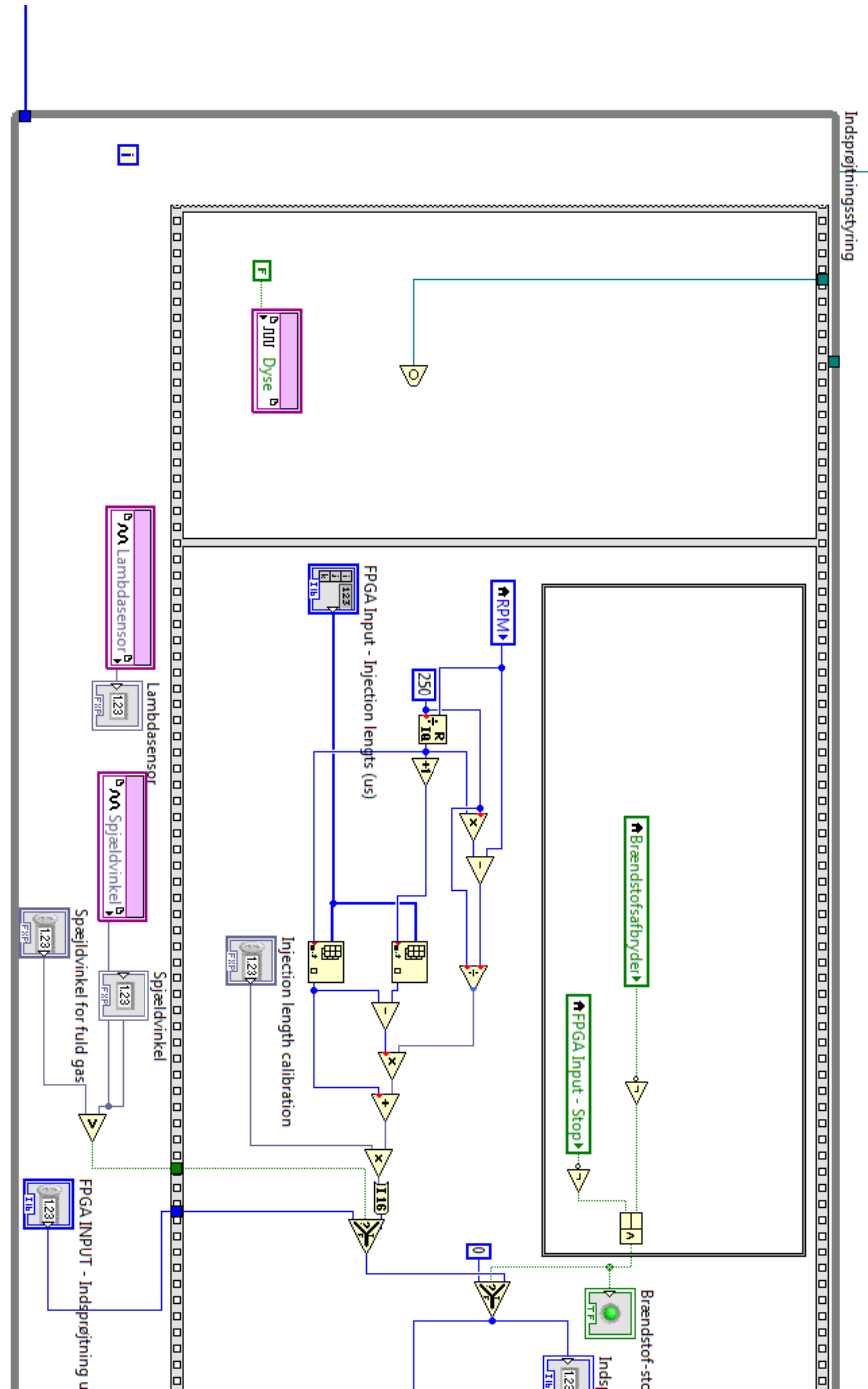
The injection length is then passed on to another selector. Here the injection length is only chosen if no fuel-cut signal is true. If the a fuel-cut signal is true, an injection length of 0 is chosen instead.

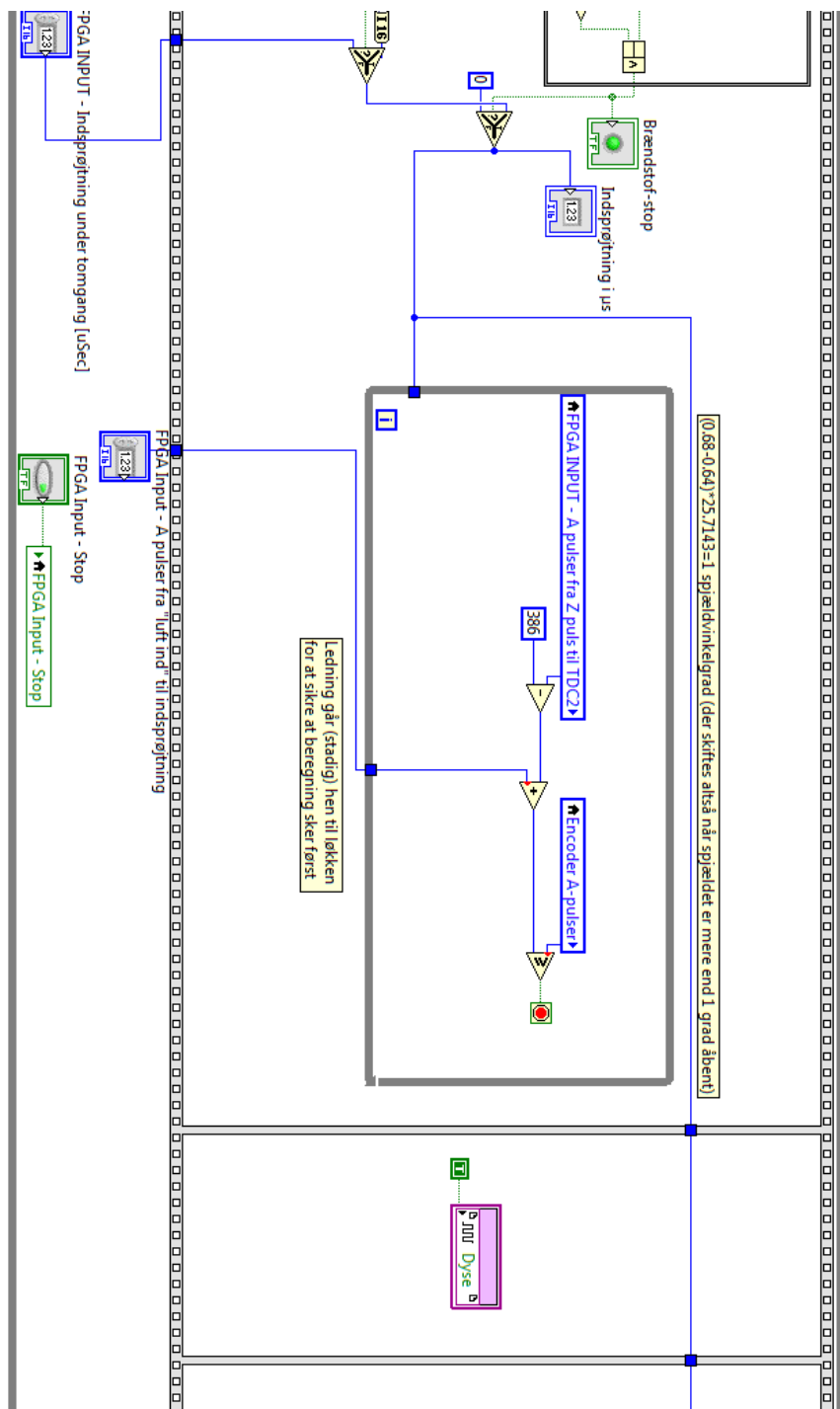
The injection length is than led to a while-loop. The injection length-string is only connected to the while-loop to ensure that the injection length is calculated before the while-loop is executed. The while-loop is running until the camshaft axle reaches the position where the fuel has to be injected. Then the while-loop is stopped and thus the 2nd step of the sequence is finished.

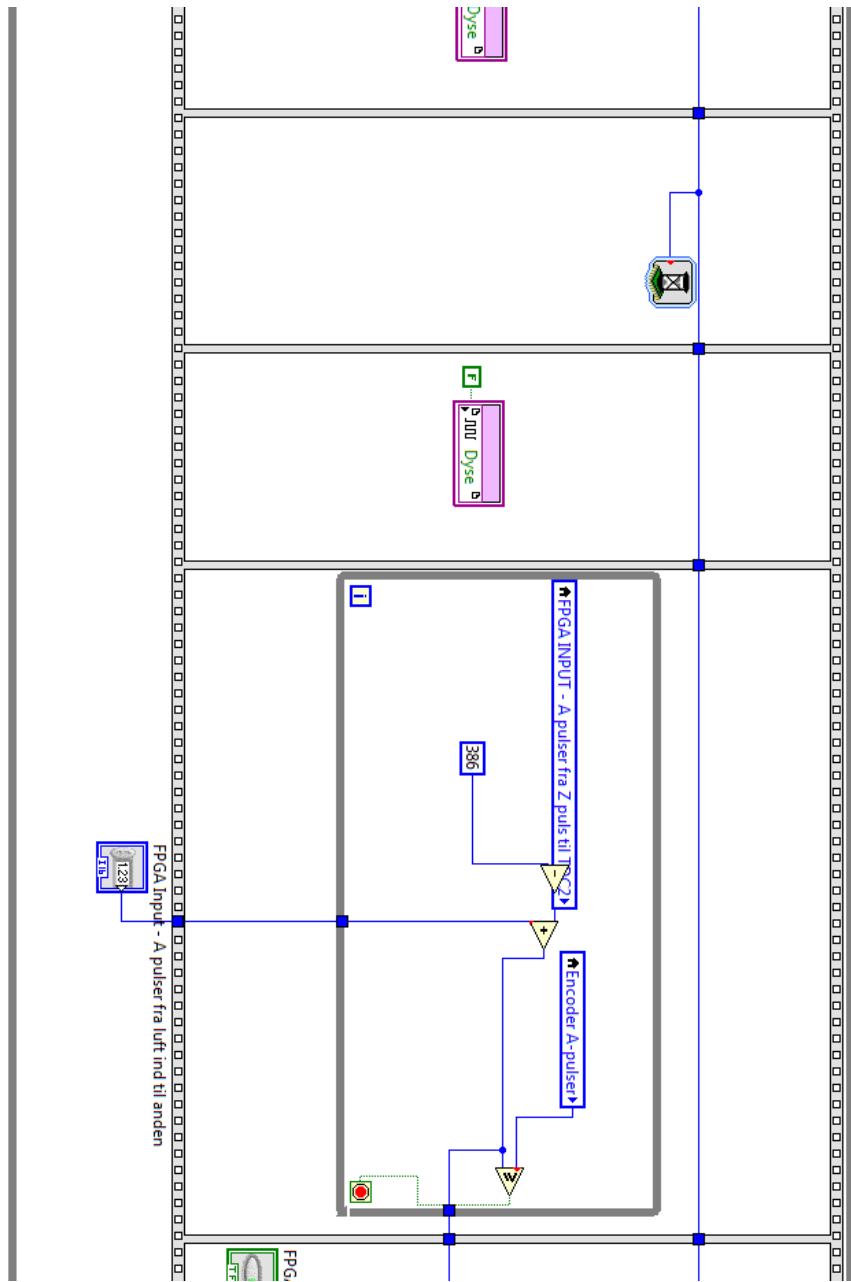
- 3 A true signal is sent to the injection nozzle so that it will open and fuel will be injected.
- 4 A wait function ( ) waits the time length of the calculated injection length. Not until then will this step finish.

- 5 A false signal is sent to the injection nozzle so that it will close and fuel will no longer be injected.
- 6 A while-loop is executing continuously until the camshaft axle is positioned for injection of the second injection.
- 7 A true signal is sent to the injection nozzle.
- 8 A wait function waits the time length of calculated injection length unless the program is set to 1 injection per cycle instead of 2. If this is the case the wait function waits 0 seconds / the step finishes immediately. In all tests presented in this report, the program was set to 1 injection per cycle. Tests were also conducted using 2 injections per cycle. From these tests it was concluded that 1 injection per cycle resulted in the most efficient combustion.
- 9 A false signal is sent to the injection nozzle.

Other than injection control, the while-loop on figure 75 also receives the input signal from the  $\lambda$ -sensor and sends it to an indicator.







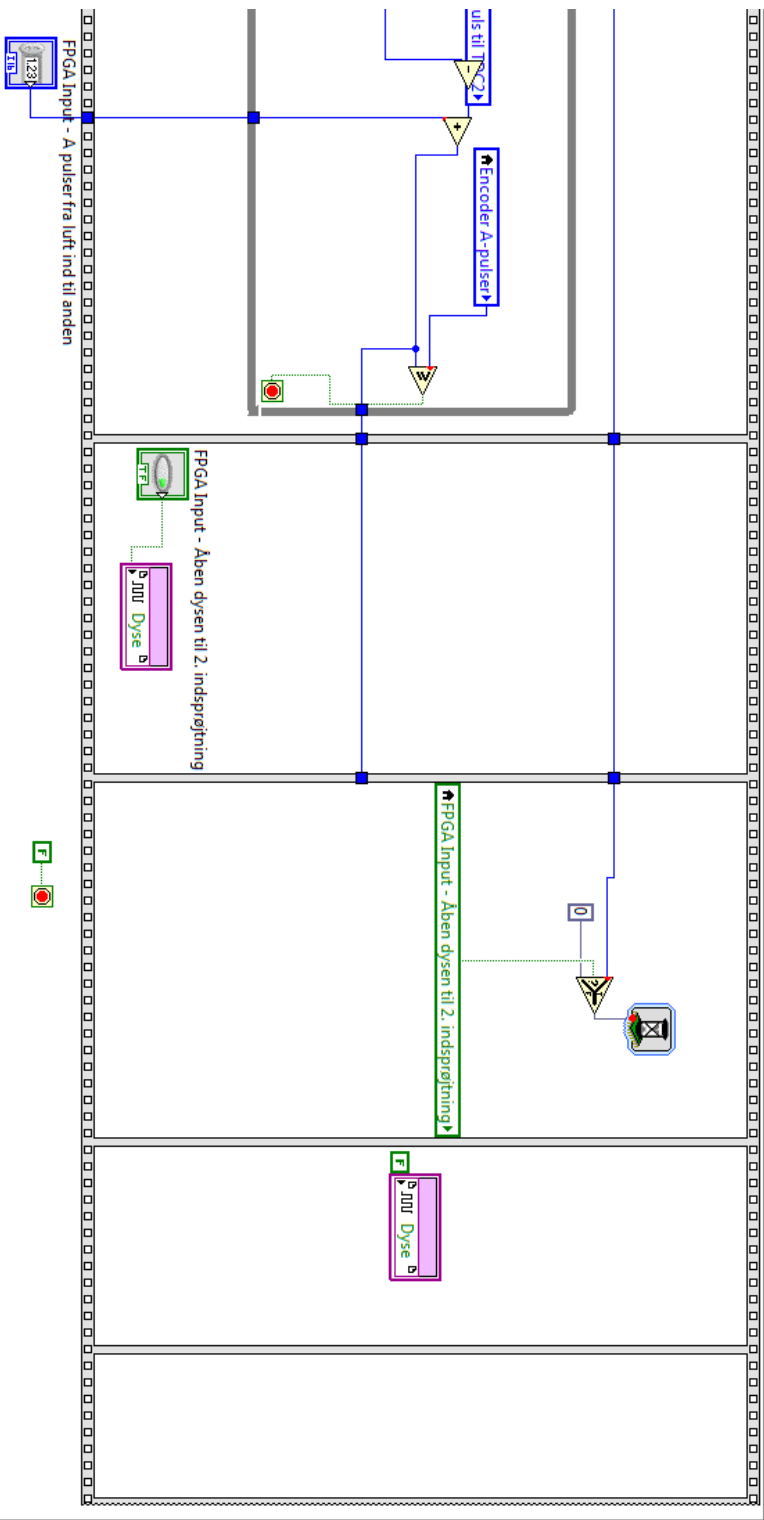
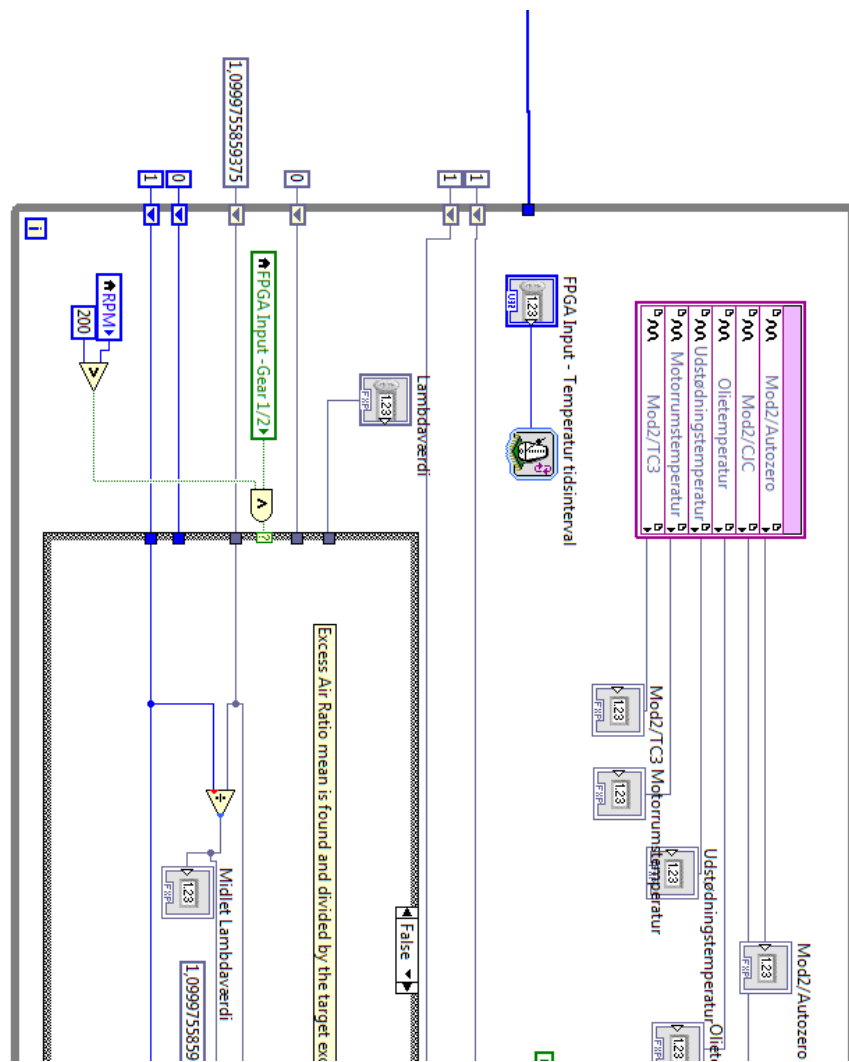


Figure 75: LabVIEW - fuel injection code

#### G.4 Closed-loop control

On figure 75 the system of closed-loop  $\lambda$  control is seen. Please note that this figure consists of 2 consecutive LabVIEW diagrams. The thick grey box is a while-loop. It is seen that a blue string is connected to the while-loop without being used. This value is sent to the loop to ensure that the loop does not start execution before an initial loop is executed once. For more information on the initial loop please see [22]. The upper part of the while-loop is measuring temperatures. Information regarding this part of the loop can be found in [22]. Inside of the while-loop, a case structure can be seen. This case structure is true whenever the engine speed is above 200 RPM and the car is in 2nd gear. When the case structure is true (figure 77), the  $\lambda$ -values are summed up. For calculation of the average, only values for when the engine speed is in the range of 2000 and 5000 RPM are used. When the case structure is false (the engine speed is below 200 RPM and the car is no longer in 2nd gear corresponding to that the gear has been changed to 1st gear which, during the race, only happens after each lap), the sum of  $\lambda$ -values is divided by the quantity of  $\lambda$ -values to obtain the average. This average is divided by 1.1 to obtain the 1-lap calibration factor (1 burn calib). This value is passed on to a selector. If the 1-lap calibration factor is the same as in last while-loop execution, the final closed-loop calibration value remains. Else, the previous closed loop calibration value is multiplied with the 1-lap calibration factor and chosen as the new final closed loop calibration factor. Before this multiplication, the 1-lap calibration factor is coerced so that it is within the range of 0.9 - 1.1. This serves as a safety barrier so that an error will not result in a too incorrect final fuel amount.



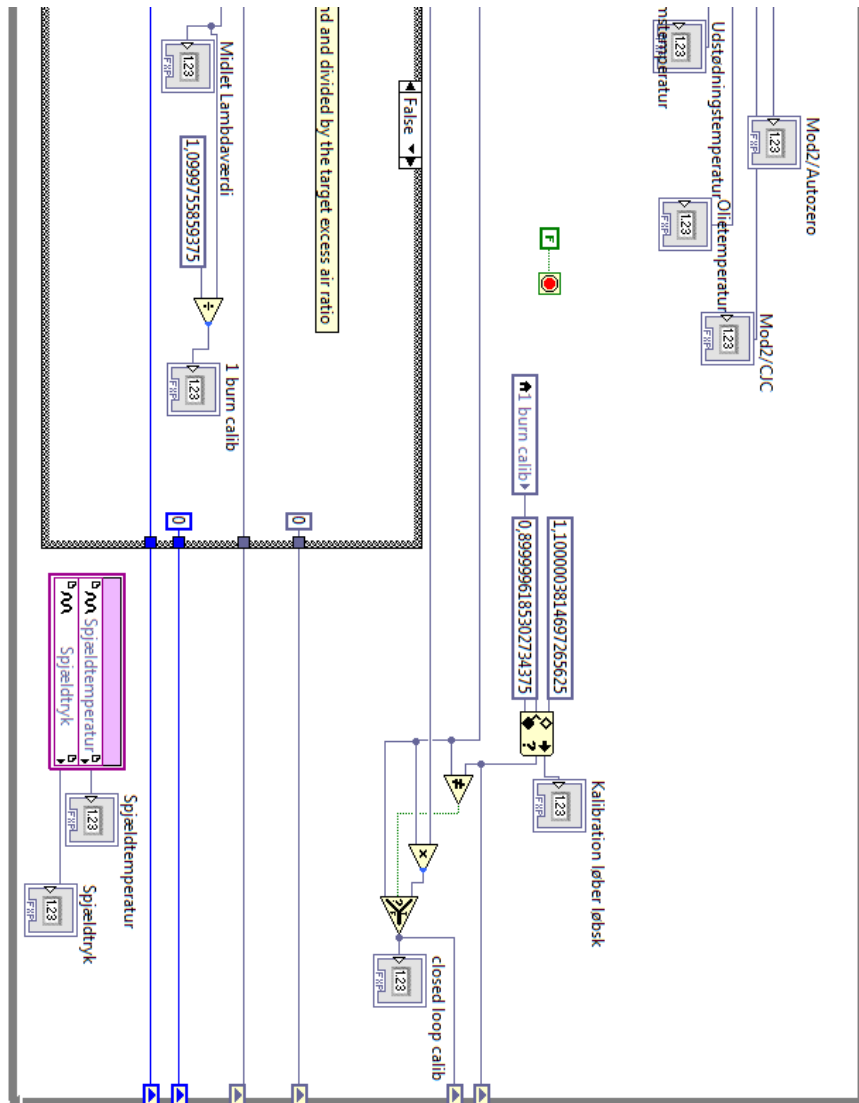


Figure 76: LabVIEW - closed-loop code

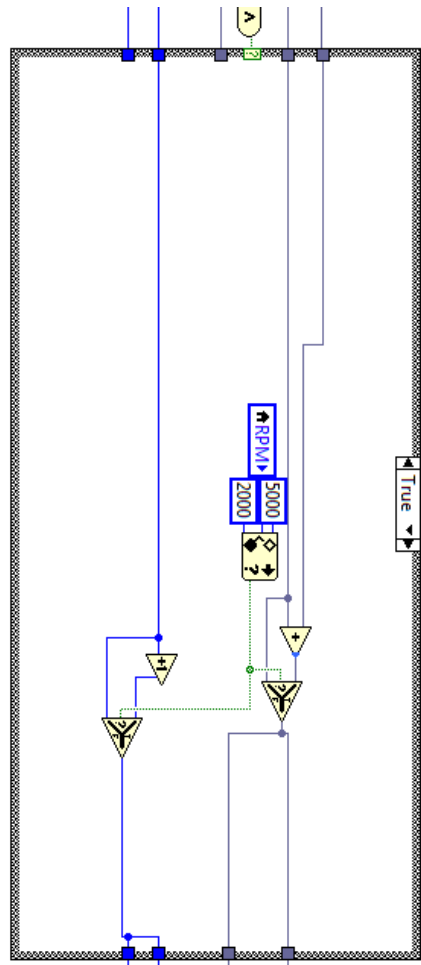


Figure 77: LabVIEW - closed-loop code, case structure true

## H Final engine map struct

0	0
250	0
500	5060
750	5568
1000	6075
1250	6126
1500	6176
1750	6329
2000	6481
2250	6004
2500	5202
2750	4771
3000	5010
3250	5200
3500	5010
3750	5101
4000	6075
4250	6731
4500	6582
4750	6537
5000	6654
5250	6633
5500	6633
5750	6481
6000	6380
6250	6380
6500	6380
6750	6380
7000	0
7250	0

Figure 78: The final engine map. The struct consists of two columns. The first column indicates the engine rotation speed in RPM and the second column indicates the injection length in  $\mu\text{s}$ .

## I Matlab code for data processing, Shell Eco Marathon 2012 data

```

1 clc
2 clear all
3 close all
4
5 startup
6 data = dlmread( 'Data/race_3.txt' , ' ', 0, 4);
7
8 db.Stop_engine=data(:,1);
9 db.WheelSpeed=data(:,2);
10 db.Lambda=data(:,3);
11 db.timeToCalcInjection=data(:,4);
12 db.Zcount=data(:,5);
13 db.GearIndicator=data(:,6);
14 db.TotalFuelInject=data(:,7);
15 db.AvgPressure=data(:,8);
16 db.MinAvgPress=data(:,9);
17 db.KolevandsTemp=data(:,10);
18 db.SpjaeldTemp=data(:,11);
19 db.MotorumTemp=data(:,12);
20 db.OlieTemp=data(:,13);
21 db.ExhoustTemp=data(:,14);
22 db.SpjaeldVinkDegree=data(:,15);
23 db.EngineRev=data(:,16);
24 db.InjLength=data(:,17);
25 db.on=data(:,18);
26 db.kobling=data(:,19);
27 db.Wheelcount=uint8(data(:,20));
28
29 % Creation of time vector:
30 sambling_rate=10;           % [Hz]
31
32 db.tid=(sambling_rate^(-1):sambling_rate^(-1):length(db.OlieTemp)/
            sambling_rate);
33

```

```

34 %Time of start and finish of race:
35 start_punkt = 24000
36 slut_punkt = 49000
37
38 %%
39 a=find(db.SpjaeldVinkDegree>50 & db.on==1 & db.Stop_engine==0 & db.
        Lambda<=1.5)
40                                     %Only relevant data is used
41
42 figure()
43 plot(db.EngineRev(a),db.Lambda(a),'*',[1500:1:6000],1.1,'g'
       ,[1500:1:6000],1.2,'r',[1500:1:6000],1,'r')
44 xlim([1500 6000])
45 ylim([0.7 1.6])
46 xlabel('Engine Speed [RPM]')
47 ylabel('Excess air ratio [-]')
48 title('Final race 2012 (611 km/l), ALL lambda-values')
49 grid on
50 hold off
51 %%
52
53 figure
54 [ax, h1, h2] = plotyy(db.tid,db.WheelSpeed,db.tid(a),db.InjLength(a))
;
55 set(get(ax(1),'Ylabel'),'String','Speed [km/h]')
56 set(get(ax(2),'Ylabel'),'String','Injection length [us]')
57 set(ax(1),'XLim',[start_punkt/10 slut_punkt/10])
58 set(ax(2),'XLim',[start_punkt/10 slut_punkt/10])
59 set(h2,'linestyle','none','marker','.')
60 xlabel('Time from beginning of warmup [s]')
61 title('Shell Eco Marathon 2012, injection length through the whole
        race')
62
63 figure
64 [ax, h1, h2] = plotyy(db.tid,db.WheelSpeed,db.tid(a),db.InjLength(a))
;

```

```

65 set(get(ax(1), 'Ylabel'), 'String', 'Speed [km/h]')
66 set(get(ax(2), 'Ylabel'), 'String', 'Injection length [us]')
67 set(ax(1), 'XLim',[4180 4276])
68 set(ax(2), 'XLim',[4180 4276])
69 set(h2, 'linestyle', 'none', 'marker', '*')
70 xlabel('Time from beginning of warmup [s]')
71 title('Shell Eco Marathon 2012, injection length through one lap')
72
73 %%
74 figure
75 plot(db.tid, db.WheelSpeed/50, ...
76      db.tid(a), db.InjLength(a)/3000, '*', ...
77      db.tid(a), db.MinAvgPress(a), '*', ...
78      db.tid(a), db.SpjaeldTemp(a)/100, '*k');
79 xlim([start_punkt/10 slut_punkt/10])
80 title('Shell Eco Marathon 2012')
81 legend('Speed [km/t/50]', 'Inj. Length [us/3000]', 'Manifold pressure [
     bar]', 'Manifold Temperature [C/100]')
82 xlabel('Time from beginning of warmup [s]')
83
84 %%
85 figure
86 plot(db.tid, db.WheelSpeed/50, ...
87      db.tid(a), db.InjLength(a)/3000, '*', ...
88      db.tid(a), db.MinAvgPress(a), '*', ...
89      db.tid(a), db.SpjaeldTemp(a)/100, '*k');
90 xlim([4180 4276])
91 title('Shell Eco Marathon 2012, values for one lap')
92 legend('Speed [km/t/50]', 'Inj. Length [us/3000]', 'Manifold pressure [
     bar]', 'Manifold Temperature [C/100]')
93 xlabel('Time from beginning of warmup [s]')
94
95 %% Lambda plot with average values:
96
97 rpm_step=10;                      % [rmp]
98 min_rpm=0;                         % [rpm]

```

```

99 max_rpm=6000; % [rpm]
100
101 step=max_rpm/rpm_step-min_rpm/rpm_step;
102
103 for i=1:step;
104     a=find(db.tid > start_punkt/10 & db.EngineRev>i*rpm_step+
105         min_rpm &...
106         db.EngineRev<(i+1)*rpm_step+min_rpm & db.Lambda<1.5 & db.
107         GearIndicator==2 ...
108         & db.Lambda> 0.53 & db.on==1);
109     rpm_int(i)=i*rpm_step+rpm_step/2+min_rpm;
110     lambda(i)=mean(db.Lambda(a));
111     lambda_std(i)=std(db.Lambda(a));
112 end
113
114 figure()
115 hold on
116 errorbar(rpm_int,lambda,lambda_std,'g')
117 plot(rpm_int,lambda,'*',[1500:1:6000],1.1,'g',[1500:1:6000],1.2,'r'
118     ,[1500:1:6000],1,'r')
119 xlabel('Engine Speed [RPM]')
120 ylabel('Excess air ratio [-]')
121 title('Final race 2012 (611 km/l), mean lambda-values')
122 grid on
123 hold off

```

## J Matlab code for data processing, Closed-loop $\lambda$ control experiment

```

1 %% 3 burns gearing=19/68
2 clc
3 clear all
4 close all
5 %% The log-file from LabVIEW is read:
6 data = dlmread( 'Dynamo 9 2013-05-18 18 04 LOG.txt' , ' ', 0, 4);
7
8 d.rpm=data(:,1); %RPM
9 d.automatgear=data(:,2); %Automatic gear true/false
10 d.aktueltgear=data(:,3); %Actual gear
11 d.gearskifte=data(:,4); %Gear shift true/false
12 d.ztid=data(:,5); %Time between wheel-Z-pulses
13 d.kmt=data(:,6); %Km/h
14 d.hjulrpm=data(:,7); %Wheel-RPM
15 d.squirtus=data(:,8); %Injection lenth [us]
16 d.squirtcalib=data(:,9); %Injection calibration
17 d.squirt2=data(:,10); %1 or 2 injections per cycle
18 d.squirttiming=data(:,11); %A-pulses from intake valve opening to
     injection
19 d.squirttiming2=data(:,12); %A-pulses from intake valve opening to 2
     nd injection
20 d.gnistbtdc=data(:,13); %Spark timing BTDC
21 d.pot=data(:,14); %Potentiometer reading
22 d.lambda=data(:,15); %Lambda-value
23 d.vandtemp=data(:,16); %Water temperature
24 d.throtdegree=data(:,17); %Throttle angle
25 d.olietemp=data(:,18); %Oil temperature
26 d.udtemp=data(:,19); %Exhaust temperature
27 d.motortemp=data(:,20); %Engine temperature
28 d.tc3=data(:,21); %Termocouple 3
29 d.lambdaavg=data(:,22); %Average lambda value
30 d.burncalib=data(:,23); %1-lap calibration factor
31 d.closedloop=data(:,24); %Final closed loop calibration factor
32 d.flow=data(:,25); %Flow signal

```

```

33 d.flowavg=data(:,26);           %Average flow signal for whole cycle
34 d.manpress=data(:,27);          %Intake manifold pressure
35 d.mantemp=data(:,28);          %Intake manifold temperature
36
37
38 % Definition of start og end values in plots:
39 st=50;
40 sl=length(d.rpm);
41 d.tid=(1:length(d.rpm));
42
43
44 %% Plot of average lambda-values as a function of engine speed:
45
46 rpm_step=10;                   % [rmp]
47 min_rpm=0;                     % [rpm]
48 max_rpm=6000;                  % [rpm]
49
50 step=max_rpm/rpm_step-min_rpm/rpm_step;
51
52 for i=1:step;
53     a=find(d.tid '>6300 & d.rpm>i*rpm_step+min_rpm &...
54             d.rpm<(i+1)*rpm_step+min_rpm &d.lambda<1.5...
55             & d.lambda> 0.53 & d.throtdegree>80);
56     rpm_int(i)=i*rpm_step+rpm_step/2+min_rpm;
57     lambda(i)=mean(d.lambda(a));
58     squirt(i)=mean(d.squirtus(a));
59     lambda_std(i)=std(d.lambda(a));
60 end
61
62 figure()
63 hold on
64 errorbar(rpm_int,lambda,lambda_std,'g')
65 plot(rpm_int,lambda,'*',rpm_int,ones(size(rpm_int))*1.1,'g',rpm_int,
       ones(size(rpm_int)), 'r', rpm_int, ones(size(rpm_int))*1.2,'r')
66 xlim([1700 4500])
67 ylim([1 1.5])

```

```

68 xlabel( 'Engine Speed [RPM] ')
69 ylabel( 'Excess air ratio [-] ')
70 title( '3rd race 2013 (602 km/1), mean lambda-values' )
71 grid on
72 hold off
73
74 %% Plot of all lambda values:
75
76 a=find(d.throtdegree>50 & d.rpm> 800 & d.gearskifte==0 & d.lambda
    <=1.5)
77 %Only relevant data is used.
78
79
80 figure()
81 plot(d.rpm(a),d.lambda(a),'*',[1500:1:6000],1.1,'g'
    ,[1500:1:6000],1.2,'r',[1500:1:6000],1,'r')
82 xlim([1700 4700])
83 ylim([0.7 1.6])
84 xlabel( 'Engine Speed [RPM] ')
85 ylabel( 'Excess air ratio [-] ')
86 title( '3rd race 2013 (602 km/1), mean lambda-values' )
87 grid on
88 hold off
89
90 %% Calibration factor plot:
91 figure()
92 hold on
93 plot(d.tid/10-630,d.lambdaavg,d.tid/10-630,(d.closedloop+1)/2)
94 ylim([0.95 1.22])
95 xlim([0 2815-630])
96 legend( 'Mean of lambda','Closed loop calibration factor' )
97 xlabel( 'Time from beginning of race [s] ')
98 title( 'Shell Eco Marathon 2013, 3rd race (602 km/1)' )
99 hold off

```

## K Matlab code for data processing, laminar flow meter experiment

```

1 %12. May 2013
2 clc
3 close all
4 clear all
5
6 %% Reading of LabVIEW log-file :
7 data = dlmread('Dynamo 9 2013-05-12 11 08 LOG.txt', ' ', 0, 4);
8
9 d.rpm=data(:,1); %RPM
10 d.automatgear=data(:,2); %Automatic gear true/false
11 d.aktueltgear=data(:,3); %Actual gear
12 d.gearskifte=data(:,4); %Gear shift
13 d.ztid=data(:,5); %time between wheel-z-pulse
14 d.kmt=data(:,6); %Km/h
15 d.hjulrpm=data(:,7); %Wheel RPM
16 d.squirtus=data(:,8); %Injection length [us]
17 d.squirtcalib=data(:,9); %Injection calibration
18 d.squirt2=data(:,10); %1 or 2 injections
19 d.squirttiming=data(:,11); %A-pulses from air in to injection
20 d.squirttiming2=data(:,12); %A-pulses from air in to 2nd injection
21 d.gnistbtdc=data(:,13); %Spark timing BTDC
22 d.lambda=data(:,14); %Lambda
23 d.vandtemp=data(:,15); %Water temperature
24 d.throtdegree=data(:,16); %Throttle angle
25 d.olietemp=data(:,17); %Oil temperature
26 d.udtemp=data(:,18); %Exhaust temperature
27 d.motortemp=data(:,19); %Engine temperature
28 d.tc3=data(:,20); %Termocouple 3
29 d.burncalib=data(:,21); %1-lap calibration
30 d.closedloop=data(:,22); %Final closed loop calibration
31 d.flow=data(:,23); %Flow signal
32 d.flowavg=data(:,24); %Average flow signal of 1 cycle
33
34 %% Creation of time vector

```

```

35 dt=0.1; %Sampling time is each 100 ms
36 d.tid=(dt:dt:length(d.rpm)*dt);
37
38 %% Air flow and engine speed as a function of time:
39 figure
40 [ax, h1, h2] = plotyy(d.tid ,d.flowavg ,d.tid ,d.rpm);
41 set(ax(1) , 'YLim' ,[2.5 2.65])
42 set(ax(2) , 'YLim' ,[0 6000])
43 set(ax(1) , 'YTick' ,[2.5:.05:2.65])
44 set(ax(2) , 'YTick' ,[0:1000:6000])
45 set(ax(1) , 'XLim' ,[1845 1875])
46 set(ax(2) , 'XLim' ,[1845 1875])
47 set(get(ax(1) , 'Ylabel') , 'String' , 'Air Flow [V]')
48 set(get(ax(2) , 'Ylabel') , 'String' , 'Engine Speed [RPM]')
49 title('Air flow and engine speed as a function of time')
50
51
52 %%
53 a=find(d.throtdegree>80 & d.aktueltgear==2);
54 %Only relevant data is used
55
56 correction=101100/((273.15+12.5)*287*1.19);
57 %The air density is divided by the
%standard air density because the
%calibration curve of prototype 5 is
%standardised.
58
59 mflow1=(-1.0364.* (d.flowavg(a)-2.5).^2+19.949.*...
60 (d.flowavg(a)-2.5))*0.111/1.1*correction;
61 %The fuel mass flow for obtaining lambda
% = 1.1 is found using the 2nd order
% polynomial trendline from the
% calibration of prototype 5.
62
63 mflowair=(-1.0364.* (d.flowavg(a)-2.5).^2+19.949.* (d.flowavg(a)-2.5))*...
correction;

```

```

64 squirtmg1=d.squirtus(a)*0.0008138-0.6695;
65 %The air mass flow is used using the 2nd
   order polynomial trendline from the
   calibration of prototype 5.
66
67 figure()
68 plot(d.rpm(a),mflow1*1000*120./d.rpm(a),'*',d.rpm(a),squirtmg1,'*')
69 xlim([1500 5500])
70 ylim([3.3 6.3])
71 xlabel('Engine speed [RPM]')
72 ylabel('Fuel mass/injection [mg]')
73 legend('Fuel mass according to laminar flow meter',...
74      'Actual injected fuel mass')
75
76 figure()
77 plot(d.rpm(a),mflow1*1000*120./d.rpm(a),'*',...
78      d.rpm(a),squirtmg1.*d.lambda(a)/1.1,'*')
79 xlim([1500 5500])
80 ylim([3.3 6.3])
81 xlabel('Engine speed [RPM]')
82 ylabel('Fuel mass/injection [mg]')
83 legend('Fuel mass according to laminar flow meter',...
84      'Actual fuel mass adjusted in relation to lambda')
85
86
87 %VOLUMETRIC EFFICIENCY PLOT:
88 figure()
89 plot(d.rpm(a),mflowair/1000*120./...
90      (101100/((273.15+12.5)*287.058)*0.000049334*d.rpm(a)),'*')
91 grid on
92 xlim([1500 5500])
93 ylim([0.6 1])
94 xlabel('Engine speed [RPM]')
95 ylabel('Volumetric efficiency')
96
97

```

```

98
99
100
101
102 %% Extraction of relevant data for lambda plot:
103 %rpm_step
104 rpm_step=10;           % [rmp]
105 min_rpm=0;            % [rpm]
106 max_rpm=6000;         % [rpm]
107
108 step=max_rpm/rpm_step-min_rpm/rpm_step;
109
110 for i=1:step;
111     a=find(d.tid >1100 & d.rpm>i*rpm_step+min_rpm &...
112             d.rpm<(i+1)*rpm_step+min_rpm &d.lambda<1.5 ...
113             & d.lambda> 0.53 & d.throtdegree>80);
114     rpm_int(i)=i*rpm_step+rpm_step/2+min_rpm;
115     lambda(i)=mean(d.lambda(a));
116     squirt(i)=mean(d.squirtus(a));
117     flow(i)=mean(d.flowavg(a));
118 end
119 %% Lambda as a function of engine speed:
120 figure
121 plot(rpm_int,lambda,'*',rpm_int,1.1)
122 title('Lambda as a funtion of engine speed – based on data from 5
burns')
123 xlabel('Engine speed [RPM]')
124 ylabel('lambda [-]')
125  xlim([1500 5500])
126  ylim([0.95 1.5])

```

## L Certification for the Meriam laminar flow meter

On the following pages the certification for the Meriam Laminar Flow element can be found



**Meriam Instrument**

a Scott Fetzer company

FILE NO. 040FB:001-19  
PAGE 1 OF 1

LETTER OF CERTIFICATION  
LAMINAR FLOW ELEMENT

CUSTOMER NAME: INSTITUTE FOR AUTO BL326

CUSTOMER ORDER NUMBER: VERBAL

MERIAM ORDER NUMBER: 777470

Meriam Instrument certifies that the completed LFE unit has been calibrated and correlated at several points of flow rate using a Meriam Standard, which is controlled per the calibration system requirements of ANSI Z540-1 and traceable to the National Institute of Standards and Technology. The collective uncertainty of the measurement standards has a 1:1 ratio to the acceptable tolerance for the flow rate being calibrated.

The total rss uncertainty of the completed laminar flow unit is +/- .86 % of reading.

MODEL NO.: 50MC2-2F SERIAL NO.: 777470-N1

FLOW CURVE/TABLE NO.: 31744, 31743

DATE OF CALIBRATION 09-09-1999 BY GEORGE ROBOTKAY

AS RECEIVED CONDITION: In Tolerance Out of Tolerance  NA

AS LEFT CONDITION :  In Tolerance Out of Tolerance NA

CALIBRATION INTERVAL: TO BE DETERMINED BY CUSTOMER BASED ON USAGE OF LFE.

FLOW STANDARD <u>SERIAL NO.</u>	DATE OF LAST CAL	DATE OF NEXT CAL
------------------------------------	------------------	------------------

WMMH10-3

APRIL 1999

APRIL 2000

The LFE unit listed hereon has been successfully calibrated in accordance with Meriam Instrument Procedure A-35822.

\_\_\_\_\_  
FLOW DATA TECHNICIAN  
MERIAM INSTRUMENT

\_\_\_\_\_  
QUALITY ASSURANCE MANAGER  
MERIAM INSTRUMENT

Standard  
LAMINAR.BAS VER 1.38 MARCH 1999

CALIBRATION DATE 09-09-1999

PLOT NUMBER 113

LAMINAR MODEL # 50MC2-2F

WORKING MASTER SERIAL # WMMH10-3

SERIAL # 777470-N1

MASTER MASTER SERIAL # 66-8275

CURVE # 31744

JOB # 777470

uut = Unit Under Test

DATA AS INPUT FROM DATA SHEET mas = Master

RH %	Tuut DEG C	Tmas DEG C	PSuut mm Hg	PSmas mm Hg	DPuut mm H2O	DPmas mm H2O
54.6	22.7	23.3	736.696	734.553	25.653	26.718
53.4	22.7	23.1	736.559	732.545	50.803	52.920
52.6	22.7	23.0	736.510	730.295	76.823	80.208
51.6	22.7	22.9	736.344	728.134	102.039	106.771
53.4	22.7	22.8	736.266	725.907	127.415	133.667
55.3	22.7	22.8	736.239	723.630	152.547	160.437
53.6	22.7	22.8	736.018	721.256	177.820	187.836
52.0	22.7	22.7	735.874	718.754	203.483	216.076

Master LFE coefficients      A1 = 2.30720E+03  
                                   B1 = -7.75223E+06  
                                   C1 = 8.71712E+09

REDUCED DATA, BASED ON MASTER LFE COEFFICIENTS:

DATA POINT	DP uut mmH2O@4C	FLOW IN ALPM BASED ON MASTER	LPM* (DATA) BASED ON MASTER	LPM* (CURVE) B*DP+C*DP^2	PERCENT ERROR**
1	25.653	371.515425	372.620517	372.004246	-0.17
2	50.803	729.076756	731.293207	731.502125	0.03
3	76.823	1094.245684	1097.572277	1098.035511	0.04
4	102.039	1442.732634	1447.071388	1447.997537	0.06
5	127.415	1788.096717	1793.474091	1794.942523	0.08
6	152.547	2123.710905	2130.167154	2133.399577	0.15
7	177.820	2460.748825	2468.552092	2468.577137	0.00
8	203.483	2800.355042	2809.326934	2803.619004	-0.20

\*LPM = ALPM x (Flowing viscosity in Micropoise / 181.87)

\*\* PERCENT ERROR = ( (CURVE-DATA) / DATA) \* 100

A Least Squares Fit of the LPM(DATA) yields the following formula and LFE uut coefficients used to generate the LPM(CURVE) values:

$$LPM(CURVE) = (B \times DP) + (C \times DP^2) \quad \text{Where } B = 1.46054E+01 \\ C = -4.06571E-03$$

A Flow of 2758.456299 LPM produces a UUT DP of 200.00 mm H2O

TERMINAL NON-LINEARITY = 2.766 %      FOR DETAILS SEE  
     INDEPENDENT NON-LINEARITY = 0.922 %      FILE NO. 501:440

PRINTOUT DATE :09-09-1999

Filename : 77747001.1NN

LAMINAR.BAS Standard VER 1.38 MARCH 1999

CALIBRATION DATE 09-09-1999

PLOT NUMBER 113

LAMINAR MODEL # 50MC2-2F

WORKING MASTER SERIAL # WMMH10-3

SERIAL # 777470-N1

MASTER MASTER SERIAL # 66-8275

CURVE # 31743

JOB # 777470

uut = Unit Under Test

**DATA AS INPUT FROM DATA SHEET**

mas = Master

RH %	Tuut DEG F	Tmas DEG F	PSuut PSIA	PSmas PSIA	DPuut In H2O	DPmas In H2O
54.6	72.8	73.9	14.246	14.204	1.010	1.052
53.4	72.8	73.7	14.243	14.165	2.000	2.083
52.6	72.8	73.4	14.242	14.122	3.025	3.158
51.6	72.8	73.1	14.239	14.080	4.017	4.204
53.4	72.8	73.0	14.237	14.037	5.016	5.262
55.3	72.8	73.0	14.237	13.993	6.006	6.316
53.6	72.9	73.0	14.232	13.947	7.001	7.395
52.0	72.9	72.9	14.230	13.899	8.011	8.507

**REDUCED DATA, BASED ON MASTER LFE COEFFICIENTS:**

DATA POINT	DP uut InH2O@4C	FLOW IN ACFM BASED ON MASTER	CFM* (DATA) BASED ON MASTER	CFM* (CURVE) B*DP+C*DP^2	PERCENT ERROR**
1	1.010	13.120336	13.159363	13.137599	-0.17
2	2.000	25.747872	25.826148	25.833526	0.03
3	3.025	38.644077	38.761558	38.777917	0.04
4	4.017	50.951145	51.104372	51.137079	0.06
5	5.016	63.147928	63.337833	63.389692	0.08
6	6.006	75.000385	75.228392	75.342548	0.15
7	7.001	86.903123	87.178701	87.179585	0.00
8	8.011	98.896562	99.213411	99.011831	-0.20

\*CFM = ACFM x (Flowing viscosity in Micropoise / 181.87)

\*\* PERCENT ERROR = ((CURVE-DATA) / DATA) \* 100

A Least Squares Fit of the CFM(DATA) yields the following formula and LFE unit coefficients used to generate the CFM(CURVE) values:

**CFM(CURVE) = (B x DP) + (C x DP^2)** Where **B = 1.31013E+01**  
**C = -9.26343E-02**

A Flow of 98.882179 CFM produces a UUT DP of 8.00 In H<sub>2</sub>O

TERMINAL NON-LINEARITY = 2.721 % FOR DETAILS SEE  
INDEPENDENT NON-LINEARITY = 0.919 % FILE NO. 501:440

PRINTOUT DATE :09-09-1999

Filename : 77747001.1NN

## M Manual for the Meriam laminar flow meter

On the following pages the manual for the Meriam Laminar Flow element can be found



10920 MADISON AVENUE • CLEVELAND, OHIO 44102  
(216) 281-1100 FAX: (216) 281-0228

MODEL 50MCZ-ZF  
SERIAL NO. 777470-N1

# LAMINAR FLOW ELEMENTS

## INSTALLATION & OPERATION INSTRUCTIONS

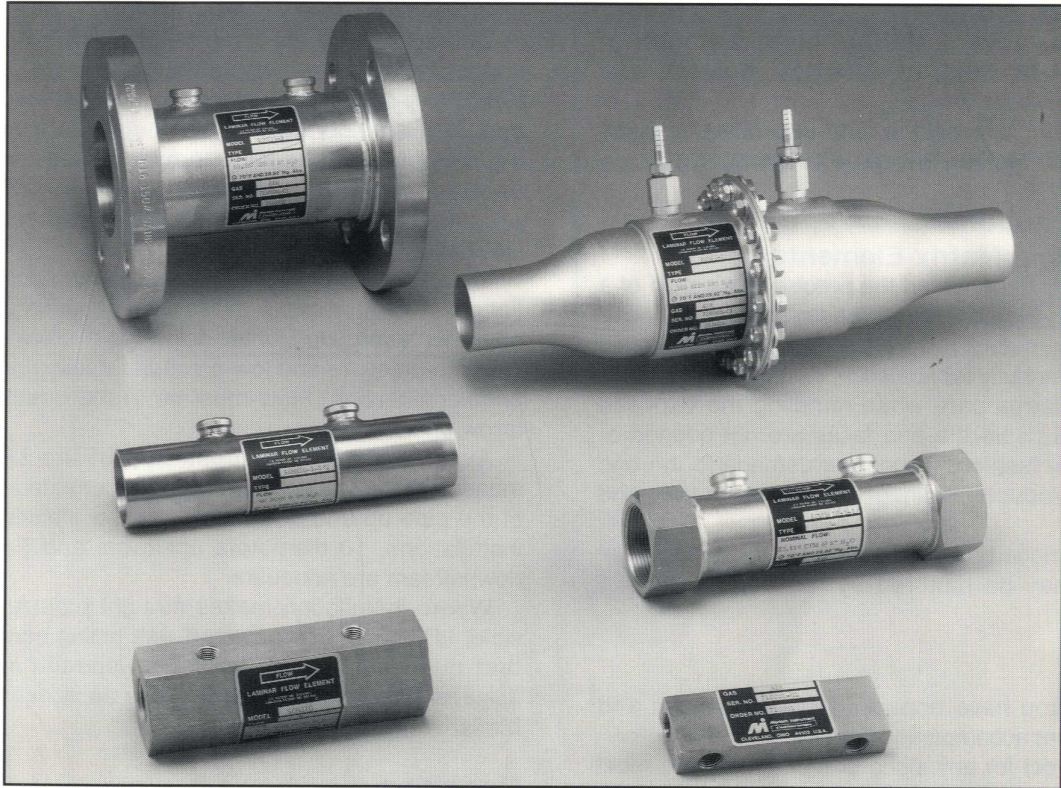


## Table of Contents

Page	Page		
Introduction .....	2	Maintenance .....	8
Inspection.....	2	Trouble shooting .....	8
Installation.....	2	Correction factor tables/curves	
Operation .....	2	Pressure .....	9
Typical Installations.....	3	Air viscosity.....	10
Calibration curve/table .....	4	Air temperature/viscosity .....	10
Actual, Standard and Mass flow equations .....	4 & 5	Temperature.....	11
Reading your laminar flow element curve/table .....	6	Air-humidity for density .....	5
		Air-humidity for viscosity .....	5

### **Introduction**

Meriam Laminar Flow Elements (LFE) are used with appropriate readout instrumentation to measure the flow of air or other gas.

This manual covers Meriam Models 50MK10, 50MW20, 50MR2, 50MJ10, 50MH10, 50MC2, and 50MY15.

For description, dimensions, and capacities of these elements, refer to Meriam Bulletin, File No. 501:215.

### **Special Precautions**

#### **When Handling Matrix Elements**

The Meriam LFE depends on the precise fabrication of a matrix metering element for its basic accuracy. These elements are manufactured from .001 in. stainless steel stock and are carefully fabricated.

Exercise extreme care when handling the exposed element to make sure the end faces are not gouged or damaged in any fashion. Gouges or damage to the end surfaces will produce nonlinear resistance to flow and introduce error.

If the end surface becomes damaged, the accuracy of the element may be restored by recalibration at the factory.

### **Inspection**

1. Make sure you have unpacked all instructions and other data that accompanied the unit.
2. Visually inspect for any signs of damage. There must be no nicks or scratches. The surfaces of the LFE should be clear.
3. Units are shipped with a cap plug in each opening. They protect the ends and pressure taps. Remove cap plugs.
4. Visually inspect matrix surface inside housing. No capillaries should be blocked except for special applications. There must be no nicks on the surface.

### **Installation**

Make sure line is free of dirt and other foreign materials. The metered gas must be clean. In-line use of filters is recommended.

Connections to the differential pressure instrument should be made with equal lengths of 1/4" I.D. hose, tubing or pipe. All instrument connections must be leak-free. Install temperature sensor 2-diameters upstream of the element. Inlet absolute pressure instrument, when needed, must be connected close to LFE at inlet pressure tap. Figure 1 shows several typical LFE installations.

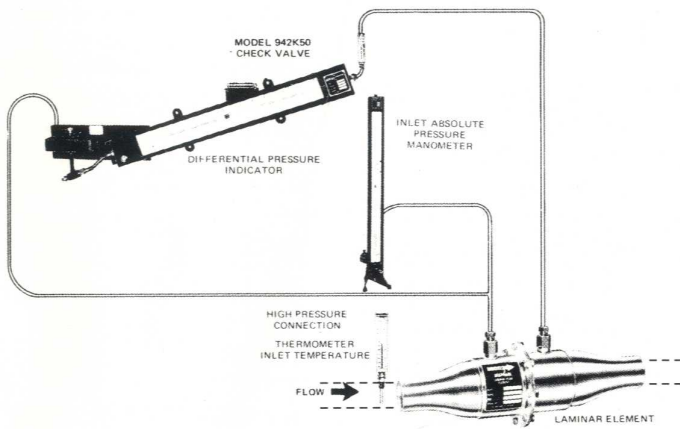
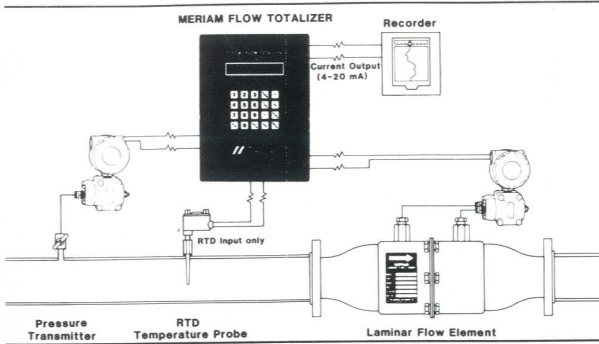
Install the LFE in the line using hose connectors, flanges, tubing or pipe, as desired. Position the LFE in any orientation. Horizontal is the most common. Orient the high-pressure and low-pressure sensing ports in any angular direction. Flow must be in the direction of the arrow on the LFE.

Avoid disturbances upstream of the LFE. Good measurement practices dictate an adequate straight run of the pipe up and downstream of the element. In most installations, 10 diameters upstream and 5 diameters downstream are adequate.

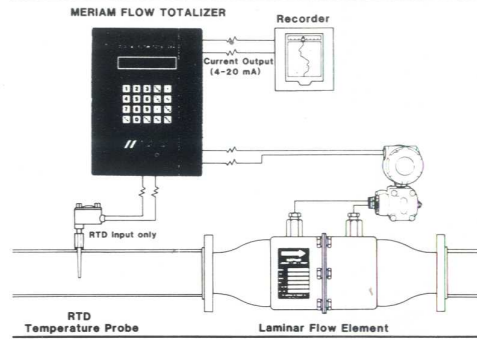
Where installation makes straight pipe runs impossible, LFE's can be calibrated with piping configurations that duplicate installation. This special calibration assures installed accuracy. In these applications, consult Meriam regarding calibration.

### **Operation**

Establish flow through the LFE. Measure differential pressure between high pressure sensing port and low pressure sensing port. Measure inlet gas temperature. For standard or mass flow rates, measure absolute line pressure. Refer to calibration curve/table instructions for flow rate calculations.

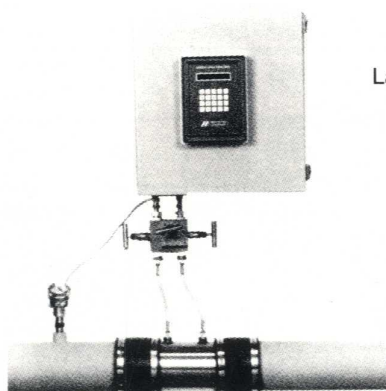


Standard or mass flow rate.



Actual volumetric flow rate.

Model LFS  
Laminar flow system



Actual, Standard or mass flow rate.

Figure 1: Typical installations of LAMINAR FLOW METER SYSTEMS.

## Calibration Curve/Table

Meriam performs an air calibration of LFE using a master flowmeter that is traceable to the National Institute of Standards and Technology (NIST). The calibration data is standardized to an equivalent dry gas flow rate at 70°F (21.1°C) and 29.92 inches Hg absolute (101.3 kPa abs.). (The customer may request another standard condition such as 0°C.) It is then possible to determine the actual or standard volumetric flow rate at your flowing conditions.

Each LFE has at least one calibration curve or table. The standard curve/table is for dry air flow rate in units of cubic feet per minute (CFM) versus the differential pressure (DP) in inches of water referenced to 4°C produced by the LFE. You may request a curve/table for a different gas and/or for different flow rate units. Each curve/ table is generated using a quadratic (second order) equation,

$$B \times DP + C \times DP^2 = Flow.$$

The calibration constants B and C are printed on each curve/table.

## Actual Volumetric Flow Rate

The LFE determines the actual volumetric flow rate. To obtain the actual volumetric flow rate, the differential pressure across the LFE and the inlet temperature to the LFE is measured. Using the calibration curve/table associated with the particular LFE, a flow rate value is obtained by either:

- 1) reading the value from the curve/table or
- 2) using the formula,  $B \times DP + C \times DP^2 = Flow$

Each curve has unique constants B and C. Multiply this flow rate value by the ratio:

$$\frac{(\text{viscosity of flowing gas at } 70^\circ\text{F in micropoise})}{(\text{viscosity of flowing gas at flowing temperature in micropoise})}$$

or  $\mu_{std} / \mu_f$ . The product is the actual volumetric flow rate. (The curve/table lists the type of gas used to generate the curve/table.)

$$\text{Actual volumetric flow rate} = (B \times DP + C \times DP^2) \times (\mu_{std} / \mu_f)$$

To help calculate the viscosity of air at flowing temperature, a viscosity equation based on temperature is included in this instruction manual (see Table A-32422 pg. 10). The equation is from "Tables of Thermodynamic and Transport Properties of Air, Argon, Carbon Dioxide, Oxygen, and Steam." All other gas viscosity equations are obtained from "Physical and Thermodynamic Properties of Pure Chemicals." Table A-31986 (page 10) lists the values of  $\mu_{std}/\mu_f$  for air from 50-159°F at 1° intervals when the standard temperature is 70°F.

\* **Note:** If you are flowing wet air, a humidity correction factor for viscosity must be used. The difference between wet-air viscosity ( $\mu_{wet}$ ) and dry-air viscosity ( $\mu_{dry}$ ) increases with temperature and humidity. At 80°F and 80% relative humidity, the ratio of  $\mu_{wet} / \mu_{dry}$  is .997.

Figure 2 (page 5) is a graph of the ratio  $\mu_{wet} / \mu_{dry}$  of air from 50 to 150°F and from 10 to 90% relative humidity. The viscosity of the flowing wet air becomes the value from the dry-air viscosity equation times the ratio  $\mu_{wet}/\mu_{dry}$ .

$$\mu_f = \mu_{wet-air} = \left( \frac{14.58x(T, K)^2}{(110.4 + T)} \right) x \left( \frac{\mu_{wet}}{\mu_{dry}} \right)$$

The curve/table may have DP units of

- 1) inches of water column (WC)
- 2) centimeters of WC
- 3) millimeters of WC
- 4) pascals
- 5) kilopascals

Whenever a pressure is expressed in units of water, the water temperature reference must be given. The calibration curve uses 4°C for the water temperature reference. Some devices use a water temperature reference of 20°C and others may use other temperature references. If no temperature reference is given on the DP instrument or in its instruction manual, consult the manufacturer. If the DP measuring device has a water temperature reference other than 4°, correct the DP reading by using the following equation:

$$DP @ 4^\circ\text{C} = DP(\text{device}) \times \frac{\text{density of H}_2\text{O} @ \text{device temperature ref.}}{\text{density of H}_2\text{O} @ 4^\circ\text{C}}$$

Water Temperature	Water Density (lbs/ft <sup>3</sup> )
4°C (39.2°F)	62.426
20°C (68°F)	62.316
15.5°C (60°F)	62.366
21.1°C (70°F)	62.301

The DP @ 4°C value should be used with the curve/ table.

## Standard Volumetric Flow Rate

The word "standard" when associated with flow rate, means the flow rate has been normalized to an assigned standard pressure and temperature. If standard volumetric flow rate is desired, the actual volumetric flow rate is multiplied by the ratios:

$$\frac{\text{standard temperature } (T_{std})}{\text{flowing temperature } (T_f)} \quad \text{and} \quad \frac{\text{flowing pressure } (P_f)}{\text{standard pressure } (P_{std})}$$

Be sure to use the same absolute units for pressure (i.e. PSIA, mm Hg absolute, ...) and temperature (°K or °R). The result is the standard volumetric flow rate at the given standard conditions.

Standard volumetric flow rate =

$$\text{Actual volumetric flow rate} \times (T_{std} / T_f) \times (P_f / P_{std})$$

This equation can be rewritten:

$$(B \times DP + C \times DP^2) \times \left( \frac{\mu_{std}}{\mu_f} \right) \times \left( \frac{T_{std}}{T_f} \right) \times \left( \frac{P_f}{P_{std}} \right)$$

Table A-31031 (page 9) lists the values of  $P_f / P_{std}$  for absolute line pressures from 26" Hg to 36" Hg at 0.05" Hg intervals. The standard pressure is 29.92" Hg absolute for this table. Table A-32422 (page 10) lists the values of  $(T_{std} / T_f) \times (\mu_{std} / \mu_f)$  for air from 50 to 159°F in 1° intervals. The standard temperature is 70°F (529.67°R) for this table.

\* Note: If you are flowing wet air, a humidity correction factor for standard volumetric flow rate must be used. The difference between wet-air density ( $\rho_{wet}$ ) and dry-air density ( $\rho_{dry}$ ) increases with temperature and humidity. At 80°F and 80% relative humidity, the ratio of  $\rho_{wet} / \rho_{dry}$  is .990. Table A-35600 (below) lists the ratio  $\rho_{wet} / \rho_{dry}$  of air from 40 to 100°F and from 20 to 100% relative humidity. The equation for standard volumetric flow rate of flowing wet air becomes :

$$\text{STANDARD VOLUMETRIC FLOW RATE}_{\text{wet air}} = (B \times DP + C \times DP^2) \times \left( \frac{\mu_{std}}{\mu_{wet-air}} \right) \times \left( \frac{T_{std}}{T_f} \right) \times \left( \frac{P_f}{P_{std}} \right) \times \left( \frac{\rho_{wet}}{\rho_{dry}} \right)$$

### Mass Flow Rate

Multiply the standard volumetric flow rate by the density of the flowing gas at standard conditions to obtain the mass flow rate of that gas.

Mass flow rate = Standard volumetric flow rate x density @ standard conditions.

### Summary

$$\text{Curve/table value } @ DP = (B \times DP + C \times DP^2)$$

$$\text{Actual volumetric flow rate} = (B \times DP + C \times DP^2) \times (\mu_{std} / \mu_f)$$

$$\text{Standard volumetric flow rate} = \text{Actual volumetric flow rate} \times (P_f / P_{std}) \times (T_{std} / T_f)$$

$$\text{Mass flow rate} = \text{Standard volumetric flow rate} \times \text{density} @ \text{standard conditions.}$$

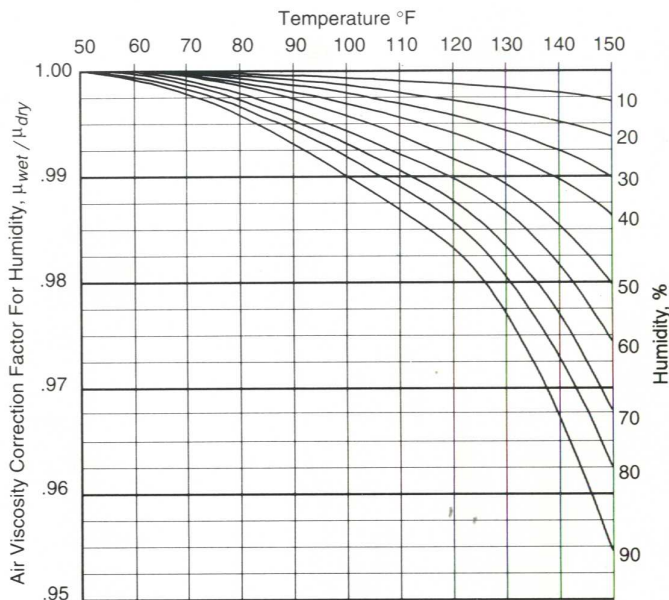


**Figure 2: Relative humidity correction factor for air viscosity. A-35500**  
Kestin & Whitelaw

**Table A-35600 (NBSIR 83-2652)**  
**Humidity correction factor for air =  $\rho_{wet} / \rho_{dry}$**

°F	% Relative Humidity				
	20%	40%	60%	80%	100%
40	.9993	.9987	.9981	.9975	.9969
50	.9990	.9981	.9973	.9964	.9955
60	.9986	.9973	.9960	.9948	.9934
70	.9981	.9962	.9944	.9925	.9907
80	.9974	.9948	.9922	.9895	.9870
90	.9964	.9928	.9892	.9855	.9818
100	.9951	.9902	.9854	.9805	.9756

## DETERMINING FLOW FROM YOUR LAMINAR FLOW ELEMENT

### Calibration Curve/Table

The curve/table of each LFE is normalized to standard conditions listed by multiplying the calibration data points by the ratio of:

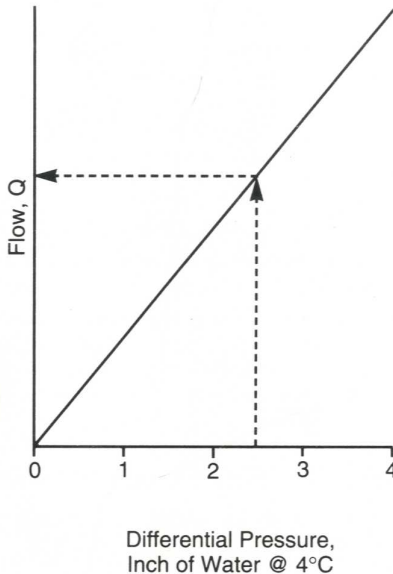
$$\frac{\text{viscosity of gas at calibration temperature}}{\text{viscosity of gas at } 70^\circ\text{F (standard temperature)}}$$

Therefore, you should NOT read the flow rate directly from the curve/table unless your flow temperature and pressure are identical to the standard conditions. The

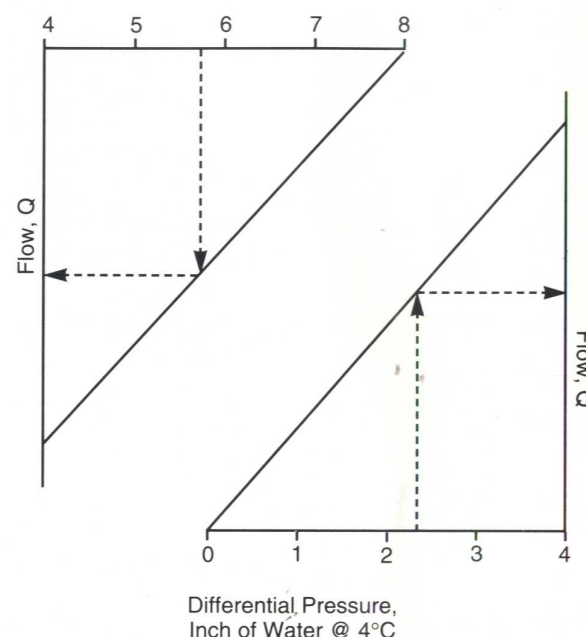
following steps must be taken to determine flow rate at flowing conditions other than standard.

1. Measure and correct to  $4^\circ\text{C}$ , if necessary, the DP across the LFE.
2. Measure and record the inlet temperature (always) and absolute line pressure (for standard or mass flow rates). Convert both values to absolute units.
3. Follow the AIR FLOW or GAS OTHER THAN AIR guidelines below.

Model 50MK10



All Other Models



### Air Flow

Select the proper flow curve/table for the LFE being used.

### STANDARD VOLUMETRIC FLOW RATE

- 1) To obtain standard volumetric flow rate if inlet pressure and temperature are other than 29.92" Hg absolute and  $70^\circ\text{F}$ , respectively, find the flow rate ( $Q$ ) that corresponds to the corrected DP. Multiply  $Q$  by temperature/viscosity and pressure corrections shown on charts A-32422 and A-31031, respectively, to bring flow to standard conditions of 29.92" Hg and  $70^\circ\text{F}$ .
- 2) At flowing conditions of  $70^\circ\text{F}$  and 29.92" Hg, read curve directly in standard volumetric flow rate.

### ACTUAL VOLUMETRIC FLOW RATE

- 1) To obtain actual volumetric flow rate at inlet flowing temperature other than  $70^\circ\text{F}$ , find the flow rate ( $Q$ )

that corresponds to the corrected DP. Multiply  $Q$  by the viscosity correction only. See chart A-31986 for corrections.

- 2) At flowing inlet temperature of  $70^\circ\text{F}$ , read curve directly in actual volumetric flow rate.

Actual volumetric flow rate equals standard volumetric flow rate when flowing conditions are  $70^\circ\text{F}$  and 29.92" Hg.

Notify Meriam if your flowing gas is not air and/or standard conditions are different from  $70^\circ\text{F}$  and 29.92" Hg absolute. A special curve/table can be provided listing the gas being flowed. The gas viscosity correction,  $\mu_{\text{std}} / \mu_f$ , will reference the gas and/or new standard temperature value, if applicable. Table A-32422 or A-31986 cannot be used for gases other than air.

## Gas Flow Other Than Air / Standard Conditions Different From 70°F and 29.92" Hg ABS

Select the proper flow curve/table for the LFE being used.

### STANDARD VOLUMETRIC FLOW RATE

- To obtain standard volumetric flow rate if the inlet temperature and pressure are different from standard, read the flow rate (Q) from the curve/table corresponding to the corrected differential pressure (DP). Calculate the viscosity at the flowing temperature using the viscosity equation for the flowing gas. Then calculate the viscosity correction factor ( $\mu_{cf}$ ) using

$$\mu_{cf} = \frac{\text{viscosity constant from curve/table}}{\text{flowing gas viscosity at flowing temperature}}$$

Locate the pressure correction factor ( $P_{cf}$ ) for the flowing inlet pressure on chart A-31031 (page 9) or calculate the correction factor using

$$P_{cf} = \frac{\text{absolute inlet line pressure}}{\text{absolute standard pressure.}}$$

Locate the temperature correction factor ( $T_{cf}$ ) for the flowing temperature on chart A-35700 (page 11) or calculate using

$$T_{cf} = \frac{\text{absolute standard temperature}}{\text{absolute flowing temperature.}}$$

Multiply Q from the curve/table by the viscosity correction factor ( $\mu_{cf}$ ), the pressure correction factor ( $P_{cf}$ ) and the temperature correction factor ( $T_{cf}$ ). This product will give the flow rate of a particular gas at the standard conditions.

- At flowing inlet conditions equal to the standard conditions, read curve/table directly in standard volumetric flow rate.

### ACTUAL VOLUMETRIC FLOW RATE

- To obtain actual volumetric flow rate if the inlet temperature is different from standard temperature, read the flow rate (Q) from the curve corresponding to the corrected DP.

Calculate the viscosity at the flowing temperature using the viscosity equation for the flowing gas. Then calculate the viscosity correction factor using

$$\mu_{cf} = \frac{\text{viscosity constant from curve/table}}{\text{flowing gas viscosity at flowing temperature}}$$

Multiply Q by the viscosity correction factor ( $\mu_{cf}$ ). This product will give the flow rate of a particular gas at the actual flowing conditions.

- At flowing inlet temperature equal to the standard temperature, read the curve/table directly in actual volumetric flow rate.



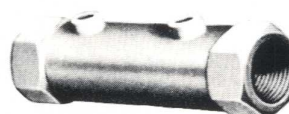
#### MODEL 50MK10

Utilizes stainless capillary tubes cemented into a stainless body. Inlet, outlet, and differential pressure connections are 1/4" NPT. Max. design: 100 PSIG and 150°F.



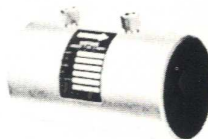
#### MODEL 50MJ10

All stainless steel unit with fused matrix. Differential pressure connections are 1/4" NPT. Line connections 1/2" NPT, except Type 9 which has 3/4" NPT. Max. design: 100 PSIG and 150°F.



#### MODEL 50MW20

All stainless steel welded unit with fused matrix. Line connections are threaded. Differential pressure connections are 1/4" NPT. Max. design: 200 PSIG and 150°F.



#### MODEL 50MH10

All stainless steel welded unit with fused matrix. Line connections are plain ends for hose connection. Differential pressure connections are 1/4" NPT. Max. design: 100 PSIG and 150°F.



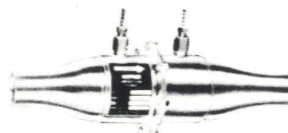
#### MODEL 50MY15

All stainless steel welded unit with fused matrix. Differential pressure connections are 1/4" NPT. Line connections are Series 15 flanges. Max. design: 150 PSIG and 150°F.



#### MODEL 50MR2

This unit is for low pressure applications. Differential pressure connections are 1/4" NPT. Aluminum Series 15 line flanges are furnished at inlet and outlet. Max. design: 20 PSIG and 150°F.



#### MODEL 50MC2

This flow element is for low pressure applications. Differential pressure connections are 1/4" NPT. Designed for use with hose for line connections at inlet and outlet. To include inlet filter, add suffix "F". Max. design: 20 PSIG and 150°F.

## Maintenance

Accumulation of dirt in the capillaries of the laminar element will affect the accuracy. When in doubt, hold the laminar in front of a high intensity light, sighting through the capillaries. Any dirt will be apparent. Loose dirt can be blown out with shop air (no more than 100 PSI) in reverse direction of flow. Shop air must be clean and dry. Brushing or rubbing the ends of the matrix element is not recommended because the matrix can be deformed, altering the calibration. Unless the customer has the facilities and primary standards to check calibration after cleaning, we recommend returning the unit to Meriam for cleaning and calibration.

## Troubleshooting

PROBLEM	PROBABLE CAUSE	REMEDY
Low or High DP Indication	Insufficient or improperly sized straight pipe downstream and/or upstream of LFE.	Use 10 diameters of straight pipe upstream and 5 diameters of straight pipe downstream of LFE. Pipe size should be same as LFE outlet size, e.g. $\frac{1}{2}$ " NPT on LFE means 10 diameters of $\frac{1}{2}$ pipe.
	One or both differential pressure connection taps plugged.	Clean or check instrument connecting line.
	If pulsation dampener is used, check stones (Model 50 MR2 and 50 MC2 only).	If plugged, replace with matched pair (Meriam part #A-31650).
	Leak in line between LFE and readout device.	Detect and repair.
	Large-volume and/or unequal-volume connecting lines to readout device.	Use small-volume and equal-volume connecting lines to readout device. See Installation on page 2.
	Piping reducers at inlet and/or outlet.	Do not use reducers immediately before or after LFE.
Pulsating/ Irregular Reading	Irregular flow pattern entering LFE.	Use at least 10 diameters of straight pipe upstream of LFE.
	Leak in system line.	Detect and repair.

**MERIAM LAMINAR FLOW ELEMENT  
PRESSURE CORRECTION FACTOR (ANY GAS)**  
BASE PRESSURE (ASSIGNED STANDARD) 29.92 INCHES MERCURY ABSOLUTE

LAMINAR INLET PRESSURE INCHES HG. ABS.		LAMINAR INLET PRESSURE INCHES HG. ABS.		LAMINAR INLET PRESSURE INCHES HG. ABS.		LAMINAR INLET PRESSURE INCHES HG. ABS.		LAMINAR INLET PRESSURE INCHES HG. ABS.	
Pcf.		Pcf.		Pcf.		Pcf.		Pcf.	
26.00	.8689	28.05	.9375	30.05	1.0043	32.10	1.0728	34.15	1.1413
26.05	.8706	28.10	.9391	30.10	1.0060	32.15	1.0745	34.20	1.1430
26.10	.8723	28.15	.9403	30.15	1.0076	32.20	1.0762	34.25	1.1447
26.15	.8739	28.20	.9425	30.20	1.0093	32.25	1.0778	34.30	1.1458
26.20	.8756	28.25	.9441	30.25	1.0110	32.30	1.0795	34.35	1.1480
26.25	.8773	28.30	.9458	30.30	1.0127	32.35	1.0812	34.40	1.1497
26.30	.8790	28.35	.9475	30.35	1.0143	32.40	1.0828	34.45	1.1514
26.35	.8806	28.40	.9491	30.40	1.0160	32.45	1.0845	34.50	1.1530
26.40	.8823	28.45	.9508	30.45	1.0177	32.50	1.0862	34.55	1.1547
26.45	.8840	28.50	.9525	30.50	1.0193	32.55	1.0879	34.60	1.1564
26.50	.8856	28.55	.9542	30.55	1.0210	32.60	1.0895	34.65	1.1580
26.55	.8873	28.60	.9558	30.60	1.0227	32.65	1.0912	34.70	1.1597
26.60	.8890	28.65	.9575	30.65	1.0243	32.70	1.0929	34.75	1.1614
26.65	.8907	28.70	.9592	30.70	1.0260	32.75	1.0945	34.80	1.1631
26.70	.8923	28.75	.9608	30.75	1.0277	32.80	1.0962	34.85	1.1647
26.75	.8940	28.80	.9625	30.80	1.0294	32.85	1.0979	34.90	1.1664
26.80	.8957	28.85	.9642	30.85	1.0310	32.90	1.0995	34.95	1.1681
26.85	.8973	28.90	.9659	30.90	1.0327	32.95	1.1012	35.00	1.1697
26.90	.8990	28.95	.9675	30.95	1.0344	33.00	1.1029	35.05	1.1714
26.95	.9007	29.00	.9692	31.00	1.0360	33.05	1.1046	35.10	1.1731
27.00	.9024	29.05	.9709	31.05	1.0377	33.10	1.1062	35.15	1.1747
27.05	.9040	29.10	.9725	31.10	1.0394	33.15	1.1079	35.20	1.1764
27.10	.9057	29.15	.9742	31.15	1.0411	33.20	1.1096	35.25	1.1781
27.15	.9074	29.20	.9759	31.20	1.0427	33.25	1.1112	35.30	1.1798
27.20	.9090	29.25	.9776	31.25	1.0444	33.30	1.1129	35.35	1.1814
27.25	.9107	29.30	.9792	31.30	1.0461	33.35	1.1146	35.40	1.1831
27.30	.9124	29.35	.9809	31.35	1.0477	33.40	1.1163	35.45	1.1848
27.35	.9141	29.40	.9826	31.40	1.0494	33.45	1.1179	35.50	1.1864
27.40	.9157	29.45	.9842	31.45	1.0511	33.50	1.1196	35.55	1.1881
27.45	.9174	29.50	.9859	31.50	1.0528	33.55	1.1213	35.60	1.1898
27.50	.9191	29.55	.9876	31.55	1.0544	33.60	1.1229	35.65	1.1915
27.55	.9207	29.60	.9893	31.60	1.0561	33.65	1.1243	35.70	1.1931
27.60	.9224	29.65	.9909	31.65	1.0578	33.70	1.1263	35.75	1.1948
27.65	.9241	29.70	.9926	31.70	1.0594	33.75	1.1280	35.80	1.1965
27.70	.9258	29.75	.9943	31.75	1.0611	33.80	1.1296	35.85	1.1981
27.75	.9274	29.80	.9959	31.80	1.0628	33.85	1.1313	35.90	1.1998
27.80	.9291	29.85	.9976	31.85	1.0645	33.90	1.1330	35.95	1.2015
27.85	.9308	29.90	.9993	31.90	1.0661	33.95	1.1346	36.00	1.2032
27.90	.9324	29.92	1.0000	31.95	1.0678	34.00	1.1363		
27.95	.9341	29.95	1.0010	32.00	1.0695	34.05	1.1380		
28.00	.9358	30.00	1.0026	32.05	1.0711	34.10	1.1397		

A-31031

For values not shown in table, interpolate or use equation.

$$\text{Pcf.} = \frac{\text{P flow}}{\text{P Base}} = \frac{\text{P flow}}{29.92}$$

Pcf. = Pressure Conversion Factor

P base = Assigned Base Pressure of 29.92 inches mercury absolute

P flow = Laminar Inlet Pressure, inches mercury absolute

The equation can be used up to and including two atmospheres absolute. It will be necessary to calibrate laminars for pressure exceeding above.

**TABLE A-31986**  
**AIR VISCOSITY CORRECTION FACTORS FOR ACFM**  
**BASE VISCOSITY 181.87 MICROPOISE AT 70°F**

$$\text{CORRECTION FACTOR} = \frac{181.87}{\mu\text{g}^*}$$

Note: These correction factors do not correct for volume changes due to temperature

Temp °F	+0	+1	+2	+3	+4	+5	+6	+7	+8	+9
50	1.03034	1.02877	1.02720	1.02564	1.02408	1.02253	1.02099	1.01945	1.01792	1.01639
60	1.01487	1.01336	1.01185	1.01035	1.00885	1.00736	1.00588	1.00440	1.00292	1.00146
70	1.0000	0.99854	0.99709	0.99564	0.99420	0.99277	0.99134	0.98992	0.98850	0.98709
80	0.98568	0.98428	0.98288	0.98149	0.98010	0.97872	0.97734	0.97597	0.97461	0.97325
90	0.97189	0.97054	0.96919	0.96785	0.96651	0.96518	0.96386	0.96253	0.96122	0.95991
100	0.95860	0.95729	0.95600	0.95470	0.95341	0.95213	0.95085	0.94957	0.94830	0.94704
110	0.94578	0.94452	0.94327	0.94202	0.94077	0.93953	0.93830	0.93707	0.93584	0.93462
120	0.93340	0.93219	0.93098	0.92977	0.92857	0.92737	0.92618	0.92499	0.92380	0.92262
130	0.92144	0.92027	0.91910	0.91794	0.91678	0.91562	0.91446	0.91331	0.91217	0.91103
140	0.90989	0.90875	0.90762	0.90650	0.90537	0.90425	0.90314	0.90203	0.90092	0.89981
150	0.89871	0.89761	0.89652	0.89543	0.89434	0.89326	0.89218	0.89110	0.89003	0.88896

**TABLE A-32422**  
**AIR TEMPERATURE/VISCOSITY CORRECTION FACTORS FOR SCFM**  
**AIR BASE TEMPERATURE 70°F, VISCOSITY 181.87 MICROPOISE**  
**REFERENCE NBS CIRCULAR 564**

$$\text{CORRECTION FACTOR} = \frac{529.67}{459.67 + ^\circ\text{F}} \times \frac{181.87}{\mu\text{g}^*}$$

$$\mu_{\text{air}} = \frac{14.58 \left( \frac{459.67 + ^\circ\text{F}}{1.8} \right)^{3/2}}{110.4 + \left( \frac{459.67 + ^\circ\text{F}}{1.8} \right)}$$

Temp °F	+0	+1	+2	+3	+4	+5	+6	+7	+8	+9
50	1.0707	1.0670	1.0633	1.0596	1.0559	1.0523	1.0487	1.0451	1.0415	1.0379
60	1.0344	1.0308	1.0273	1.0238	1.0204	1.0169	1.0135	1.0101	1.0067	1.0033
70	1.0000	.9966	.9933	.9900	.9867	.9834	.9802	.9770	.9737	.9705
80	.9674	.9642	.9611	.9579	.9548	.9517	.9486	.9456	.9425	.9395
90	.9365	.9335	.9305	.9275	.9246	.9216	.9187	.9158	.9129	.9100
100	.9072	.9043	.9015	.8987	.8959	.8931	.8903	.8875	.8848	.8820
110	.8793	.8766	.8739	.8712	.8686	.8659	.8633	.8606	.8580	.8554
120	.8528	.8503	.8477	.8452	.8426	.8401	.8376	.8351	.8326	.8301
130	.8276	.8252	.8227	.8203	.8179	.8155	.8131	.8107	.8083	.8060
140	.8036	.8013	.7990	.7966	.7943	.7920	.7898	.7875	.7852	.7830
150	.7807	.7785	.7763	.7741	.7719	.7697	.7675	.7653	.7632	.7610

\* When flowing gas other than air, use the viscosity in micropoise of the gas at flowing temperature in the Correction Factor equation.

**TABLE A-35700**  
**TEMPERATURE CORRECTION FACTOR**  
**BASE TEMPERATURE = 70°F**

$$T_{cf} = \frac{529.67}{(459.67 + {}^{\circ}\text{F})}$$

Temp °F	+0	+1	+2	+3	+4	+5	+6	+7	+8	+9
50	1.0392	1.0372	1.0352	1.0332	1.0311	1.0291	1.0271	1.0252	1.0232	1.0212
60	1.0192	1.0173	1.0153	1.0134	1.0115	1.0095	1.0076	1.0057	1.0038	1.0019
70	1.0000	0.9981	0.9962	0.9944	0.9925	0.9906	0.9888	0.987	0.9851	0.9833
80	0.9815	0.9797	0.9778	0.976	0.9742	0.9725	0.9707	0.9689	0.9671	0.9654
90	0.9636	0.9619	0.9601	0.9584	0.9567	0.9549	0.9532	0.9515	0.9498	0.9481
100	0.9464	0.9447	0.943	0.9414	0.9397	0.938	0.9364	0.9347	0.9331	0.9314
110	0.9298	0.9282	0.9265	0.9249	0.9233	0.9217	0.9201	0.9185	0.9169	0.9153
120	0.9137	0.9122	0.9106	0.909	0.9075	0.9059	0.9044	0.9028	0.9013	0.8998
130	0.8982	0.8967	0.8952	0.8937	0.8922	0.8907	0.8892	0.8877	0.8862	0.8847
140	0.8833	0.8818	0.8803	0.8789	0.8774	0.876	0.8745	0.8731	0.8716	0.8702
150	0.8688	0.8674	0.8659	0.8645	0.8631	0.8617	0.8603	0.8589	0.8575	0.8561

Dear LFE User,

When you decide to have your LFE cleaned, please be aware of the various capabilities of recalibrating LFE's at Meriam. The following procedures (procedure #'s in parentheses) can be performed. All calibrations include: 6-8 calibration points; data sheet with raw data and reduced data; calibration curve; and instruction manual.

Calibrations	NIST certificate	Accuracy % Reading
{ } Clean (A-33555) and recalibrate (A-33558) using working masters.	{ x }	±0.86% R
{ } Clean and recalibrate using master masters.	{ x }	±0.7% R
{ } As received (before) calibration (A-34777), clean, recalibrate (after) using working masters.	{ x }	±0.86% R
{ } As received (before) calibration (A-34777), clean, recalibrate (after) using master masters.	{ x }	±0.7% R
{ } ANSI/NSCL Z540-1(MIL STD 45662A) same as (3).	{ x }	±0.86% R
{ } ANSI/NSCL Z540-1(MIL STD 45662A) same as (4).	{ x }	±0.7% R
{ } Nuclear or safety related application (A-33544). 8 calibration points.	{ x }	±0.7% R

Options

- { } 2 extra calibration points beyond full scale value.
- { } Extra calibration points beyond full scale value.  
at the following settings \_\_\_\_\_.
- { } Extra calibration points below 1/8 full scale value  
at the following settings \_\_\_\_\_.
- { } Oxygen cleaning (A-50558).
- { } Helium leak check (A-34759).
- { } Pneumatic pressure test (A-70763).
- { } Calibrate LFE with differential pressure transmitter (A-33881).

The usual unit for flow rate is cubic feet per minute. Other available units include

{ }	Liters	Per	{ }	second
{ }	Cubic centimeter		{ }	minute
{ }	Meters		{ }	hour
{ }	Pounds (include flowing temperature and pressure)			
{ }	Kilograms (include flowing temperature and pressure)			
{ }	Other _____.			

The usual unit for differential pressure is inches of water at 4°C. Other available units include

{ }	Millimeters of water @4°C	{ }	Kilopascals
{ }	Centimeters of water @4°C	{ }	Other _____
{ }	Pascals		

A second data sheet and calibration curve using the listed units will be included with the recalibration.



10920 MADISON AVENUE • CLEVELAND, OHIO 44102  
(216) 281-1100 FAX: (216) 281-0228